NASA CONTRACTOR REPORT

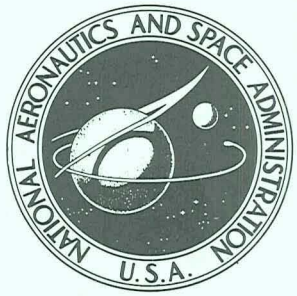

NASA CR-2351

NASA CR-2351

NONLINEAR ANALYSIS OF STRUCTURES

by H. Armen, H. Levine, A. Pifko, and A. Levy

Prepared by
GRUMMAN AEROSPACE CORPORATION
Bethpage, N.Y. 11714
for Langley Research Center

NATIONAL AERONAUTICS AND SPACE ADMINISTRATION • WASHINGTON, D. C. • MARCH 1974

1. Report No. NASA CR-2351	2. Government Accession No.	3. Recipient's Catalog No.
4. Title and Subtitle NONLINEAR ANALYSIS OF STRUCTURES		5. Report Date March 1974 6. Performing Organization Code
7. Author(s) H. Armen, H. Levine, A. Pifko, and A. Levy		8. Performing Organization Report No. RE-454
9. Performing Organization Name and Address Grumman Aerospace Corporation Research Department Bethpage, N. Y. 11714		10. Work Unit No. 760-60-01-01 11. Contract or Grant No. NAS 1-10087
12. Sponsoring Agency Name and Address National Aeronautics and Space Administration Washington, D.C. 20546		13. Type of Report and Period Covered Contractor Report 14. Sponsoring Agency Code

15. Supplementary Notes

This is a topical report.

16. Abstract

The material presented in this report is representative of the current state of the development of nonlinear analysis techniques within the framework of the finite-element method. Although the emphasis here is concerned with those nonlinearities associated with material behavior, a general treatment of geometric nonlinearity, alone or in combination with plasticity is included, and applications presented for a class of problems categorized as axisymmetric shells of revolution. Effects due to creep and other time-dependent material properties are not considered. The scope of the nonlinear analysis capabilities includes: 1) a membrane stress analysis, 2) bending and membrane stress analysis, 3) analysis of thick and thin axisymmetric bodies of revolution, 4) a general three dimensional analysis, and 5) analysis of laminated composites.

Applications of the methods are made to a number of sample structures. Correlation with available analytic or experimental data range from good to excellent.

17. Key Words (Suggested by Author(s))	18. Distribution Statement
Finite element Plastic Nonlinear Deflection	Unclassified - Unlimited

19. Security Classif. (of this report)	20. Security Classif. (of this page)	21. No. of Pages	22. Price*
Unclassified	Unclassified	128	$4.50

*For sale by the National Technical Information Service, Springfield, Virginia 22151

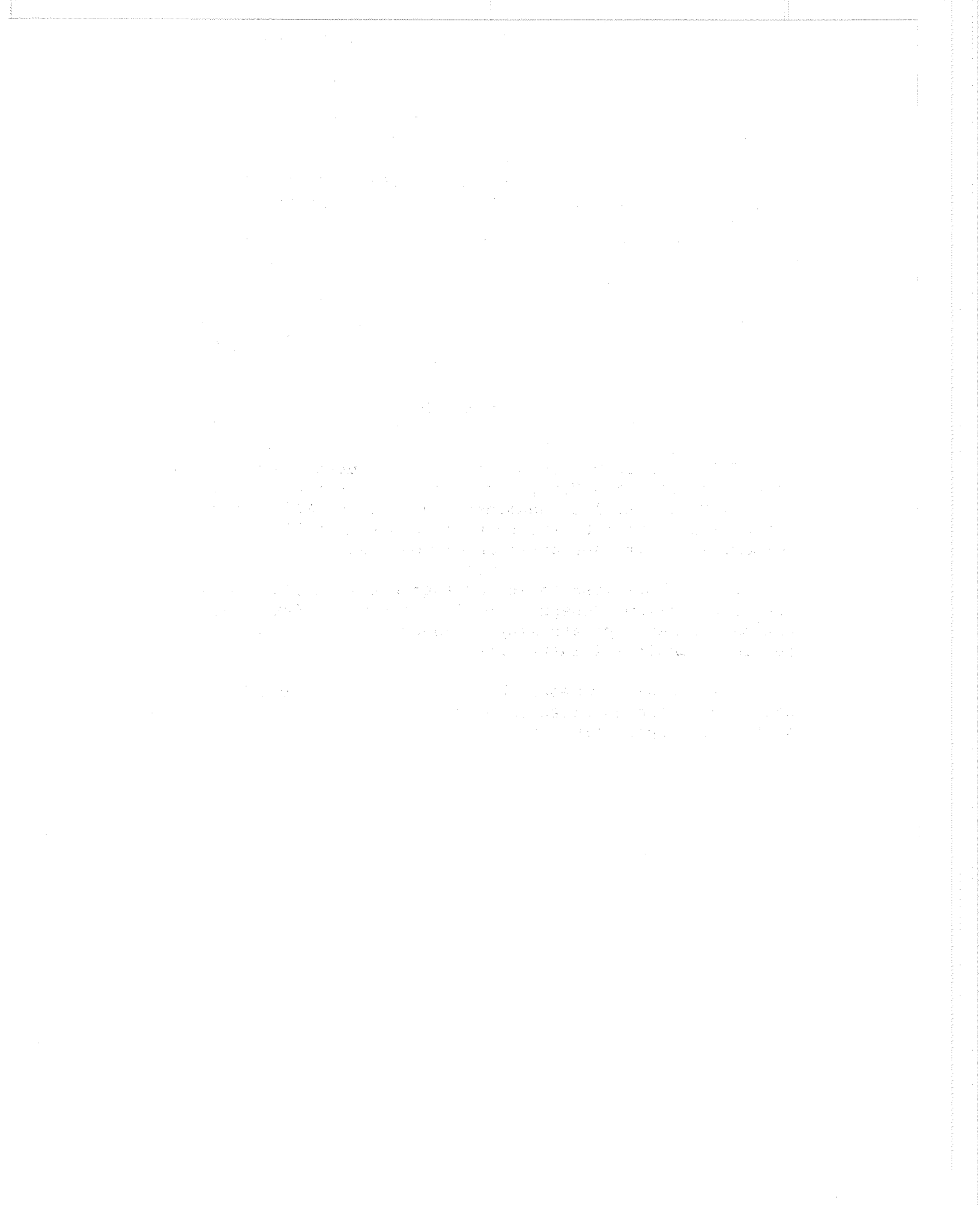

FOREWORD

This program was conducted by the Grumman Aerospace Corporation, Bethpage, New York, under partial support of Contract NAS 1-10087, entitled "Nonlinear Analysis of Structures." The work was performed by the Research Department of Grumman Aerospace Corporation, with support from Grumman Data Systems.

The authors wish to acknowledge the valuable contribution of Patricia Zirk and Joseph S. Miller of Grumman Data Systems for digital computer programming. Thanks also go to Catherine O'Regan for the technical illustrations.

This volume presents the analytical investigations and results obtained in the application of the methodology to several representative sample structures.

TABLE OF CONTENTS

LIST OF ILLUSTRATIONS

LIST OF SYMBOLS

c	hardening coefficient
e^e	elastic strain
e_{ij}	linear component of strain-displacement relation
e^T	total strain
E	Young's Modulus
F	body forces
f	yield or loading function
n	shape parameter used in Ramberg-Osgood stress-strain relation
P	generalized forces
Q	effective plastic load
R	residual load for equilibrium correction
S	surface area of finite element
T	surface tractions
U	strain energy
u	generalized displacement
V	volume of a finite element
α_{ij}	coordinate of center of loading surface
Δ	denotes an incremental quantity
ϵ_{ij}	plastic strain components
$\tilde{\epsilon}_{ij}$	Green's strain tensor

η_{ij} nonlinear components of total strain

$d\lambda$ scalar quantity associated with flow rule

$d\mu$ scalar quantity appearing in Ziegler's hardening rule

ν Poisson's ratio

Σ_{ij} components of initial stress at the start of a load increment

σ_{ij} components of stress

σ_o yield stress

$\sigma_{0.7}$ parameter in Ramberg-Osgood stress-strain relation

ω_{ij} combination of independent incremental components of stress and plastic strain for elastic-ideally plastic materials; infinitesmal components of rotation

Matrices:

$[A]$ matrix relating total strains in structure to applied loads

$[C]$ matrix relating plastic strain increments to stress increments for strain-hardening materials

$[E]$ matrix relating elastic strains to stresses in a finite-element

$[\bar{E}]$ matrix representing condition of normality of plastic strain increment vector to yield or loading surface in an individual ideally-plastic element

$[\tilde{E}]$ matrix representing condition of normality of plastic strain increment vector to yield or loading surface in an individual ideally-plastic element

$[k^0]$ conventional element elastic stiffness matrix

$[k^1]$ initial strain stiffness matrix for a finite-element

$[N]$	matrix relating displacements to generalized nodal displacements
$[W]$	matrix relating linear components of strain to generalized nodal displacements
$[\Omega]$	matrix relating nonlinear components of strain to generalized nodal displacements

Notation:

$\{\ \}$	column vector
$[\ ]$	square or rectangular matrix
$[\ ]'$	transpose of matrix
$[\ ]^{-1}$	inverse of matrix
i	used as a subscript denotes nodal quantities
k	used as a superscript denotes k^{th} incremental load step

SUMMARY

The material presented in this report, although primarily concerned with the author's investigations, is representative of the current state of the development of nonlinear analysis techniques within the framework of the finite-element method. Although the emphasis here is concerned with those nonlinearities associated with material behavior, a general treatment of geometric nonlinearity, alone or in combination with plasticity is included, and applications presented for a class of problems categorized as axisymmetric shells of revolution. Effects due to creep and other time-dependent material properties are not considered.

The report represents an extension of two previous studies reported in NASA Contractor's Reports CR-803 and CR-1649. The emphasis of the two previous investigations was on the development of methods, along with sufficient computer programming and computation to establish their validity and effectiveness. The purpose of the currently reported effort is to develop a comprehensive program that implements the methods and procedures of the two previous investigations, and thus provides practical tools to the designer and analyst. To accomplish this requires that the capabilities and capacity of the programs be sufficiently broad in scope so as to permit the analysis of realistic structures and that close attention be paid to efficiency, so that computations can be made more economically.

The scope of the nonlinear analysis capabilities resulting from this study includes: 1) a membrane stress analysis, 2) bending and membrane stress analysis, 3) analysis of thick and thin axisymmetric bodies of revolution, 4) a general three dimensional analysis, and 5) analysis of laminated composites.

Applications of the methods are made to a number of sample structures. Correlation with available analytic or experimental data range from good to excellent.

A catalog of the finite-elements used in developing this comprehensive program and a general discussion of three plasticity theories are presented in respective appendices.

1. INTRODUCTION

The application of finite-element methods to treat the nonlinear behavior of structures has reached a sufficient state of maturity so that the results obtained from these analyses can be accepted with a high level of confidence. While these methods are generally analysis oriented, their application to industrial design is gaining momentum in this country [1-3].

Although it is not customary in design practice to allow a structure to enter the plastic range, the need for developing a capability for treating the nonlinear behavior of structures nevertheless exists. An obvious reason for this capability is that the prediction of failure loads (elastic and plastic instability) under realistic loading conditions provides a consistent, meaningful application of factors of safety. In addition, predicting the redistribution (whether by design or from unavoidable circumstances) of stresses resulting from the nonlinear behavior of a structure is a necessary ingredient toward its design as an efficient, safe, well proportioned structure.

Compendium of Previous Studies

While solutions exist in the literature that are applicable to numerous structures and materials, many of these solutions involve such gross simplifications that they must be used with caution. These simplifications were made because the complexities associated with plastic behavior render the solution of all but the simplest problems a formidable task. First, the laws of material behavior under complex multiaxial stress states have not been precisely defined. The stress-strain relations do not simply involve the current values of the stress components, as is the case for linear elastic behavior; rather, they depend as well upon the past histories of these components, i.e., the material has a memory associated with its behavior. In addition, the material laws appear to be different for each material. One approach to this difficulty is the use of approximations that provide a reasonably realistic representation of the essential experimentally observed features of inelastic material behavior.

Another complexity associated with the general plasticity problem is its nonlinearity. Thus, the chances of obtaining a closed-form solution to a specific problem are fairly remote. As was the

case with linear elastic stress analysis, solutions to specific problems had to be matched to a catalog (however limited) of predetermined solutions. If the geometry and system of loads did not fit these known solutions, the analyst was forced to consider a simplified geometry and loading system that approximated the one in question. The nonvalidity of the principle of superposition added an extra dimension of complexity to the nonlinear analysis. Therefore, the analyst sought numerical solution techniques of the repetitive type. These are usually classified as iterative or stepwise. In the first, the iterative approach, the entire load may be applied at once, and a solution is effected by using an appropriate convergent iterative technique. In the stepwise approach, the response of the structure is assumed to be linear over small increments of load. There are merits in both approaches, as well as in their combined use.

A major difficulty with the repetitive type of solution is that it generally requires quite an extensive computing effort. To circumvent this difficulty, it is necessary not only to develop higher-speed machines of larger capacity but also to develop methods of analysis that minimize the computing effort.

Despite these complexities, substantial progress has recently been made in developing general methods of plastic analysis. This progress is largely due to advances in the field of numerical methods of structural analysis, specifically, the finite-element method. The treatment of nonlinearities, both physical and geometric, within the framework of existing finite-element techniques permits analysis of structures of arbitrary shape and consideration of a variety of loading and boundary conditions.

References 4-16 are representative of recent investigations concerned with incorporating the effects of plastic behavior in finite-element analysis. These studies describe techniques to treat plasticity by means of various algorithms that linearize the basically nonlinear problem. These techniques have been divided into two general categories: a) the initial strain and b) the tangent-modulus methods.

In the initial-strain method, the equivalence between temperature gradients and body forces in causing a strain field is extended to include plastic strains. Thus plastic effects are treated by interpreting plastic strains as initial strains. This analogy, first introduced in Ref. 17 reduces the nonlinear analysis to the analysis of an elastic body of identical shape and boundary conditions, but

with an additional set of applied loads, here termed "effective plastic loads." The initial-strain method is advantageous because of the ease with which it can be implemented in a finite-element analysis and because the stiffness matrix developed for the elastic behavior of the structure remains unaffected by changes in material properties.

In the tangent-modulus method (outlined in Refs. 6 and 9), the incremental linear constitutive relation, based on the plasticity theory, is introduced directly into the governing equilibrium equations. This method requires modification of the element stiffness influence coefficients at each incremental load step.

Despite differences in application of the initial-strain and the tangent-modulus concepts, there is, in some respects, a close relationship between them. References 9 and 16 discuss this relationship and the comparative merits of the methods as applied to membrane stress problems, while Ref. 18 discusses the relative merits of each of these approaches for combined nonlinear problems.

The development of nonlinear finite-element analysis has not been limited to the area of plasticity. Considerable effort has been directed toward the treatment of geometric nonlinearity. Effects resulting from geometric nonlinearities alone [19-21] have been considered extensively, and in several instances the simultaneous effects of both types of nonlinearity have been treated [18, 22-24]. In general, these studies have been concerned solely with monotonic loading conditions where the load reaches a specified maximum value, or until structural failure occurs. Only in rare instances have unloading and reversed loading been considered [11, 16, 23].

In many cases, when one considers the problem of combined geometric and material nonlinearity, the solution technique used for the treatment of plasticity alone (i.e., an incremental approach) becomes especially attractive. Since the relations derived from the flow theory of plasticity are themselves incremental, the modifications necessary to incorporate the effects of geometric nonlinearity are minimal.

However, the choice of using the tangent modulus or effective load approach to account for material and geometric nonlinearity is of utmost importance because of the extensive computer times required for repetitive solutions to these problems. In addition, the choice of solution algorithm (e.g., Cholesky decomposition, Gauss-Seidel iteration, etc.) and solution procedure (Newton-Raphson, first order self-correcting, etc.) in conjunction with either of the

above two methods can have an appreciable effect on the accuracy, efficiency (time), and stability of the solution. Various aspects of these problems have been discussed in two recent papers [18, 23].

Grumman-NASA Investigations

Since 1965 NASA/Langley has partially supported several efforts concerning the development of methods for the inelastic analysis of complex aeronautical structures. A chronological summary of these efforts is presented in Fig. 1. The goal of these studies has been to provide a feasible analytical means for determining the behavior of structures under conditions approaching failure and for loadings of a realistic nature. The methods developed under these contractual investigations, cited in Refs. 16 and 25, are based on and represent an extension of, the displacement method in finite-element techniques of structural analysis.

In the earliest of the previous studies (Ref. 25), consideration was given to the development of discrete-element methods for the plastic analysis of complex built-up structures in states of biaxial membrane stress, with particular emphasis on the effect of cyclic loading causing stress reversals into the plastic range. To accommodate this case, the methods implemented a plasticity theory that can take into account the Bauschinger effect. This theory is the kinematic hardening theory of Prager (Refs. 26 and 27) as modified by Ziegler (Ref. 28). It can represent the salient features of the plastic behavior of structural metals, and is readily implemented in a discrete-element analysis.

The governing linear matrix equation relating nodal displacements to applied loads and initial strains was modified for the treatment of membrane stress states to the form of a linear matrix equation relating stress increments directly to increments of applied load and initial strain. The solution to this equation was obtained by means of two alternative procedures. In the first, termed a predictor procedure, estimated values of initial (plastic) strain increment are used in the governing equation to yield stress increment. In the second, termed the stepwise linearization procedure, the flow rule of the plasticity theory chosen is used directly to obtain a matrix equation in terms of the unknown stress increment. These two methods are discussed in detail in Ref. 4. The computer programs for this analysis follow a two-step procedure. First, an elastic finite-element program must be used to develop the coefficient matrices to be used in the governing equation for the stress increments. The program accepts nodal and member topological information, forms the stiffness matrix for the structure, and subsequently performs the necessary matrix operations to form the

coefficient matrices relating the stress increments to the increments of applied load and initial strain. Constant stress or linearly varying stress elements are used in computing these coefficient matrices. As a second step, computer programs are written, independent of the type of finite-element used, to perform the plasticity analysis.

The simplicity of this technique for membrane stress analysis stems from the fact that the coefficient matrices, initially developed from an elastic analysis, remain unchanged during the course of the plastic analysis, and thus may be used without further modification.

In the follow-on effort, reported in Ref. 16, the methods previously developed for membrane stressed structures were extended to include the treatment of bending alone or in combination with membrane stresses.

An added complexity in a plastic bending analysis is that plastically deforming elements cannot be treated as wholly plastic. The regions of plasticity extend through only a portion of the thickness, consequently, it is necessary to locate elastic-plastic boundaries within the thickness of the element. A technique developed to accomplish this both for bending alone and for bending in combination with membrane stresses, involves an assumed distribution of plastic strain across the thickness (i.e., each component of plastic strain was assumed to vary linearly from the extreme fibers to an elastic-plastic boundary). A subsequent technique, developed under the present effort, does not require an a priori assumption concerning the representation of plastic strains or the elastic-plastic boundary through the thickness. Instead, the integrations necessary to obtain the components of the initial strain stiffness matrices are performed numerically by using the Gaussian quadrature scheme for in-plane integrations and Simpson's rule for the plastic strain integrations through the thickness. In addition, states of stress are evaluated at selected points through the thickness. Constitutive relations from the plasticity theory are used to evaluate states of plastic strain at these points, and the resulting variation is used in evaluating the pertinent integrals associated with those matrices required in the plastic analysis. While the previous approach is quite satisfactory for cases involving monotonic loading conditions, it is nevertheless restrictive and leads to great complexities when consideration is given to unloading and cyclic loading involving reversed plastic deformation. The new technique avoids such complexities.

At the completion of Contract NAS 1-7315, the methodology had been extended so that the "library" of elements available for plastic analysis included a beam of rectangular cross section, triangular and rectangular flat plate elements, and constant strain and linear strain triangular membrane elements. Also included in this study was an investigation to determine the feasibility of including the treatment of geometric nonlinearity within the framework of the plasticity methods. An incremental method was used to account for the effects of the changing geometry of the structure as it deforms, and application of the combined nonlinear procedure was made to beam and arch structures, as reported in Refs. 13 and 16.

The emphasis of the two NASA contracts was on the development of methods, along with sufficient computer programming and computation to establish the validity and effectiveness of these methods. The results obtained for almost all of the sample structures considered during the course of the contracts were compared with experimental and/or previous analytical work, and the correlation ranged from good to excellent. On this basis, we believe that the methods and procedures developed under these contracts can be used with a high level of confidence. The acceptance of these plasticity methods as a practical means for determining the nonlinear response of structures subjected to realistic loadings now required that they be made available on a convenient basis to the structural designer and analyst. This requirement led to the currently reported effort, Contract NAS 1-10087, the purpose of which is to develop a comprehensive program that implements the methods and procedures of the two previous investigations, and thus provides practical tools for the designer and analyst. To accomplish this requires that the capabilities and capacity of the programs be sufficiently broad in scope so as to permit the analysis of realistic structures and that close attention be paid to efficiency, so that computations can be made more economical.

The scope of the nonlinear analysis capabilities resulting from the study reported on here is presented in Fig. 2a. The capabilities are cataloged in terms of the types of analysis that can be treated. Finite-element programs, written for each of the analyses, take full advantage of the distinctions associated with each type of analysis for which they were written. The final comprehensive program consists of these programs under an executive that will selectively load and supervise the execution of individual programs as selected by the user. An organization chart of this structure is shown in Fig. 2b. A more detailed description of the organization of PLANS (PLastic ANalysis of Structures) is discussed subsequently in this report and in detail in a companion report.

One of the principal requirements of a comprehensive finite-element plastic analysis computer program is that it contains a library of finite-elements of sufficient variety that it is capable of accurately describing the state of stress and deformation existing in a wide variety of structures. These elements should be of a basic shape such that arbitrary geometric configurations may be represented to any desired accuracy. A catalog of the specific finite-elements to be available in the developed plasticity program is presented in Appendix A. A brief discussion of each element is presented in this appendix in which each element is classified according to the type of analysis to which it is applicable.

2. GOVERNING MATRIX EQUATIONS

The method employed in the present report uses an incremental formulation for the large deflection, elasto-plastic problem and is based on a variational principle presented in Ref. 29. The approach used here is identical in concept to that outlined in Ref. 24, with the exception that plasticity is treated by means of the initial strain concept [30, 31] in the present work, whereas the tangent modulus method [10] is used in Ref. 24.

The use of either approach requires the use of constitutive relations for an elastic-plastic engineering material. In general, the matrix equations governing the response of a structure to some arbitrary history of loading are used to solve for displacement and total strain increment. It is necessary, therefore, to develop incremental relations linking plastic strain or stress to total strains. These relations are presented here in matrix form for strain hardening and ideally plastic behavior. A more detailed discussion is presented in Appendix B and Refs. 16 and 25.

Plasticity Relations

Appropriate incremental plasticity relations to determine values of stress and plastic strain developed during the history of loading are now considered. Hill's yield criterion [32] for an orthotropic material, which reduces to the Von Mises yield condition for isotropic materials, is used to predict initial yield and to obtain the flow rules of plasticity. The capability of handling both strain hardening and ideally plastic behavior is included in the analysis. While orthotropic behavior is included in the case of ideal plasticity,

only isotropic behavior is now allowed when the material strain hardens. There are several theories to treat the plastic behavior of strain hardening orthotropic materials, but the acceptance of a suitable one awaits further experimental verification. A discussion of three theories for the treatment of strain hardening materials is presented in Appendix B. Two of these theories (isotropic hardening and kinematic hardening) have been developed for initially isotropic materials; the third theory (work-hardening modulii) can treat initially anisotropic materials.

Regardless of the theory used, linear incremental constitutive relations can be developed and incorporated into an equation relating generalized loads to generalized displacements of an arbitrary structure. These constitutive relations can be conveniently represented in matrix form.

Matrix Relations - Strain Hardening

We can, for small strain increments, decompose the total strain increment $\{\Delta e^T\}$ into elastic $\{\Delta e^e\}$ and plastic $\{\Delta \epsilon\}$ components, as

$$\left\{\Delta e^T\right\} = \left\{\Delta e^e\right\} + \left\{\Delta \epsilon\right\} \quad . \tag{1}$$

The elastic strain increments are related to the stress increments $\{\Delta \sigma\}$ by

$$\left\{\Delta e^e\right\} = [E]^{-1} \left\{\Delta \sigma\right\} \quad , \tag{2}$$

where $[E]^{-1}$ is an array whose elements are combinations of elastic material constants.

Regardless of the plasticity theory used, a linear incremental constitutive relation between plastic strains and stresses can be written. This relationship can be represented as

$$\left\{\Delta \epsilon\right\} = [C] \left\{\Delta \sigma\right\} \quad . \tag{3}$$

Therefore, substituting Eqs. (2) and (3) into (1) we can write

$$\left\{\Delta\sigma\right\} = [R]^{-1} \left\{\Delta e^{T}\right\} \quad , \tag{4}$$

where $[R] = [E]^{-1} + [C]$.

Matrix Relations - Perfect Plasticity

The treatment of multiaxial elastic ideally plastic behavior requires that the following conditions be satisfied:

- The stress increment vector must be tangent to the loading surface.
- The plastic strain increment vector must be normal to the loading surface, where the loading surface is the representation in stress space of the initial yield function or the subsequent yield function after some plastic deformation has occurred.

If $f(\sigma_{ij})$ represents the yield surface, the first condition can be expressed analytically as

$$\frac{\partial f}{\partial \sigma_{ij}} d\sigma_{ij} = 0 \quad , \tag{5}$$

and provides a linear relationship among the components of stress increment. Thus, one of the components may be expressed in terms of the others. In matrix form, this can be written as

$$\left\{\Delta\sigma\right\} = [\underline{E}] \left\{\underline{\Delta\sigma}\right\} \quad , \tag{6a}$$

where $\{\underline{\Delta\sigma}\}$ represents the independent stress components.

The normality condition provides a linear relation among the various components of the plastic strain increment. This condition is derived from the flow rule of Eq. (B-3), and provides a linear relationship in which each of the components of plastic-strain increment can be written in terms of any one component. This relationship may be represented in the following form

$$\left\{\Delta\epsilon\right\} = [\underset{\sim}{E}] \left\{\underset{\sim}{\Delta\epsilon}\right\} \quad , \tag{6b}$$

where $\{\underset{\sim}{\Delta\epsilon}\}$ is the independent plastic strain increment.

It is apparent from Eq. (5) that the independent increments of stress and plastic strain can be combined and written as the components of a vector, $\{\Delta\omega\}$ (see Ref. 33), so that Eqs. (6) can be written, respectively, as

$$\left\{\Delta\sigma\right\} = [\underline{E}]\left\{\Delta\omega\right\} \tag{7a}$$

$$\left\{\Delta\epsilon\right\} = [\underset{\sim}{E}]\left\{\Delta\omega\right\} \quad . \tag{7b}$$

Combining the above equations with Eqs. (1) and (2), we can form the following relation for the independent quantities

$$\left\{\Delta\omega\right\} = [E^*]^{-1}\left\{\Delta e^T\right\} \quad , \tag{8}$$

where $[E^*] = [E]^{-1}[\underline{E}] + [\underset{\sim}{E}]$.

Thus, it is apparent that, upon the selection of an appropriate plasticity theory to represent the nonlinear material behavior, the constitutive relations can be represented in terms of a linear matrix relation. There are several alternatives towards incorporating this relation into the final equation relating loads to deformations. The approaches we have found to be convenient (in terms of required machine time) and accurate when compared with previous solutions and/or experiments, are outlined in the following subsections.

Development of Load-Deflection Relations

As the initial step towards the development of the governing matrix equation, we choose a reference state, Γ_R, in the body, for which the states of stress, strain, and deformation are known. We now choose the next state to be incrementally adjacent to the initial state with all quantities referred to the reference state, i.e., $x_i = X_i + \Delta u_i$, where x_i are the new coordinates of an arbitrary point, X_i are the original coordinates in the local coordinate system, and Δu_i are the incremental deflections of the point in going from the reference state to the current state [29].

At the start of a load increment, let the stresses, surface tractions, and body forces acting on the structure be denoted by Σ_{ij}, T_i^0, and F_i^0. These quantities are referred to a unit of "undeformed" area, i.e., before the addition of the current load increment. They take into account the effects of any previous initial strains present in the body. The application of an incremental load to the body, expressed in terms of ΔT_i and ΔF_i, result in additional stresses $\Delta\sigma_{ij}$, displacements Δu_i, plastic (initial) strains $\Delta\epsilon_{ij}$, and the distortion of the body to its new configuration given by x_i.

The total stresses, surface tractions, and body forces, referred to the unit undeformed area and in the new coordinate directions x_i, are

$$\begin{aligned} \sigma_{ij} &= \Sigma_{ij} + \Delta\sigma_{ij} \\ F_i &= F_i^0 + \Delta F_i \\ T_i &= T_i^0 + \Delta T_i \quad . \end{aligned} \tag{9}$$

The development of the governing matrix equation may be approached by one of several alternative procedures. The authors choose here the principle of virtual work, which, for an incremental method, may be written as [29]:

$$\begin{aligned} \int_V (\Sigma_{ij} + \Delta\sigma_{ij})\delta(\Delta\tilde{\epsilon}_{ij})dV = &\int_S (T_i^0 + \Delta T_i)\delta(\Delta u_i)dS \\ &+ \int_V (F_i^0 + \Delta F_i)\delta(\Delta u_i)dV \quad . \end{aligned} \tag{10}$$

Here $\Delta\tilde{\epsilon}_{ij}$ is Green's strain tensor that refers to the original or "undeformed" volume of the element

$$\Delta\tilde{\epsilon}_{ij} = \Delta e_{ij} + \Delta\eta_{ij} \quad . \tag{11}$$

In this expression Δe_{ij} are the terms that represent a linear strain-displacement relationship, while $\Delta\eta_{ij}$ are those associated with the nonlinear terms in the strain-displacement relationship. The incremental constitutive equations are taken to be in the following form

$$\Delta\sigma_{ij} = E_{ijkl}(\Delta\epsilon_{kl} - \Delta\epsilon_{kl}) \quad , \tag{12}$$

where $\Delta\epsilon_{kl}$ are the initial or plastic strains developed in the current increment based upon the "undeformed" geometry. These are assumed to be small and independent of the total strains. The terms, E_{ijkl}, are the linearly elastic material properties.

Substituting the stress-strain relations, Eqs. (12) and (11) into Eq. (10) yields

$$\int_V \left[\Delta e_{ij} E_{ijkl} \delta(\Delta e_{kl}) + \Sigma_{ij} \delta(\Delta\eta_{ij})\right] dV =$$

$$\int_S \Delta T_i \delta(\Delta u_i) dS + \int_V \Delta F_i \delta(\Delta u_i) dV$$

$$+ \int_V \Delta\epsilon_{ij} E_{ijkl} \delta(\Delta e_{kl}) dV - \left(\int_V \Sigma_{ij} \delta(\Delta e_{ij}) dV \right. \tag{13}$$

$$\left. - \int_S T_i^0 \delta(\Delta u_i) dS - \int_V F_i^0 \delta(\Delta u_i) dV \right)$$

$$- \left(\int_V \Delta\eta_{ij} E_{ijkl} \delta(\Delta e_{kl}) dV + \int_V \Delta\sigma_{ij} \delta(\Delta\eta_{ij}) dV \right) \quad .$$

We now have an equation that is similar in form to that presented in Ref. 24, with the exception of those terms associated with initial strains. As in Ref. 24, it is assumed that, although total strains may be large, incremental strains from one neighboring state to the next are small, and thus the last two terms of Eq. (13) (which are cubic and quartic in displacement increments) may be neglected when compared to terms that are quadratic in displacement increments. These terms that are neglected lead to the matrices $[N_1]$ and $[N_2]$ of Ref. 34 and must be retained in a total Lagrangian formulation. An additional matrix due to the presence of initial strains is also generated from the last term of Eq. (13), but as it contributes terms of the same order of magnitude as the other termsneglected, it too need not be retained.

We then have

$$\int_V \left[\Sigma_{ij}\delta(\Delta\eta_{ij}) + \Delta e_{kl}E_{ijkl}\delta(\Delta e_{ij})\right]dV =$$

$$\int_S \Delta T_i\delta(\Delta u_i)dS + \int_V \Delta F_i\delta(\Delta u_i)dV$$

$$+ \int_V \Delta\epsilon_{ij}E_{ijkl}\delta(\Delta e_{kl})dV \qquad (14)$$

$$+ \left(\int_S T_i^0\delta(\Delta u_i)dS + \int_V F_i^0\delta(\Delta u_i)dV - \int_V \Sigma_{ij}\delta(\Delta e_{ij})dV\right) .$$

If the initial stress state, Σ_{ij}, T_i^0, and F_i^0, is in equilibrium at the start of the incremental step, then the last three terms of Eq. (14) vanish and we get the following incremental initial strain, large deflection relation:

$$\int_V \left[\Sigma_{ij} \delta(\Delta\eta_{ij}) + \Delta e_{kl} E_{ijkl} \delta(\Delta e_{ij}) \right] dV = \int_S \Delta T_i \delta(\Delta u_i) dS + \int_V \Delta F_i \delta(\Delta u_i) dV + \int_V \Delta \epsilon_{ij} E_{ijkl} \delta(\Delta e_{kl}) dV \quad . \tag{15}$$

The first term of this equation yields the initial stress stiffness matrix after the rotations (or other nonlinear terms) have been expressed in terms of nodal degrees of freedom. The second term leads to the conventional stiffness matrix. The first two terms on the right side lead to the consistent load vectors for surface tractions and body forces, respectively. The last term on the right side leads to the initial strain stiffness matrix which is multiplied by a vector of plastic (initial) strains to be used as an "effective" plastic load vector.

Because we use a predictor procedure, however, the initial stress state may not be in equilibrium before the current load step. The results for the next step may be adjusted or corrected for this imbalance by introducing a residual force given by [24].

$$R_i = \int_S T_i^0 \delta(\Delta u_i) dS + \int_V F_i^0 \delta(\Delta u_i) dV - \int_V \Sigma_{ij} \delta(\Delta e_{ij}) dV \quad . \tag{16}$$

Any discrepancies due to the neglect of the change in direction of the load are also accounted for in Eq. (16), because the total load is applied to the structure in its current configuration. The total stresses σ_{ij} obtained at the end of load increment N become the initial stresses for step $(N + 1)$. These must now be related to the new deformed area (which is the undeformed area for step $N + 1$). The transformation that accomplishes this is presented in Ref. 24 and written here as

$$\Sigma_{ij} = (1 - \Delta e_{kk})\sigma_{ij} + (\Delta e_{jk} + \Delta\omega_{jk})\sigma_{ik} + (\Delta e_{ik} + \Delta\omega_{ik})\sigma_{jk} \quad , \tag{17}$$

where the $\Delta\omega_{ik}$ are the incremental rotations. Similar transformations must be carried out for the surface tractions, body forces, and initial strains.

We will, at this point, mention that the last two terms of Eq. (13) need not be neglected and can be included without the formation of any additional stiffness matrices besides the required initial stress stiffness matrix and initial strain sitffness matrix. These terms may be retained in a predictor process in which values for $\Delta\sigma_{ij}$ and $\Delta\eta_{ij}$ obtained from the previous step (appropriately extrapolated) are used in the formulation of the appropriate stiffness matrices for the next incremental step. This should permit the use of larger step sizes in the current formulation. This latter concept was not used to obtain the results presented here.

Final Matrix Equations and Solution Procedures

The final form of the incremental equations used in the finite-element formulation is obtained from Eq. (14). The displacements $\{\Delta u\}$, linear total strains $\{\Delta e_{ij}\}$, and rotations $\{\Delta\omega_{ij}\}$ are related to the nodal generalized displacements $\{\Delta u_i\}$ via the following matrix relations:

$$\begin{aligned} \{\Delta u\} &= [N]\{\Delta u_i\} \\ \{\Delta e_{ij}\} &= [W]\{\Delta u_i\} \\ \{\Delta \omega_{ij}\} &= [\Omega]\{\Delta u_i\} \quad . \end{aligned} \tag{18}$$

We then have

$$\left([k^0] + [k^1]\right)\{\Delta u_i\} = \{\Delta P_i\} + \{\Delta Q_i\} + \{R_i\} \tag{19}$$

where

$$[k^0] = \int_V [W]^T[E][W]dV$$

$$[k^1] = \int_V [\Omega]^T [\Sigma_{ij}][\Omega] dV$$

$$\{\Delta P_i\} = \int_S [N]^T \{\Delta T^0\} dS$$

$$\{\Delta Q_i\} = \int_V [W]^T [E] \{\Delta \epsilon\} dV$$

$$\{R_i\} = \int_S [N]^T \{T^0\} dS - \int_V [W]^T \{\Sigma'_{ij}\} dV$$

and body force terms have been neglected, as they are not considered in this report. Here $[k^0]$ is the conventional stiffness matrix, $[k^1]$ is the "initial stress" or geometric stiffness matrix, $\{\Delta P_i\}$ is the vector of applied loads, $\{\Delta Q_i\}$ is the effective plastic load vector, and $\{R_i\}$ is the vector of residual forces due to the existence of any equilibrium imbalance that may exist because of the predictor nature of the numerical solution procedure.

Equation (19) is derived by using a moving coordinate system fixed to the body. It is valid for large elastic-plastic deformations, provided the appropriate nonlinear terms are retained in the strain-displacement relations and the total strain increment can be simply decomposed into elastic and plastic components. Additionally, proper transformations from the previous to current coordinate systems must be used so that the changes in orientation and volume of the elements must be accounted for [23, 24]. In this report, consideration is restricted to small strain, moderate rotation problems. Alternative solution techniques to solve Eq. (19) are presented and comprehensively discussed in Ref. 33. For completeness, a brief summary of these techniques is presented here.

Material Nonlinearity

If we initially neglect the effects of changing geometry and the equilibrium correction term, and write the elastic stiffness matrix as

$$[k^o] + [k^1] = [k_e] \quad , \tag{20}$$

and use the superscript "k" to denote the "k^{th}" load increment, then Eq. (19) may be written as

$$[k_e]^k \{\Delta u_i\}^k = \{\Delta P_i\}^k + \{\Delta Q_i\}^k \quad . \tag{21}$$

It should be noted that the initial stress stiffness matrix $[k^1]$ is not necessarily associated only with geometric nonlinearity; it may also be required in such other cases as the bending of plates subjected to membrane stress.

In Ref. 33, Eq. (21) is put into alternative forms suitable for numerical solution; distinctions among the basic forms employed are accomplished by using the term "method," and distinctions among the solution procedures are effected by using the term "procedure."

Displacement Method – Predictor Procedure. In the first "method" to be treated, the "effective plastic loading" is taken to be equal to that computed in the preceding load increment, and is thus taken as a known quantity in the equation.

The final form of Eq. (21) is

$$[k_e]^k \{\Delta u_i\}^k = \{\Delta P_i\}^k + \{\Delta Q_i\}^{k-1} \quad , \tag{22}$$

where k-1 is the preceding load step. The use of this type of predictor procedure obviates the necessity of introducing the plastic stress-strain relations explicitly into the governing matrix equation.

The incremental solution technique using Eq. (22) reduces to a sequence of linear problems in which the applied loading is constantly modified by the effective plastic load vector. Thus, with the increments of generalized displacement obtained from Eq. (22), the strain-displacement relations and Eqs. (4) and (3) are used to obtain the complete solution for increments of total strain, stress, and plastic strain, respectively, assuming elastic strain-hardening material behavior. The corresponding relations [replacing Eqs. (4) and (3)] for an elastic, ideally-plastic material are given in Eqs. (7) and (8). After summing all incremental quantities to determine current values of the pertinent variables, new values of

the increments of fictitious load $\{\Delta Q\}$ are determined for each element in the plastic range, and the procedure is repeated until the end of the loading process is reached. A further discussion of the use of the effective plastic load concept in conjunction with the basic governing matrix equation, Eq. (22), can be found in Refs. 13, 16, and 25.

Strain Method – Predictor Procedure. The predictor procedure solution technique can also be applied in an alternative formulation of the problem involving a direct solution for the increments of total strain. This alternative formulation is applicable to those problems in which an explicit solution for displacements, or their increments, is not required, and where the initial strain stiffness matrix $[k^*]$ does not change throughout the loading range. The governing matrix equation in this formulation is determined by substituting Eq. (20) into Eq. (19), and making use of the nodal strain-displacement relation of the following form:

$$\{\Delta e_i^T\} = [A]\{\Delta P_i\} + [J]\{\Delta \epsilon_i\} \quad , \tag{23}$$

where

$$[A] = [W_i][k_e]^{-1} \quad ,$$

and

$$[J] = [W_i][k_e]^{-1}[k^*] \quad ,$$

with

$$[k^*] = \int_V [W]^T [E] dV$$

where $[W_i]$ represents the matrix relating the linear component of the strain-displacement equations to the nodal degrees of freedom.

If we wish to use a predictor procedure to solve Eq. (23), we must write this relation in the following form:

$$\{\Delta e_i^T\}^i = [A]\{\Delta P_i\}^i + [J]\{\Delta \epsilon_i\}^{i-1} \quad . \tag{24}$$

Using values of $\{\Delta \epsilon_i\}$ estimated in this way, we can find the unknown total strain increments from Eq. (24), and then find the increments of stress and plastic strain from Eqs. (4) and (3) for strain-hardening behavior, or from Eqs. (7) and (8) for ideally plastic behavior. In Refs. 4, 6, 7, and 25 the predictor procedure is also formulated in terms of a governing matrix equation relating increments of stress to increments of load and plastic strain, similar to that of

Eq. (23). This procedure, referred to as a "constant stress" procedure, has been shown to lead to a characteristic numerical instability [4, 7, 25]. No such instability occurs when the predictor procedure is used in conjunction with Eq. (22) or Eq. (24).

The predictor procedure, involving the use of estimated values of plastic strain in Eq. (22) or Eq. (24), has computational advantages since the solution requires only matrix multiplication in each load step once the corresponding effective plastic load vector is formed, provided the matrix $[k_e]$ is constant and thus need be inverted only once. This differs from the direct substitution procedure, to be discussed below, in which matrix inversion or simultaneous equation solution is required at each load step. However, a disadvantage associated with the predictor procedure solution technique is a "drifting" of the numerical results from the true solution as plastic strain proceeds. One may choose to use small load increments for improved accuracy, thereby reducing the computational advantage of this procedure, or the results for any increment may be adjusted or corrected toward the true solution by introducing a residual force $\{R_i\}$ to ensure equilibrium of the total system. At any step, the residual force may be computed from the governing equations written in terms of total quantities. Thus, for the displacement method we have

$$\{R_i\}^k = - [k_e]^k \{u_i\}^k + \{P_i\}^k + \{Q_i\}^{k-1} \quad , \tag{25}$$

and for the strain method

$$\{R_i\}^k = - \{e_i^T\}^k + [A] \{P_i\}^k + [J] \{\epsilon_i\}^{k-1} \quad . \tag{26}$$

The value of the residual force is used in the next incremental load step, i.e.,

$$[k_e]^k \{\Delta u_i\}^k = \{\Delta P_i\}^k + \{\Delta Q_i\}^{k-1} + \{R_i\}^k \quad . \tag{27}$$

Displacement and Strain Method – Direct Substitution Procedure. The use of Eqs. (22) or (24) is usually associated with the initial strain method of finite-element plasticity analysis. An alternative approach, commonly referred to as the tangent modulus method, involves the direct substitution of the incremental constitutive plasticity relations into the governing matrix equation, Eq. (21). For an elastic, strain-hardening material, Eqs. (3) and (4) may be

combined to yield an incremental relation between plastic strains and total strains. For an elastic, ideally-plastic material the incremental relation between plastic strains and total strains is obtained from Eq. (8). Thus, regardless of material behavior, an equation of the following form may be written at those nodes or elements in the plastic range:

$$\{\Delta\epsilon_i\} = [S]\ \{\Delta e_i^T\} \quad , \tag{28}$$

where [S] reflects strain-hardening or ideally-plastic behavior and is a null matrix at those nodes or elements in the elastic range.

An incremental plastic strain-displacement relation is obtained by substituting the total strain-displacement relation into Eq. (28), so that we can write

$$\{\Delta\epsilon_i\} = [S][W_i]\ \{\Delta u_i\} \quad . \tag{29}$$

A linear incremental load-displacement relation of the form

$$\{\Delta P_i\} = [k_T]\ \{\Delta u_i\} \quad , \tag{30}$$

where $[k_T] = [k_e] - [k^*][S][W_i]$, results from substituting Eq. (29) into Eq. (19). Alternatively, after extensive manipulation (see [33]),

$$[k_T] = [k_p] + [k^1] \quad , \tag{31}$$

where

$$[k_p] = \iiint_V [W_i]'[M][W_i]dv \quad ,$$

$$[M] = [R]^{-1} \quad \text{for strain-hardening behavior}$$

$$= [E^*]^{-1} \quad \text{for perfectly plastic behavior.}$$

A direct formulation of the equations in the tangent modulus form has been presented in [22, 24].

The matrix $[k_p]$ in Eq. (31) may be regarded as a "plastic stiffness matrix" since it explicitly contains the effect of plasticity and enters into the analysis as an additional component of the total stiffness matrix. Further, since the elements of $[k_p]$ are functions of the instantaneous stress state, they must be evaluated at each incremental step. Similarly, substituting the incremental plastic strain-total strain relation of Eq. (29) into Eq. (23) results in the following equation:

$$\{\Delta e_i^T\} = [Y] \{\Delta P_i\} \quad , \tag{32}$$

where $[Y] = [A] + [J][S]$.

The direct substitution procedures, as is the case with the predictor procedures, may make use of an equilibrium correction to account for errors associated with the linear incrementation of the problem. For example, in the displacement method we can write

$$[k_T] \{\Delta u_i\} = \{\Delta P_i\} + \{R_i\} \quad , \tag{33}$$

where $\{R_i\} = [k_T] \{u_i\} - \{P_i\}$.

Summary of Methods for Plastic Analysis

A distinction among the various formulations is associated with the solution procedures used, which may be named the predictor and the direct substitution procedures. In the former, estimated values of plastic strain are used in the governing linear matrix equation. Thus, plastic effects are treated in the linear matrix equation by a modification that is external to the stiffness influence coefficient matrix. In the direct substitution procedure, plasticity is accounted for by means of an "internal" modification of the stiffness matrix.

The direct substitution or internal modification procedure, though it retains the errors associated with stepwise linearization, does eliminate the propagation of error associated with the predictor or external modification procedure. This improvement in accuracy for a given magnitude of the load increment is, however, accompanied by an increase in the number of numerical operations required to obtain a solution. These operations can be computationally expensive, since the elements of the influence coefficient matrices, $[k_T]$ of Eqs. (30) or (31) or $[Y]$ of Eq. (32), must be recomputed at each incremental step of loading. The effect of this

can be mitigated by increasing the magnitude of the load increment, but at the cost of greater inaccuracy. A choice between the two basic procedures thus involves a tradeoff between smaller load increment but less computation per increment, in the case of the predictor procedure, and larger load increment but more computation per increment, in the case of the direct substitution procedure. This choice will not be obvious in any given problem.

An approach that combines the two procedures might prove to be the most effective. For example, the predictor procedure may be sufficiently accurate in those regions of a structure where plastic flow has begun but has not yet been substantially developed. In those regions where plastic effects are predominant, the direct substitution procedure could be used.

Implementation of Combined Plasticity and Geometric Nonlinearity

A primary consideration in choosing a method for the analysis of geometric nonlinearity from among the several currently available is the ease with which it can be combined with methods of plastic analysis. For this reason, our approach is based upon a linearized incremental formulation, i.e., one in which the nonlinear analysis is reduced to the solution of a sequence of linear incremental equations. In Refs. 6, 10, and 35, this approach was used to solve problems involving geometric nonlinearity. Since the plasticity relations are themselves incremental, and the methods discussed in the preceding section depend upon a revision of the governing matrix equation in each loading step, the modifications necessary to incorporate "large deflection" terms are minimal.

The method of solution of the small strain, geometrically nonlinear problem discussed here involves the solution of a sequence of "beam-column" type problems, using Eq. (19), in which values of the membrane stress resultants and the geometry of the deformed structure are updated in each increment of loading. For sufficiently small loading increments, the increments of rotation in any finite-element will be small as measured with respect to a local coordinate system that translates and rotates with the element in successive loading steps (but is assumed to remain fixed within any one loading step). Consequently, squares and products of the increments of rotation may be neglected in computing increments of membrane strain [29].

Because of the presence of geometric nonlinearity, the entire element stiffness matrix $[k_e]$ in Eq. (20) must be reformed in

each loading step, with current stress levels and geometry being used. In the discussion of the development of the elastic stiffness matrix, it was mentioned that the only component matrices required are the conventional stiffness matrices (those not dependent upon the presence of stress) and the initial stress stiffness matrix. The latter matrix accounts for the change in bending stiffness due to the presence of membrane loads. In the development of the initial stress stiffness matrix, the membrane stresses taken into account are those present at the beginning of the loading step, any further changes in these stresses occurring during the loading step being neglected in that development. This constitutes the linearization of the procedure during an increment of loading.

Some investigators (see [21, 22]) have indicated the need for an additional matrix, termed "the initial displacement" matrix, for the treatment of geometric nonlinearity. Because the current analysis uses a "moving" local coordinate system, this additional stiffness matrix is not required (see [24] for a more complete discussion of this point).

For the large deflection elastic-plastic analysis, the load is applied in small increments from the initial unloaded state. At the end of each increment, new increments of deflection, stress, strain, and plastic strain are calculated. Total quantities, such as the initial stresses, are calculated by using appropriate transformations, and the geometry of the structure is updated. Again the plastic strain increments used are those calculated in the previous step. The total stiffness matrix is reformed at every increment, together with the incremental load vector, plastic load vector, and residual load vector. The element contributions are then assembled and the system of linear incremental equations is again solved and the process repeated until the maximum specified load is reached or structural failure occurs. If the response to cyclic loads is desired, the load increment is reversed at the maximum load, and the incremental process is repeated until the new maximum (minimum) load is reached. This procedure is then repeated for as many load cycles as desired.

For the large deflection problem, the most time-consuming feature is the reassembly of the stiffness matrix and solution of the linear incremental equations. It becomes convenient, therefore, to consider the possibility of treating the large deflection terms as well as the plasticity effects as effective loads. This may be done by rewriting Eq. (19) as

$$[k^o]\ \{\Delta u_i\}^k = -\ [k^1]\ \{\Delta u_i\}^{k-1} + \{\Delta P_i\}^k + \{\Delta Q_i\}^{k-1} + \{R_i\} \quad , \quad (34)$$

where the product of the initial stress stiffness matrix and the vector of displacement increments of the previous step is now treated as an "effective geometric load." The stiffness matrix $[k^o]$ may be re-formed every M steps $(M \geq 1)$, with the possibility of saving considerable time. The use of this solution procedure may lead to numerical instabilities when the nonlinearities become large [20], although none were observed in the limited number of problems solved by the authors. The use of the geometric terms as effective loads is not new, and has been used in many Lagrangian formulations with great success [20].

If large deflection terms are not important, considerable simplification results. For the problem of material nonlinearity alone if we consider the displacement method-predictor procedure, the sequence of computations followed is to calculate the value of the load at which plastic deformation first occurs. From this point, the load is incremented to a maximum value, with new increments of displacement, plastic strain, and stress calculated at each step and total values obtained by summing incremental values. The plastic strain increments used in the plastic load vector are those calculated from the previous step. Because this is a small deflection analysis, the stiffness matrix need never be re-formed. The residual force vector was not used in any of the small deflection problems presented although it could have been so used. At the maximum load, a new critical load for which yielding begins in the reverse direction is calculated, based upon elastic unloading to this point. Procedures for determining this load are presented in Refs. 16 and 25. This critical load may occur before all the load is removed from the structure because of the presence of residual stress and the existence of the Bauschinger effect. At this new critical value, the load is incremented to the new specified maximum (minimum) value, and this procedure is repeated for as many half cycles as desired.

3. APPLICATIONS OF NONLINEAR METHODS

The methods and procedures of the previous section have been applied to a variety of problems during the course of several years of investigation by the authors. Comparison between the predictor

procedure and the direct substitution procedure involving plasticity alone is made and evaluated for the strain method as applied to membrane stress problems [25], and for the displacement method for problems involving bending stresses [16]. A survey and thorough evaluation of procedures for combined geometric and material nonlinearity is presented in Ref. 36.

The development of practical methods of treating the nonlinear response of structures within the framework of finite-element techniques has required that they be made available on a convenient basis to the structural designer and analyst. This requirement has led to the development of a comprehensive program that provides a practical tool for the designer and analyst. A brief description of this program is presented in the next section and, in more detail, in a companion report. To accomplish the development of such a program requires that the capabilities and capacity be sufficiently broad in scope to permit the analysis of realistic structures and that close attention be paid to efficiency, so that computations can be made economically.

On the basis of the authors' experience we have found that for plasticity problems alone, the displacement method-predictor procedure is the most attractive in terms of generality and ease of application. Furthermore, it is highly competitive in terms of efficiency and accuracy as compared with various other algorithms discussed in this report. Hence, in the program developed in this study and for the results to be subsequently presented, this technique has been used exclusively. For problems involving combined material and geometric nonlinearity the predictor procedure is used for both geometric and material nonlinearity until the geometric nonlinearities become "large." From then on the geometric nonlinearities are included via the tangent modulus approach while the material nonlinearities are still handled via the effective load technique. The equilibrium correction term is used in each increment. This procedure is effective [23] although not necessarily the most efficient [18].

Elastic-Plastic Analysis of Representative Two and Three Dimensional Structures

Our basic philosophy of program organization for material nonlinearity alone, as presented in the next section, is to separate classes of analysis into individual groups, with each group defined by the physical problem to be solved. For example, groups can be defined for membrane structures, combined bending and membrane

structures, thick or thin bodies of revolution, general three dimensional solids, or laminated composites. On the basis of this concept, each group is in itself an independent finite-element computer program, with an associated element library that can be individually loaded and used to solve the problem class of interest. In this manner any simplification or specialization germane to the individual analysis can be incorporated.

Each group can contain subprograms common to all other program groups as well as subprograms distinct to its group alone. Linkage to any individual program group is made through an executive program that performs the function of loading the individual analysis programs. Data set management and core allocation are handled by each of the group programs, and linkage to any group can be made only through the executive routine.

Representative problems from each of the individual analysis programs are presented to demonstrate the scope, accuracy, and general adaptability of the analysis techniques.

Membrane Stress Analysis

The element library for this program contains the following elements: 1) constant strain triangle, 2) linear strain triangle, 3) hybrid triangles linking the constant strain and linear strain triangles, 4) warped quadrilateral shear panel [37], 5) stringer elements, and 6) a beam element. This program is designed to be used for the analysis of arbitrarily shaped structures (stiffened or unstiffened) in which the loads are those that generate primarily membrane stresses.

Uniformly Loaded Sheet with a Central Crack. An illustration of the application of the membrane stress program is that of a uniformly loaded sheet with a central crack. The idealization of a quadrant of the sheet, as shown in Fig. 3, involves 455 elements, 219 vertex nodes, and 250 mid-side nodes, resulting in 902 degrees-of-freedom when symmetry boundary conditions are applied. A mixture of linear strain elements (used in the region surrounding the crack tip), transition elements, and constant strain elements are used to make up the network shown.

Results from the analysis in the form of the distribution along the horizontal axis of symmetry of the stress component in the direction of loading is shown in Fig. 4a. Results from the finite-element analysis for the elastic behavior compare favorably

with a continuum solution [38]. Results for the plastic behavior are shown for two levels of loading corresponding to stress levels for which the gross section stress (σ_o) is 37.6 percent and 75.3 percent of the yield stress of the material. The effect of plasticity in decreasing the stress gradient in the vicinity of the crack tip is clearly evident from the figure. Also shown are the residual stress distributions that result from complete unloading from the respective maximum loads of 37.6 percent and 75.3 percent of yield stress. The residual stresses in the vicinity of the crack tip are significant and can be expected to represent an important factor in determining the fatigue life of such structures.

The displacement profile of one-half of the crack is shown in Fig. 4b. Once again, a comparison of the finite-element results, assuming elastic behavior compares favorably with the continuum solution. The results from the finite-element analysis for loading in the plastic range indicate that the displacement profile is virtually unchanged from the elastic profile. This is attributed to the fact that plasticity is localized to a rather small region around the crack tip. That is, for monotonically increasing loads, the localized region of plasticity does not appreciably affect the deflection profile to the extent that it influences the stress distribution in the vicinity of the crack tip. However, because of the development of a plastic zone there is a residual displacement profile along the entire crack length as shown in Fig. 4b. This profile has a "dog-bone" type pattern, i.e., the maximum opening occurs near the crack tip and becomes uniform toward the center of the crack.

The propagation of the plastic zone in the uniformly loaded sheet with a central crack is shown in Fig. 5a for monotonically increasing loading and in Fig. 5b for unloading from the maximum load. The zones are determined by drawing a curve through the centroid of those elements that are plastic at the corresponding load. As shown in Fig. 5b, prior to the removal of all the load ($\sigma_o/\sigma_{yield} = 0.345$) a compressive plastic zone develops in the region of the crack tip. The plastic zone that remains upon the complete removal of the loads is also shown in this figure.

Additional problems, typical of the type that can be treated by this module of the program, have been presented in previous publications by the authors (i.e., 11, 16, and 25). Although not illustrated here, the current capability includes the treatment of general out-of-plane stiffened and unstiffened structures.

Bending and Membrane Stress Analysis

This module of the comprehensive program is to be used for the general analysis of structures in which bending and membrane stresses are generated. Its finite element library consists of flat triangular bending [39] and membrane elements, and a general beam element to represent stiffeners.

A wide range of applications of prototypes of this program appear in several of the author's previous publications (i.e., 13, 16, and 40). The problems considered to date include initially flat rectangular, circular, and annular plates subjected to loads causing bending alone and combined bending and membrane stress states. The current capability includes the treatment of general out-of-plane stiffened and unstiffened structures.

Axisymmetric Analysis of Bodies of Revolution

The element library for this program consists of a revolved triangle [41] for general thick walled bodies of revolution, an isoparametric shell element [23, 42], and a ring element [43].

Full Sphere. The problem of a full sphere subjected to a "$\cos^2\theta$" loading is used to illustrate the accuracy of the elastic solution obtained by using the revolved triangles or the shell element. An idealization of a quadrant of the sphere, as shown in Fig. 6, consists of 153 triangular elements, 95 nodes, resulting in 183 degrees-of-freedom when symmetry boundary conditions are applied. An idealization using the shell element consists of 15 elements, 16 nodes and results in 60 degrees-of-freedom. The meridional segments shown in Fig. 6 represent the meridional lengths of the shell elements.

A comparison of results for the radial displacement distribution versus the meridional direction is shown in Fig. 7. The results from the two separate finite-element solutions are compared with an elasticity solution [44]. The correlation of results between the three solutions is quite good, with a maximum divergence occurring at, and in the neighborhood of, the apex. A similar correlation exists when a comparison is made for the circumferential stress versus the meridional direction, as shown in Fig. 8.

Thick Tube Under Uniform Internal Pressure. The elastic-ideally plastic behavior of an internally loaded circular tube was considered to be a representative test of the accuracy of the non-linear analysis using the triangular elements. Results from the finite-element analysis are compared to the results from a solution obtained in Ref. 45, and shown in Figs. 9-11. For this particular case, the ratio of the outer to inner radius equals 2. The external radial displacement and radius of the elastic-plastic boundary versus the internal pressure p are plotted in Fig. 9. The comparison of results between the two solutions is good for the entire range of loading considered. The resulting radial and circumferential stress distributions for various positions of the elastic-plastic boundary are shown in Figs. 10 and 11. The correlation with the results of Ref. 45 is again seen to be quite good, despite a discontinuous distribution of circumferential stress at the elastic-plastic boundary as shown in Fig. 11. It should be noted that the stresses plotted represent the "average" stress at a node; that is the average value of the stresses in all those elements common to a node.

Sheet with an Oversized Fastener. Another illustration of the use of this module of the program considers the residual stress field surrounding a hole in a sheet into which an oversized fastener has been driven. As shown in Fig 12, the "head" of the fastener, which must be driven through the hole, is tapered to a maximum diameter D_1, with the shank stepped down to a diameter, D_2. Results for the residual circumferential and radial stress distribution along a radial line on the outer surfaces of the sheet are shown in the figure for three cases of prescribed interference, D_1-2a. These stresses apply with the fastener shank in the hole. Linear strain hardening material behavior is assumed for the sheet material in the plastic range. It is significant to note the small increase in favorable compressive residual stress at the edge of the hole as compared to the substantial increase in tensile stresses at some distance from the edge. For the case involving the largest interference, the level of this tensile stress was found to be unacceptable from both fatigue and stress corrosion considerations.

Torispherical Shell. The accuracy of the shell element, used in this module of the PLANS program, is demonstrated in Ref. 42 in the form of an extensive number of applications and comparisons with existing solutions. An application of the use of this element for a plastic analysis is presented in Fig. 13 where the load versus apex deflection for a torispherical shell under uniform internal pressure is presented for various load increments, and a comparison

is made with the results obtained in Ref. 46 where elastic-perfectly plastic behavior was assumed. The results from Ref. 46 were obtained by using load increments of 1.03×10^4 N/m^2, and are virtually identical with those of the present analysis, where a load increment of 2.76×10^3 N/m^2 was used. As seen in the figure, halving this load increment produces a significant change in the results only at a load above the theoretical collapse load predicted by limit analysis [47]. The use of the initial strain method, wherein the plastic behavior is accounted for by an "effective plastic load" vector, requires smaller load increments than a tangent modulus method [16]. However, increment size alone is not the sole criterion governing the efficiency of one method versus another. The increase in computing time associated with the use of smaller increments in the initial strain method is offset by the fact that the stiffness matrix need never be reformed after the first step. Additional evidence that indicates that the initial strain procedure is competitive from the standpoint of computer time requirements is presented in Ref. 48.

Figure 14 shows the load versus apex deflection curve for the same shell for one full cycle of loading. The load is varied between amplitudes of ±80 psi ($\pm 5.52 \times 10^5$ N/m^2) and back to zero. It is interesting to note that the deflections, moments, etc., obtained by unloading from the maximum load and subsequent loading to -80 psi (-5.52×10^5 N/m^2) are virtually the same as those that would be obtained simply by loading monotonically to -80 psi (-5.52×10^5 N/m^2) from the initial state. It is conjectured that this occurs as a combined result of assuming elastic-perfectly plastic behavior, neglecting the effects of geometric nonlinearity, and the fact that the same material properties were assumed to exist in reversed loading. Moreover, the values of residual stress, strain, and deflection obtained at the end of one full cycle are virtually the negatives of those values obtained by unloading to zero load from the maximum load.

Simply Supported Circular Plate. To investigate the generality of these results, a different structure, a simply supported circular plate subjected to a uniform pressure applied centrally over a circular area with radius 0.0718 of the plate radius, was cycled through various load ranges. Again, elastic-perfectly plastic behavior was considered. The material properties assumed were $E = 10.5 \times 10^6$ psi (7.24×10^{10} N/m^2), $\nu = 0.33$, $\sigma_o = 4000$ psi (2.76×10^7 N/m^2). The radius of the plate was 2.61 in. (6.63×10^{-2} m), and the thickness was 0.2615 in. (6.64×10^{-3} m). The load ranges considered were ±2000 psi (1.38×10^7 N/m^2), ±3000 psi (2.07×10^7 N/m^2), ±3500 psi (2.41×10^7 N/m^2), and ±4000 psi (2.76×10^7 N/m^2). The results are presented in Fig. 15. In all cases

except the last, the displacements, moments, etc., at the maximum negative load obtained by unloading from the maximum positive load are the same as would be obtained merely by loading monotonically to the maximum negative load from the virgin state. For the last case [±4000 psi (±2.76 x 10^7 N/m^2) load range] the load increments used during reversed loading are too large from the standpoint of accuracy, and consequently, the plastic strains computed are smaller than those that actually occur [4000 psi (2.76 x 10^7 N/m^2) is near the theoretical collapse load of 4280 psi (2.95 x 10^7 N/m^2) for this structure]. These cases tend to corroborate the hypothesis that for elastic-ideally plastic material one need only consider one-half cycle of loading to obtain information concerning full cycle behavior when the effects of geometric nonlinearity are ignored.

Clamped Circular Plate. A strain hardening problem is considered next. A uniformly loaded clamped circular plate was cycled between ±560 psi (±3.86 x 10^6 N/m^2). The same problem was considered for monotonic loading up to 560 psi (3.86 x 10^6 N/m^2) in Ref. 49, and the results for this range are compared. Excellent agreement up to the maximum load was achieved (see Fig. 16). The discrepancies at this load may be attributed to the use of different plasticity theories (kinematic versus isotropic hardening) and the difficulty in reproducing the stress-strain data from Ref. 49. Furthermore, the load-deflection curve does exhibit all of the characteristics of strain hardening behavior. The absolute magnitude of the center deflection at the maximum negative load is larger than that developed at the maximum positive load, and the full cycle residual deflections are triple those of the half cycle.

Stiffened Shallow Spherical Shell. Results for a uniformly loaded shallow spherical shell with a stiffened circular hole at the apex are presented next. This problem demonstrates the beneficial effects of a stiffening ring on the elastic-plastic behavior of a shell, although for this particular problem it is seen that large deflection terms are also important and should be included. The pertinent geometric and material parameters defining the problem are shown in Figs. 17 and 18. The ratio of the hole radius to shell base plane radius (b/a) is 0.1, and elastic-perfectly plastic material behavior was assumed for the shell.

Figure 17a shows the normal displacement versus the applied pressure at the ring hole interface and at an interior point approximately halfway between the hole and the outer edge boundary

for an unstiffened hole and one with a stiff ring. As seen from Fig. 17a there is a substantial difference between the displacement at the hole boundary for the case of an unstiffened and for that of a stiffened hole. In fact, at the collapse load the displacement for the stiffened hole changes sign and is in the direction opposite to that of the applied uniform pressure. In effect, the region in the vicinity of the hole moves as a rigid body as the displacements in the interior become unbounded. This is due to the restraining effect of the ring in preventing the hole circumference from contracting. Since the effect of the hole is localized, the displacements in the interior (Fig. 17b) for the stiffened and unstiffened case are indistinguishable. As indicated, sudden collapse of the shell is evidenced at $qa^4/Et^4 \simeq 15000$. This occurs when the entire cross section in a substantial portion of the interior is plastic for both cases considered. However, since the ring carries a portion of the load, there is a wholly elastic section between the hole boundary and completely plastic interior cross section at collapse. This contrasts with the unstiffened case, for which the wholly plastic cross sections begin at the hole boundary and propagate towards the interior with increasing load.

Figures 18a and b show the distribution of circumferential stress resultant at the yield load and at an intermediate load in the plastic range. As expected (Fig. 18a), the peak value for the unstiffened hole is at the hole boundary. As the region of plasticity expands, this peak value moves toward the interior and is located approximately at the elastic-plastic boundary. Figure 18b shows results at the same two loads for the stiffened hole. It can be seen that the stiff ring substantially reduces the stress resultant at the hole boundary.

Analysis of Three Dimensional Bodies

The isoparametric hexahedra family of elements presented in Ref. 50 represents the element library for this program.

End-Loaded Rectangular Prism. Results for the longitudinal and transverse stress distributions in a rectangular prism subjected to prescribed end forces, shown in Figs. 19a and b, are used to demonstrate the accuracy of this element for elastic behavior. The idealization used to represent a quadrant of the prism consists of 128 members and 225 nodes and resulted in 560 degrees-of-freedom when the simple 8-node linear displacement field element was used throughout the idealization. The results are compared with a three dimensional elasticity solution

presented in Ref. 51. As seen from these figures the correlation is quite good although it should be noted that the elasticity solution corresponds to points along the x-axis with $y = 0$ and $z = 0$, whereas the results from the finite-element analysis are plotted at points corresponding to the centroid of those elements adjacent to the axes of symmetry.

Uniformly Loaded Rectangular Laminate. The elastic stress distribution in a laminated fibrous composite is studied by means of the three dimensional finite-element module of the PLANS program. Of interest are the normal and shear stress components in the interlaminar region, which cannot be predicted by using classical plate theory. The influence of interlaminar deformation on the delamination and general failure of laminates is currently under investigation.

The stress distribution in each layer of a boron-aluminum laminate with a symmetric $[90/90/0/0]_s$ layup is shown in Fig. 20. The interlaminar normal (σ_z) and shear (τ_{yz}) stresses are seen to be significant only in the vicinity of the free edges. This effect was noted in several previous studies, and it has been shown that the interlaminar stresses decay beyond a distance that is of the order of the thickness of the laminate.

For the layup and loading considered, the interlaminar normal stress is a favorable compressive stress tending to retard delamination. A reversal in applied stress or layup (e.g., $[0/0/90/90]_s$) would result in an unfavorable tensile normal stress.

Infinite Plate Containing a Circular Hole. The classical problem of an infinite plate containing a circular hole is chosen to demonstrate the use of the three dimensional element for a problem involving material nonlinearity. The thickness-to-hole diameter ratio was taken as 0.75 so that a plane stress analysis would not be valid [52]. The finite-element model consisted of four layers of eight-node hexahedra elements to represent the half-thickness, with each layer consisting of sixty elements.

Results of this analysis are shown in Fig. 21 for the variation of circumferential stress σ_θ, along the axis of symmetry perpendicular to the load at the maximum elastic load. The elastic distribution along the middle and upper surfaces compares quite favorably with published results [52]. The values of stress, obtained from the finite-element analysis, at the edge of the hole are obtained by extrapolation, since centroidal stresses are used exclusively in this analysis.

The dashed curve in Fig. 21 represents, the distribution of σ_θ at almost twice the maximum elastic load, for elastic-perfectly plastic behavior, and reveals a substantial reduction in peaking of the stress field in the vicinity of the hole. Although the plate yields initially at the middle surface, the elastic-plastic boundary quickly propagates through the thickness and thereafter follows a pattern that is similar to the behavior associated with a plane stress state.

Plane Stress Analysis of Laminated Composites

A finite-element to model the interlaminar behavior of multi-layered fibrous composites under plane stress loadings has previously been presented and discussed [53,54]. The idealized model separates the membrane and interlaminar properties of a laminated composite by using alternating orthotropic fiber-bearing segments, which are assumed to remain elastic throughout the entire load history, and isotropic, elastic-plastic shear segments. The constant stress triangle is used to represent the orthotropic segments that carry in-plane stresses only; the shear segments carry only interlaminar shear stresses, and are in a state of pure shear.

Results for several sample problems are presented and discussed in detail in Ref. 54. One such problem involves a flat panel with a circular cutout, loaded along two opposite edges. The dimensions of the panel were chosen such that the stress field around the cutout is not influenced by the external boundaries. A typical idealization is shown in Fig. 22, which contains 223 members and 138 nodes. A fine network of elements are used around the edge of the hole since the interlaminar region in which the stress fields diverge from the classical plate solution comprises a narrow region along the stress free edge of the laminate. The interlaminar shear stress distribution around the edge of the hole is shown in Fig. 23 at the maximum elastic load $(\sigma_o/\tau_{yield} = 2.95)$, maximum and minimum loads in the plastic range $(\sigma_o/\tau_{yield} = \pm 7.37)$, and at a load corresponding to complete unloading from the minimum load. As indicated in the figure, high residual shear stresses occur for $\theta < 45°$, and relatively low residual shear stresses occur for $\theta > 45°$.

Geometric Nonlinearity

Circular Plates

The capability of treating geometric nonlinearity and combined geometric and material nonlinearity has been developed under the

present contract for axisymmetric shell structures. The analysis uses the shell element reported in Ref. 42, and a presentation of the application of the element for combined nonlinear analysis is presented in Ref. 23. The accuracy of the procedure for geometric nonlinearity in the case of purely elastic behavior is demonstrated in Figs. 24 and 25 where a comparison of results obtained from the present analysis is made with those obtained in Ref. 55 for a clamped, uniformly loaded, elastic circular plate. Poisson's ratio was chosen to be 0.3. Figure 24 is a plot of central deflection versus load, and Fig. 25 is a plot of bending and membrane stresses at the center and edge versus deflection. For the increment size chosen, excellent agreement was obtained between the solution presented in Ref. 55 and our numerical results.

In the present investigation, results for this problem were obtained by using both the "tangent modulus" method and the "effective" load method for the same increment size. For the latter case, the stiffness matrix was re-formed every five increments. No equilibrium correction term was included for either method for this problem. The deflections and bending stresses in both cases were identical, while slightly smaller membrane stresses were predicted by the effective load method. Of most significance was the reduction in CPU time from 386.28 seconds for the tangent modulus method to 202.08 seconds for the effective load method, an approximately 47 percent time savings at no appreciable loss in accuracy. Similar time savings of from 40 to 50 percent were noted for other problems.

Spherical Cap

Figure 26 illustrates the need for the equilibrium correction term in problems involving a high degree of nonlinearity. An exact load-deflection curve obtained from Ref. 20, based upon results presented in Ref. 56, is shown for an elastic, clamped spherical cap loaded by a central concentrated load. Also shown are results obtained from the current analysis using a straight incremental approach with 1/8 lb (0.56 N) increments and an incremental-plus-equilibrium correction solution using 1 lb (4.45 N) increments. The results obtained in the current analysis are virtually identical (for both incremental and incremental-with-equilibrium correction solutions) to the numerical results given in Ref. 20.

Combined Material and Geometric Nonlinearity

Circular Plate

Figure 27a shows a load versus central deflection plot for a centrally loaded, simply-supported plate with a diameter-to-thickness ratio of 40.6. The numerical results are compared with test data obtained from the experimental program described in Ref. 23. Shown are the linear elastic, nonlinear elastic, elastic-plastic and combined nonlinear predictions using the tangent modulus approach with the incremental and incremental-with-equilibrium correction solution procedures. Although for these combined problems the equilibrium correction affords a considerable improvement over the incremental approach, without equilibrium correction, a more extensive iteration scheme is probably needed to close the theoretical-experimental gap. In Figs. 27b and 27c the radial distribution of circumferential strain at the lower and upper surfaces, respectively, for this plate is illustrated for several load levels and compared with theory. Despite the only fair-to-good correlation of the displacement data at high loads, excellent correlation with experiment for the strains is noted, except, as might be anticipated, directly under the loading rod for higher loads. The discrepancy at this point might be the result of local shear and penetration effects.

Spherical Cap

Wilkinson and Fulton [57] have presented results for the elasto-plastic buckling of uniformly loaded shallow spherical caps with both simple and clamped support at the edges. Several comparison test cases were chosen to verify their results and determine the present program's ability to predict buckling loads of such structures. The cases run were for $\alpha = 0.1$, $\beta = 0.002$, and $\lambda = 4$ and 5.5 for the clamped cap, and $\lambda = 4$ for the simply-supported cap. Here α is the ratio of tangent modulus to Young's modulus, β is the ratio of yield stress to Young's modulus, and λ is the geometric shell parameter $2[3(1 - \nu^2)]^{\frac{1}{4}}(H/h)^{\frac{1}{2}}$, with ν being Poisson's ratio, H the maximum shell rise, and h the shell thickness. As can be seen from Fig. 28, excellent agreement for these cases was obtained. The buckling pressures are 3 percent higher than those predicted by the analysis of Ref. 57. The results from the previous analysis are probably more accurate than those obtained here, since the present analysis makes no attempt to refine the load increment size in the vicinity of the critical load. The tangent modulus method was used to account for the effects of geometric nonlinearity.

Cyclic Loading of Simply-Supported Circular Plate

Results in the form of load versus central deflection of a simply-supported, centrally loaded mild steel circular plate are shown in Fig. 29. These results involve a history of loading to a maximum load in the plastic range and then the removal of the load. A comparison with the experimental data presented in Ref. 58 indicates that the finite-element results predict larger displacements than those obtained experimentally. This may be partially explained by the fact that no information (except the yield stress) was available in Ref. 58 concerning the strain hardening properties of the material used in the experiment. The finite-element analysis was performed by assuming elastic-ideally plastic behavior, which is a good representation of the stress-strain behavior for mild steel for strains less than 2 percent. The larger displacement prediction from analysis is consistent with this assumption. When the strains in the plate become larger than 2 percent, mild steel experiences strain hardening. Indeed at loads above 15,000 lb (66.73×10^3 N) the theoretically predicted strains exceed 2 percent in a considerable region of the plate, and divergence of the results occurs. As a consequence of the overprediction of the maximum displacement, the residual displacement predicted by the analysis is considerably greater than that experimentally observed. However, the general shape of the load-deflection curve upon unloading parallels the experimental curve.

Ring-Stiffened Cylinder

The circular cylinder is a structural component that is currently under consideration as an energy-absorbing device to improve the crashworthiness of small land and air vehicles. A reasonably accurate prediction of the load-deformation behavior of this device is required to evaluate its efficiency as compared to other devices of a similar kind. Toward this goal the prototype program was used to describe the elastic-plastic, large deflection behavior of a simply-supported ring-stiffened circular cylinder shown in Fig. 30.

Results for the axial displacement versus axial stress resultant (Fig. 30a) and the radial displacement (Fig. 30b) are shown for elastic and elastic-ideally-plastic, large deflection behavior. The rings ($EA = 10^6$ lbs $= 4.45 \times 10^6$ N) remain elastic throughout the entire load history, but the influence of material nonlinearity in the cylinder significantly influences its behavior and decreases its buckling load. From the results for the radial displacements, it is apparent that the rings have a negligible influence on the behavior

of this cylinder. To verify this conclusion, the problem was re-analyzed (elastic and elastic-plastic) for the unstiffened cylinder, and it was found that the removal of the rings had virtually no effect on the buckling load or mode shape.

Unstiffened Circular Cylinders

Results for the end-load versus end-deflection for a clamped circular cylinder fabricated from 6061-0 aluminum alloy are presented in Fig. 31a. They indicate a buckling load of about 1600 lb/in. (280×10^3 N/m) or 39,800 pounds (177×10^3 N) total load for this structure. This compares quite favorably with experimentally determined buckling loads of 35,650 pounds (159×10^3 N) (two specimens) and 41,250 pounds (183×10^3 N) (one specimen) obtained at NASA/Langley. In the course of the analysis, it was found that the buckling load is extremely dependent on an accurate determination of the material properties. A Ramberg-Osgood three parameter representation of the stress-strain curve for 6061-0 aluminum alloy was used for the analysis, i.e.,

$$\epsilon = \frac{\sigma}{E} + \frac{3\sigma}{7E}\left(\frac{\sigma}{\sigma_{0.7}}\right)^{n-1} .$$

We chose E as 10^7 psi (6.9×10^{10} N/m^2), $\sigma_{0.7}$ = 5050 psi (3.5×10^7 N/m^2), and n = 4.8. A proportional limit (σ_{pl}) of 4300 psi (2.97×10^7 N/m^2) was used. These properties were derived from data obtained from the Materials Selector Handbook and verified by tests performed in the Grumman Research Department Applied Mechanics Laboratory. Pertinent geometric data for the clamped circular cylinder are given in Figs. 31a and b. Calculations were then performed, using the same configuration and material properties, but with simple supports at the ends to determine the effect of edge restraint on the buckling load of this cylinder. As anticipated, the reduction in buckling load resulting from the change in edge restraint was extremely small and virtually negligible (see Fig. 31a).

Figure 31b shows the radial deflection profile versus axial length for the clamped and simply-supported cylinders at end-loads of 1050 lb/in. (184×10^3 N/m) and 1575 lb/in. (276×10^3 N/m), which is immediately before buckling. The initial buckling profiles are quite evident, with the wavelength of the simply-supported cylinder being smaller than that of the clamped cylinder, and the maximum displacement amplitude of the simply-supported shell approximately $1\frac{1}{2}$ times that of the clamped cylinder at this load, indicative of the slightly lower critical load for the simply-supported cylinder.

Clamped Truncated Circular Cone

A clamped truncated circular cone was then analyzed in an initial effort to determine what qualitative and quantitative beneficial effects tapering the sides might introduce into the energy absorption capacity of a vehicle. The first cone chosen had the dimensions of one specimen of the test program at Langley. It, too, was fabricated from 6061-0 aluminum alloy and its dimensions are presented in Figs. 32a and b. The cone angle, α, is 17.09 degrees. The critical load for this structure was calculated to be 42,575 pounds (189×10^3 N), corresponding to an axial stress resultant applied at the larger end of 670 lb/in. (117×10^3 N/m). This represents an increase of almost 7 percent over the calculated critical load for the clamped circular cylinder previously analyzed. The cone has the same thickness and axial length as the cylinder and its smaller diameter is equal to the diameter of the cylinder. Figure 32a shows an applied load versus end-deflection curve for this structure, and Fig. 32b presents a normal displacement profile versus axial distance for loads of 420 lb/in. (74×10^3 N/m), and 660 lb/in. (116×10^3 N/m) (i.e., immediately preceding buckling). It can be seen that the structure buckles at the smaller diameter end.

Several additional analytical cases have been considered because the experimental buckling loads obtained for the cone with $\alpha = 17°$ were considerably lower than those obtained analytically assuming clamped edges. It was observed during the experiment that, at the small diameter end, the edges "curled" as the load increased, indicating that clamped edge conditions are not justifiable. To determine the extent of the effect of edge restraints, the same cone was analytically buckled with the small diameter end simply supported and free (axially restrained with no radial force or bending moment allowed). The critical load for the simply supported case was slightly lower than for the clamped case and was equal to 38,800 lbs (172.7×10^3 N). For the left end free, the buckling load was drastically reduced from 42,575 lbs (189×10^3 N), for the clamped case to 13,000 lbs (57.9×10^3 N), a 69.4 percent change. (See Fig. 32a for load-end deflection curves for the simply supported and free end cases.) The experimentally observed actual load of 25,000 lbs (111×10^3 N) lies between the two extremes of edge restraint represented by simple supports and a free edge, thus indicating the importance of accurately reproducing the restraint conditions for the plastic buckling analysis of conical shells.

4. PROGRAM DEFINITION

As mentioned in Section 1, the computer program PLANS for the PLastic ANalysis of Structures is organized as shown in Fig. 2b. The basic philosophy of program organization is to separate classes of analysis into individual groups, with each group defined by the physical problem to be solved. For example, as indicated in the figure, groups can be defined for membrane stressed structures (PLANE), combined bending and membrane stressed structures (BEND), bodies of revolution (REVBY), three dimensional solids (HEX), and membrane stressed laminated composites (COMPEL). On the basis of this concept, each group is in itself an independent finite-element computer program, with an associated element library, that can be individually loaded and used to solve the problem class of interest. In this manner any simplification or specialization germane to the individual analysis can be incorporated. Each group can contain subprograms common to all other program groups as well as subprograms distinct to its group. Linkage to any individual program group is made through an executive program indicated in the figure. As shown, linkage to any program group can be made only through this executive routine with no horizontal linkage between group programs.

A brief discussion of the significant features of several components of the program follows. A more detailed discussion is presented in a separate report.

Executive Program

The executive program performs the function of loading the individual analysis programs. Data set management and core allocation are handled by each of these programs. The system allows a user to store many program decks on a magnetic tape or direct access volume, and to use these programs conveniently. During a single computer run, the user may call for a "Select-Load-Go" procedure to execute routines in a previously created object file, or he may issue a series of easily-learned commands to change the old source file, thereby generating new source, index, and object files incorporating the desired changes. These new files can then be made available for a "Select-Load-Go" as part of the same run.

The executive system comprises three separate collections of subprograms to accomplish this. These are:

- A source update program to allow a user to selectively edit and compile a new source program.

- An object update program that maintains updated files of compiled source programs.

- A file select program that selectively loads programs from the object file for execution.

While the file select program can accept commands to load individual programs, it can also load groups of programs by simply supplying a group name that has been previously defined. In addition, each group definition may contain other group names in its definition. This feature is particularly meaningful for our purposes since each program in Fig. 2b naturally defines a group, and programs common to all groups (such as the solution package) are naturally subgroups. Thus, as shown in Fig. 2b, groups can be set up corresponding to PLANE, BEND, HEX, etc., and subgroups can be set up defining, for example, the solution package.

Thus, the capability to maintain source and object files and selectively load programs by groups is the most significant feature of the executive program. In addition, this system will have the ability to update files by rereading complete groups and is able to define new groups as additional programs are added to the PLANS system.

Basic Flow of Analysis Programs

Figure 33a is a gross schematic representation of the flow of each of the analysis programs. As shown in the figure, each module has three components: a main calling routine (MAIN); and elastic analysis group (ELAS); and the plastic analysis group (PLAS). A brief description of these components follows.

Main Program

Each individual computer program defining a group is controlled by a main calling program. This program sets up core allocation for principal arrays and the data set specifications for auxiliary storage. It then transfers control to subroutine ELAS. ELAS is a finite-element elastic analysis program that performs the elastic analysis and calculates the initial yield load. Control is then transferred back to the main program, which calls Subroutine PLAS only if requested. PLAS manages the plastic analysis and maintains control of the analysis until the complete plastic analysis is performed. At this point control is transferred to the main program either to terminate the job or call ELAS again to work

another problem. By so organizing the program it should be possible with a minimum amount of changes to use PLAS with other available finite-element elastic analysis programs.

ELAS

Figure 33b shows a block diagram of the computational flow of ELAS. This program is a special purpose finite-element program for the elastic analysis of structures. Accordingly, its first major task is to read all inputs. The input is read in functional groups as follows:

- Problem title.
- Nodal coordinates and control variables.
- Member topology describing connectivity.
- Nodal boundary conditions. Single and multi-point constraints on the displacements are specified in addition to fixed or free conditions.
- Load vector – includes the consistent member load vector for a distributed load.
- Material properties – tables of elastic and plastic material properties and member geometric properties are set up along with applicable members. Complete generality has been maintained so that orthotropic material behavior can be specified.

Other variables controlling output are also specified. The input scheme has been written so as to minimize the amount of card handling for any problem.

The next step is to form all element stiffness, stress, and initial strain stiffness matrices. This routine also places the elements of the stiffness matrix along with their position in the total stiffness matrix on an auxiliary storage device.

The total stiffness matrix and load vector are assembled by sequentially reading this information, stacking that portion of the stiffness matrix that fits in core, and then reading it onto an auxiliary storage device. This process is repeated until the entire load vector and stiffness matrix have been formed.

At this point it is appropriate to mention that our basic design philosophy is to make alterations, perform certain matrix multiplications, account for boundary conditions on the element level, and then to assemble these quantities into total arrays. In this manner we need not make use of a matrix interpretive system to manipulate large matrices.

With the total stiffness matrix and load vector assembled, the next step is to solve for displacements. Two solution packages are currently being used for this purpose, both based on the Cholesky factorization method. Their differences are based on the system used to store the stiffness matrix. PIRATE is based on partitioning the structure so that the stiffness matrix is explicitly in block tridiagonal form. The second routine, PODSYM, is based explicitly on the banded nature of the stiffness matrix, so that only elements within the lower triangle that lie between the semibandwidth need be assembled. In addition, this routine "packs" the rows of the stiffness matrix before writing it on auxiliary storage by suppressing all consecutive zeros.

The unit load stresses are calculated next from displacements. These stresses are used to calculate the initial yield load, and this yield load is used to scale the displacements and to calculate yield load stresses and strains. Control is then returned to the main program.

Subroutine PLAS

Figure 33c shows a block diagram of the computational flow of Subroutine PLAS. This program supervises the entire plastic analysis after initial processing has been carried out by ELAS. The principal information that must be communicated to PLAS is:

- Factored stiffness matrix and unit load vector
- Element stress and initial strain matrices
- Initial yield load
- Plastic material properties.

With this information, the routine increments the load and checks the yield condition for each member. Members that were previously plastic are also checked against an unloading criterion.

The effective plastic load vector is then formed as the product of the member's initial strain matrices and the plastic strains and added to the vector of applied load. This combined load vector is then used as the right hand side of the matrix equation to calculate

nodal displacements. It should be noted that, at this point, the stiffness matrix has been factored so that the solution involves only the multiplication necessary to perform the forward and backward solution.

In the next step, a subroutine is called that implements the plastic constitutive relations. This segment of code, calculates increments of total strain, stress, and plastic strain (shift in the yield surface when kinematic hardening is used) for each member from the increments of displacement, and sums the results with total quantities calculated previously.

After control is returned from the above subroutine a test is made to see if the maximum specified load has been reached. If not, the load is incremented and the steps discussed above are repeated.

When the maximum load is reached, the final effective plastic load vector is formed and displacements calculated with the applied load vector set equal to zero. Stresses and strains are calculated on the basis of these displacements. If subsequent yielding occurs in the reversed cycle at a load that is opposite in sign to the load previously completed, then these stresses and strains represent residual quantities. This is checked next by computing a new yield load. This calculation involves the solution of a quadratic equation for each member. One root of this solution represents the previously reached maximum load and the other the new yield load in the reversed direction. This load level is used as a starting point for the next cycle of loading.

At this point, a check is made to see if another cycle of loading is desired. If not, control is returned to the main program. If an additional cycle of loading is specified, new plastic material parameters can be read as input and inserted into the material property tables. This is followed by the formation of the effective plastic load vector. This load vector is then added to the load vector, and the sum is used to solve for the new critical load displacements and the corresponding stresses and strains. Transfer is then made to the beginning of PLAS in order to increment the load and proceed as described above.

Representative Time Requirements

The cost involved in obtaining an elastic solution to a particular problem depends upon a multitude of parameters. These include the core requirements, number of operating system calls, the total and central processing time, etc. An attempt to uniquely define the cost requirements for a problem of a given size, run under any one of the current operating systems, is unfeasible.

Although a realistic accounting procedure would consider some or all of the variables mentioned, it nevertheless remains true that the central processing time (CPU) is a significant factor in determining the total cost. On this basis we have indicated (Fig. 34) representative elastic solution time requirements versus problem size for the PLANE module. The problem size is represented in the figure by the number of degrees-of-freedom and the semi-bandwidth. The two curves in Fig. 34 were not obtained independently. That is, as illustrated in the figure, a problem involving 700 degrees-of-freedom requires 13 seconds of CPU if the semi-bandwidth is 90.

The time requirements for the solution to an elastic-plastic problem is measured as the summation of the time required for each increment of load. As discussed in Section 2, the displacement method-predictor procedure (used by all the modules of PLANS) does not require the reformulation and successive decomposition of the elastic stiffness matrix for each step beyond the initial maximum elastic load value. Thus, the time required for each incremental load step is considerably less than the elastic solution requirement. In general, it has been found that one-tenth of the elastic solution time represents a fairly reliable estimate for determining the CPU time for each increment in the plastic range.

A schematic curve of total system time versus problem size (degree-of-freedom x semi-bandwidth) is presented in Ref. 59, in addition to an excellent discussion on the cost of computing for a nonlinear analysis system.

5. CONCLUDING REMARKS

The material presented in this report, although primarily concerned with the authors' investigations, is representative of the current state of the development of nonlinear analysis techniques within the framework of the finite-element method. In addition to this report, recent surveys of the literature reveal that these methods have been developed to the point where a broad spectrum of structures of considerable complexity can be analyzed through the plastic range. Particular emphasis has been placed here on cyclic loading conditions involving reversed loading into the plastic range. Information concerning the behavior of structures subjected to realistic load spectra of this type should be of great value in treating the problem of low-cycle fatigue.

Although deficiencies still remain in the development of accurate constitutive relations describing elastic-plastic large deformation behavior, we do not believe that this should inhibit the development of analytical methods and their associated computer programs. Whether any one of the currently available plasticity theories represents an "exact" model for material nonlinearity is of less significance than the fact that the finite-element method allows us to perform numerical experiments to aid in the development of theories that more realistically describe complex material behavior. The programs also provide a guide for the experimentalist so that he can determine the type of experiments to perform, the properties to measure, and the data to monitor so that more accurate theories may be formulated. On this basis it is anticipated that further inroads can be made into those areas of investigation that, in the authors' opinion, require further insight. These problem areas include: anisotropic plasticity, temperature dependent plasticity, and dynamic loading effects.

During the course of the present study a substantial effort was devoted toward the development of a user-oriented computer code, briefly described in this section, that implements the plastic analysis techniques favored by the authors. To translate these theoretical approaches into a user-oriented, practical computing tool, one must recognize that those problems that exist in the development of such a tool for an elastic analysis are magnified for a nonlinear analysis. The constraints imposed by the range of validity of any particular theoretical analysis must be understood by the user and the data obtained from it carefully interpreted to ensure its proper application. For these reasons it would be potentially dangerous to consider such a tool as a "black box." Thus, a desirable feature of such a program, i.e., its ease of application, perhaps represents its greatest liability.

Recently, considerable attention [18] has been turned toward considering problems of efficiency, accuracy, and the resultant economic feasibility of large scale use of numerical nonlinear analytic systems. On the basis of the improvements in solution procedures, equation solving algorithms and computer hardware, one can now envision the time when it will become unnecessary to guess at or design around a problem involving complex nonlinearities. In considering the cost of using such a tool, however, one must always weigh the cost of the analysis versus the cost and risk involved in the possibility of designing a system on the basis of partial information or instituting an experimental program to gain the same information.

APPENDIX A

CATALOG OF FINITE-ELEMENTS

Plane Stress (Membrane States Only)

1. Constant Strain Triangle (CST) (Fig. 35) — This well-known plane stress membrane element was used successfully for the idealization of structures considered under Contract NAS 1-5040. Its derivation is based upon the assumption of a linear distribution for the in-plane displacements u and v, and consequently, leads to a constant strain state within the element. Each vertex is allowed two degrees of freedom (the in-plane displacements u and v) for a total of six degrees of freedom for the element. Consistent with the total strain distribution, the initial strains (plastic strains) are assumed to be constant within each element. Stiffness and initial strain matrices have been developed and successfully used in Contracts NAS 1-5040 and NAS 1-7315, Refs. 25 and 16.

2. Linear Strain Triangle (LST) (Fig. 36) — In regions of high strain gradient, the CST triangle is not sufficiently accurate to be used in a plasticity analysis unless a very fine grid is employed. The linear strain triangle (LST) remedies this shortcoming of the CST element. The assumption of a quadratic distribution for the in-plane displacements allows for a linear strain variation within the triangle. Two degrees of freedom at each node (u,v) for each of the six nodes (three vertex and three midside nodes) give this element a total of 12 degrees of freedom. The initial strains are assumed to be constant within each element and are evaluated at the centroid. Both stiffness and initial strain matrices have been developed and successfully used in Contract NAS 1-7315.

3. Hybrid Triangles — In transition regions, i.e., regions in which stresses and strains change from rapidly varying to slowly varying, it becomes convenient and efficient to switch from linear strain triangles to constant strain triangles. This is accomplished by using four and five node triangles to maintain compatibility with both the CST and LST elements. These elements together with the CST and LST elements were originally used in Ref. 6, and are referred to as the TRIM 3 through TRIM 6 family. For these mixed formulation hybrid elements, the displacements along edges may vary quadratically or linearly, depending upon whether an LST or CST triangle is contiguous to the respective sides. Again, the plastic strain distribution is assumed constant within each element.

4. Warped Quadrilateral Shear Panel (Fig. 37) — For many aircraft structures the stiffness properties may be adequately represented by an assemblage of beams, bars, and shear panels. The shear panels, as their name implies, provide resistance only to shearing forces. The normal and bending stresses are carried by the bars and beams. The shear panel used in the analysis is based upon the original formulation and approximation proposed by Garvey (Ref. 37). It is quadrilateral in planform and all four nodes need not lie in a plane. The out of plane "twisting" is taken up by "kick" forces f_i as shown in Fig. 37. The plastic behavior of this element is assumed to be uniaxial, i.e., the single stress or strain component at the centroid of the element is used to compute the plastic strain at that point.

5. Stringers (Fig. 38) — For many aircraft structures, e.g., fuselages, wings, etc., local stiffening is required to provide adequate stability in compression. Special one dimensional finite-elements are required to represent the stringers used for this purpose. Uniform cross section stringer elements have been developed using both constant and linearly varying strain assumptions, so that compatibility with both the CST and LST elements can be maintained. For the constant strain stringer, a linear axial displacement and a constant initial (plastic) strain distribution within the element are assumed. The linear strain stringer stiffness matrix is based upon a quadratic displacement assumption and the initial (plastic) strains are constant within the element

Bending

1. Triangular Element (Bell) (Fig. 39) — While a rectangular element is excellent for rectangular regions, a triangular element is necessary to treat plates with arbitrary boundaries, including curved boundaries. The fully conforming triangular bending element developed by Bell (Ref. 39) and several other authors (Refs. 60 and 61) has proved to be extremely effective for the analysis of bending of plates with curved boundaries. This element was used effectively in Ref. 16 to treat triangular, circular, annular, and rectangular plates. The lateral displacement w is assumed to be a complete quintic polynomial in x and y, the in-plane coordinates. Six nodal degress of freedom $(w, w_{,x}, w_{,y}, w_{,xx}, w_{,xy}, w_{,yy})$ at each vertex node and three normal slopes at the midpoints of the sides $(w_{,n})$ are initially prescribed. The latter three degrees of freedom are then eliminated by imposing a cubic variation of the normal slope along the edges, resulting in an 18 degree of freedom element. The plastic strain distribution is allowed to vary arbitrarily in the plane of the element. Plastic strains are evaluated at Gauss

points and the plastic load vector is formed using two dimensional Gauss-Legendre integration in the plane of the element. The plastic strain variation through the thickness at each Gauss point is monitored at a given number of points through the thickness (layered approach). The strains are then numerically integrated through the thickness for use with the initial strain stiffness matrix to form the plastic load vector. For problems involving combined bending and stretching the in-plane displacements are assumed to vary linearly, as in the constant strain membrane triangle or cubically (see Ref. 10) as in Felippa's formulation. Stiffness, initial stress stiffness, and initial strain matrices have been derived and successfully employed in the work of Ref. 16.

2. Beam Element (Fig. 40) — The effects of local stiffening may be represented by a beam element that assumes the gross geometric and elastic properties of the actual stiffener. Such a beam element with a rectangular cross section has been developed and used extensively in Refs. 13 and 62 for bending, combined bending and stretching, geometric nonlinearity, and integrally stiffened plate problems. Bending, membrane, and torsional rigidity are all accounted for in the stiffness matrix. The lateral deflections are assumed to be cubic in the axial coordinate, while the axial displacement is linear. Torsional rigidity is included through the assumption of a linear variation of the angle of twist.

In addition to this standard beam element, another element has been developed for use as a stiffener in conjunction with the triangular plate element. This element, depicted in Fig. 40, employs a cubic displacement assumption for both lateral displacements and the axial displacement. The angle of twist is assumed to vary linearly from node to node.

Plasticity is accounted for by assuming a linear variation from node to node of plastic strains along the beam axis and allowing an arbitrary variation of plastic strains through the cross-sectional area. The plastic strain distribution is integrated across the area using Gauss-Legendre integration and along the length in closed form.

Axisymmetric Bodies of Revolution

1. Axisymmetric Solid Element (Fig. 41) — The analysis of thick solids of revolution subjected to arbitrary mechanical loads is of basic interest in the aerospace industry. A triangular element of revolution used to analyze these problems was developed by Wilson (Ref. 41) and others. This is essentially a two dimensional

element with the formulation modified to account for hoop stresses and strains (due to the curvature of the structure). Its derivation is based upon a linear assumption for the radial and axial displacement components. A modification to this element to include a torsional degree-of-freedom is incorporated for the element included in this module. Thus, the element has three degrees-of-freedom at each nodal circle. Because of its triangular shape, it is capable of representing arbitrary bodies of revolution. The plastic strain distribution to be used in the formation of the initial strain matrix is assumed constant within each element. Stiffness and initial strain matrices have been developed and incorporated into the program. It should be mentioned that good elastic results have been obtained by using this element (Ref. 63), and Marcal (Ref. 64) and Armen, Levine, and Pifko (Ref. 65) have obtained good results in elastic-plastic analyses.

2. Axisymmetric Thin Shell Element (Fig. 42) — For shells whose thickness-to-mean-radius ratio is less than 1/10 (in many cases this ratio may be as high as 1/3) and where local effects are negligible (e.g., junctures, branches, welds), the use of a three dimensional element becomes wasteful. For such structures, shell theory, which is a two dimensional approximation to three dimensional elasticity theory, gives an accurate description of the state of stress and deformation. Moreover, since thickness effects are included in the kinematic model, only the circumferential and meridional variation of pertinent variables must be considered. This results in a considerable saving with regard to computer storage, since a smaller number of elements is required to describe the structure.

The shell of revolution is a basic component of many aerospace structures. Cylinders, spheres, cones, and various combinations thereof are widely used. For these reasons, an axisymmetric thin shell element capable of treating arbitrary shells of revolution under axisymmetric loading is included in the plasticity program.

The shell element chosen for use here is based upon the element developed by Levine and Armen in Ref. 42. The derivation of the stiffness properties of this element is based upon a shell theory proposed by Sanders (Ref. 66) that uses Kirchoff's hypothesis and Love's first approximation. The meridional displacement is assumed to be a cubic function of the meridional coordinate ξ (see Fig. 42) and the normal displacement is also chosen to be cubic in ξ. The actual meridional shape of the shell is represented by a cubic variation within the element. Plasticity has been accounted for by dividing the shell into layers through the thickness. For the current analysis, the plastic strains are assumed to vary linearly along the meridian in the derivation of the

initial strain matrix. Initial strain, initial stress, and conventional stiffness matrices have been developed and successfully employed in combined problems of material and geometric nonlinearity.

3. Axisymmetric Thin Ring Element — A thin ring element to account for the effects of local stiffening on the behavior of axisymmetric structures has been developed. The ring may be of arbitrary cross section and eccentrically attached to the structure. Torsion, extension, and bending are accounted for. The effects of prestress, warping, and shear deformation have been neglected, and the shear center and centroid must coincide. The element is basically similar to that presented by Cohen (Ref. 43). Plastic effects are included by numerically integrating the plastic strains over the cross-sectional area of the ring for use with the effective plastic load vector.

Three Dimensional Analysis

Isoparametric Hexahedron Element Family Ranging from 8 Nodes (at the Corners) to 20 (8 Corner and 12 Mid-edge) Nodes (Fig. 43 and Ref. 50) — For the 8 node element the displacement function is represented by a set of linear interpolating functions. Quadratic interpolation functions are used for the 20 node element. In local coordinates the element is a cube; in global coordinates, however, the position of all nodes is arbitrary. Each edge of the cube is either a quadratic curve in space or a straight edge, depending upon whether the edge is defined by the location of three or two node points. Thus, curved boundaries are represented by quadratic interpolating polynomials.

A constant plastic strain within each element has been incorporated.

Laminated Composite Plate Analysis —

- Constant stress element
- Pure shear element

} Composite Element (Fig. 44)

Interlaminar shear deformation, the mechanism by which load is transferred through a matrix material between two stiff laminae as the laminae tend to slide over each other, cannot be predicted by using classical plate theory. This type of deformation develops along the edges of a laminate and can be important with respect to

strength predictions of composite structures, especially for a laminate with a relatively low transverse shear strength. Analogous behavior is found to exist in bonded structural joints.

The idealized model used in the analysis separates the membrane and interlaminar properties of a laminated composite by using alternating orthotropic fiber-bearing segments and isotropic shear segments, as shown in Fig. 44a. The orthotropic segments carry in-plane stresses only, and may be considered to be in a state of plane stress; the shear segments carry only interlaminar shear stresses, and are in a state of pure shear.

The composite element consistent with the idealized model is shown in Fig. 44b. The membrane segments are triangular orthotropic elements in which the total strains are assumed to be uniform. Here the strain-displacement relation is based on a linearly varying displacement field. The stiffness properties of the interlaminar shear segments are also based on a linear displacement field, so that the shear strains may be written in terms of the nodal displacements in the following manner:

$$\gamma_{xz} = \frac{\partial u}{\partial z} = \left(u_i^{\ell-1} + u_j^{\ell-1} + u_k^{\ell-1} - u_i^{\ell} - u_j^{\ell} - u_k^{\ell}\right) \Big/ 3t$$

$$\gamma_{yz} = \frac{\partial v}{\partial z} = \left(v_i^{\ell-1} + v_j^{\ell-1} + v_k^{\ell-1} - v_i^{\ell} - v_j^{\ell} - v_k^{\ell}\right) \Big/ 3t \ , \qquad \text{(A-1)}$$

where u and v are displacements in the x and y directions, respectively; subscripts identify elements vertices; and superscripts identify element faces as shown in Fig. 44. Since the displacements vary linearly in the plane of a membrane segment, the interlaminar shear strain is computed on the basis of centroidal values of displacement, and thus the shear segment may be regarded as a shear-resisting medium connecting the centroids of adjacent membrane segments. Any number of segments may be stacked through the thickness to form the multilayered composite element.

Plastic behavior of the plate is assumed to be confined to the softer matrix material. A uniform plastic shear strain is assumed to exist in the interlaminar region. A detailed discussion of this element and its potential usage is presented in Ref. 54.

APPENDIX B

PLASTICITY RELATIONS

Considerable efforts have been made in the experimental exploration of the nonlinear behavior of many of the commonly encountered structural materials. A motivating force underlying much of this effort can be attributed to basic investigations concerned with low cycle fatigue (Refs. 67 and 68). From a metallurgical viewpoint, the mechanism associated with the behavior of ductile materials experiencing cyclic plastic deformation to fracture appears to be overwhelmingly complex. Because of this complexity no universally applicable laws governing the behavior of materials in the plastic range have yet been developed. If the structural analyst is to predict the gross deformation behavior of structures in the plastic range, he is required to choose from among the several available plasticity theories one that successfully combines mathematical simplicity with a reasonably faithful representation of some of the more obvious experimentally observed features of material behavior.

We here present and briefly discuss plasticity relations for three particular theories associated with strain-hardening behavior. These are the kinematic hardening and isotropic hardening theories and a third theory that incorporates features of both. Isotropic hardening is restricted to monotonic loading conditions, whereas the last two are specifically developed to treat cyclic loading conditions involving stress reversals. In addition, consideration is given to those relations appropriate to ideally plastic material behavior.

For isotropic, isothermal conditions, we can define a function of the stress components to be used in describing the limits of elastic behavior. This function generally represents one or a combination of stress invariants and can be a smooth continuous function (von Mises) or discontinuous piecewise linear (Tresca).

In the case of subsequent yielding from a plastic state, the function used to define the elastic limit is referred to as the subsequent yield or loading function, and the corresponding yield condition can be represented as

$$f(\sigma_{ij},\alpha_{ij}) - (\sigma_o)^n = 0 \ , \qquad \text{(B-1)}$$

where f is a homogeneous function of order n of its arguments, σ_{ij} are the stress components, α_{ij} represents a measure of the degree of work hardening, and σ_o is the yield stress.

The yield and loading conditions serve to establish criteria for loading, unloading, or neutral loading from elastic or plastic states, respectively (Ref. 25). Additional information, in the form of a constitutive relation between increments of plastic strain, stress, and stress increment, is required to describe the plastic behavior of a material. This constitutive relation, termed the flow rule, is based on the maximum plastic work inequality (Ref. 69):

$$(\sigma_{ij} - \sigma^{o}_{ij})d\epsilon_{ij} \geq 0 \ , \tag{B-2}$$

where $d\epsilon_{ij}$ represents the plastic strain increment components resulting from the stress state σ_{ij} on the subsequent loading surface, and σ^{o}_{ij} is any other stress state on the surface beneath it. In addition to providing the convexity condition on the loading surface, the inequality leads to the normality condition associated with the plastic strain increment vector. Thus, the flow rule is represented as

$$d\epsilon_{ij} = d\lambda \frac{\partial f(\sigma_{ij},\alpha_{ij})}{\partial \sigma_{ij}} \tag{B-3}$$

where $d\lambda$ is a positive scalar quantity.

Having selected a yield condition and flow rule, we must now choose a function that will establish conditions for subsequent yielding from a plastic state. Choice of a hardening rule depends on the ease with which it can be applied in the chosen method of analysis as well as on its capability of representing the actual hardening behavior of structural materials. These requirements and the necessity of maintaining mathematical consistency with the yield function constitute the criteria for final choice of a hardening rule. An appraisal of some of the available hardening rules follows.

Kinematic Hardening

The hardening behavior postulated in this theory assumes that during plastic deformation the loading surface translates as a

rigid body in stress space, maintaining the size, shape, and orientation of the yield surface. The primary aim of this theory, due to Prager (Refs. 26 and 27), is to provide a means of accounting for the Bauschinger effect. Such a capability is of particular importance in the strength prediction of aircraft structures, since severe loadings tend to be random, and failure may occur as the cumulative effect of a small number of such loadings.

An illustration of kinematic hardening, as applied in conjunction with the von Mises yield curve in the σ_1, σ_2 plane, is provided in Fig.45. The yield surface and loading surface are shown here for a shift of the stress state from point 1 to point 2. Denoting the translation of the center of the yield surface by α_{ij}, we may represent the loading function f in the form $f(\sigma_{ij} - \alpha_{ij})$; the subsequent yield condition is given as

$$f(\sigma_{ij} - \alpha_{ij}) - \sigma_o^2 = 0 \ . \qquad \text{(B-4)}$$

As a consequence of assuming a rigid translation of the loading surface, kinematic hardening predicts an ideal Bauschinger effect for completely reversed loading conditions. That is, the magnitude of the increase of yield stress in one direction results in a decrease of yield stress of the same magnitude in the reverse direction. Kadashevitch and Novozhilov (Ref. 70) have independently developed a hardening rule almost identical to Prager's. In their theory, the total translation of the yield surface is regarded as associated with "internal microstresses" that remain in the body upon unloading. It is these internal microstresses that are considered to be responsible for the Bauschinger effect.

The kinematic hardening theory as set forth by Prager postulates that the increments of translation of the loading surface in nine dimensional stress space occur in the direction of the exterior normal to the surface at the instantaneous stress state. This geometric relation can be expressed analytically by

$$d\alpha_{ij} = c\,d\epsilon_{ij} \ , \qquad \text{(B-5)}$$

where $d\epsilon_{ij}$ is the increment of plastic strain, which, according to the flow rule, Eq. (B-3), is in the direction of the exterior normal to the loading surface, and c is a parameter characterizing the hardening behavior of the material.

As indicated in Refs. 71 - 73, inconsistencies arise when the theory is applied in various subspaces of stress, that is, when the symmetry of the stress tensor or the fact that some of the stress components are zero is taken into account in reducing the number of dimensions of the stress space.

These inconsistencies produce the result that the loading surface will not, in general, translate in the direction of the exterior normal in a subspace of stress when it is made to do so in the full nine dimensional stress space. Reference 72 specifies stress conditions under which a linear transformation of variables enables the loading surface, in the transformed subspace, to translate in the direction of the exterior normal.

To avoid this difficulty in implementing complete kinematic hardening, Ziegler (Ref. 28) has proposed a modification of Prager's rule. This replaces Eq. (B-5) with the following expression for the increment of translation

$$d\alpha_{ij} = d\mu(\sigma_{ij} - \alpha_{ij}) \qquad d\mu > 0 \ . \tag{B-6}$$

The geometrical significance of this modification is shown in Fig. 46, where the increment of translation $d\alpha_{ij}^{(P)}$, computed on the basis of Prager's rule, is compared with the increment of translation $d\alpha_{ij}^{(Z)}$, computed on the basis of Ziegler's modified rule. Note that in the latter case the increment of translation $d\alpha_{ij}^{(Z)}$ is in the direction of the vector from the center of the yield or loading surface to the point representing the instantaneous stress state.

The scalar $d\mu$ in Eq. (B-6) is determined from the condition that the stress state must remain on the translated loading surface during plastic deformation. From Fig. 47 it can be seen that this condition may be represented as

$$(d\sigma_{ij} - d\alpha_{ij}) \frac{\partial f}{\partial \sigma_{ij}} = 0 \ . \tag{B-7}$$

Substituting Eq. (B-6) into Eq. (B-7), we have

$$d\mu = \frac{\frac{\partial f}{\partial \sigma_{ij}} d\sigma_{ij}}{(\sigma_{ij} - \alpha_{ij}) \frac{\partial f}{\partial \sigma_{ij}}} \tag{B-8}$$

An expression for the scalar factor $d\lambda$ associated with the flow rule, Eq. (B-3), can be determined by recognizing that the vector $cd\epsilon_{ij}$, shown in Fig. 47, is the projection of $d\sigma_{ij}$ on the exterior normal to the loading surface at the instantaneous stress state. Thus, we can write

$$(d\sigma_{ij} - cd\epsilon_{ij}) \frac{\partial f}{\partial \sigma_{ij}} = 0 \ . \tag{B-9}$$

Using the flow rule, Eq. (B-3), to substitute for $d\epsilon_{ij}$ in Eq. (B-9) results in the following expression for $d\lambda$

$$d\lambda = \frac{1}{c} \frac{\frac{\partial f}{\partial \sigma_{ij}} d\sigma_{ij}}{\left(\frac{\partial f}{\partial \sigma_{k\ell}}\right) \left(\frac{\partial f}{\partial \sigma_{k\ell}}\right)} \ , \tag{B-10}$$

where the summation convention is adopted in 9-space. The flow rule now becomes

$$d\epsilon_{ij} = \frac{1}{c} \frac{\partial f}{\partial \sigma_{ij}} \frac{\frac{\partial f}{\partial \sigma_{mn}} d\sigma_{mn}}{\left(\frac{\partial f}{\partial \sigma_{k\ell}}\right) \left(\frac{\partial f}{\partial \sigma_{k\ell}}\right)} \tag{B-11}$$

Isotropic Hardening

This theory assumes that during plastic flow the loading surface expands uniformly about the origin in stress space, maintaining the same shape, center location, and orientation as the yield surface. Figure 48 illustrates, on the basis of a simplification to a two dimensional plot, the yield and loading surfaces when the

stress state shifts from point 1 to 2. Unloading and subsequent reloading in the reverse direction result in yielding at the stress state represented by point 3. The path 2-3 will be elastic, and 0-2 is equal to 0-3.

It can be seen that the isotropic type of representation of work hardening does not account for the Bauschinger effect exhibited by most structural materials. In fact, this theory provides that because of work hardening the material will exhibit an increase in the compressive yield stress equal to the increase in the tensile yield stress. Furthermore, since plastic deformation is an anisotropic process, a theory that predicts isotropy in the plastic range cannot be expected to lead to realistic results when nonproportional loading paths (not necessarily completely reversed) are considered. This conclusion has been indicated experimentally in Refs. 74 -77. For monotonic loading conditions, however, isotropic hardening is satisfactory and is commonly used.

In the case of isotropic hardening, $f(\sigma_{ij})$ in Eq. (B-1) retains its original form, except that σ_o increases in magnitude to provide for the expansion of the yield surface as work hardening proceeds. Equation (B-1) then serves to define σ_o, which is referred to as the "effective stress." The corresponding relationship between plastic strain increments and stress increments for the case of isotropic hardening is obtained by introducing the expression for $f(\sigma_{ij})$ in Eq. (B-1) into the flow rule of Eq. (B-3), with σ_o treated as a constant.

Work-Hardening Moduli

A theory that combines kinematic and isotropic work hardening would require the yield condition of Eq. (B-1) to be modified as follows.

$$f(\sigma_{ij} - \alpha_{ij}) - F(\lambda) = 0 \ , \qquad \text{(B-12)}$$

where $F(\lambda)$ is a measure of the expansion of the yield surface in stress space, and, during plastic deformation, λ is a monotonically increasing scalar function. Equation (B-12) reduces to the case of kinematic hardening when $F(\lambda)$ = constant, and to isotropic hardening when $\alpha_{ij} = 0$ and $F(\lambda)$ is monotonically increasing.

From experimental considerations concerned with the behavior of metals under cyclic loading, it has been observed that a steady cycle of alternating plastic flow is reached after a certain number of cycles (Ref. 78). For some materials under a fixed strain (or stress) range, fully reversed cyclic tension-compression tests may tend to increase the stress (or strain) range toward a fixed steady-state value (work stiffening). Conversely, in some metals initially cold worked into the plastic range or heat treated, the stress (or strain) range can be lowered to the same steady-state value during plastic cycling (work softening). The hypotheses of isotropic and kinematic hardening cannot, in general, predict this observed phenomenon. In the uniaxial case shown in Fig. 49, for instance, for stress cycling between the limits $\pm\sigma_B$, the isotropic hardening model predicts completely elastic behavior beyond the first half-cycle, whereas kinematic hardening predicts steady cyclic plastic straining beyond the first cycle — neither of which may represent the actual behavior.

In proposing a work-hardening model to account for the behavior of metals under cyclic loading conditions, Mróz (Refs. 79 and 80) has introduced the notion of a field of work-hardening moduli and the variation of this field during the course of plastic deformation. In this proposed model, a stress-strain curve of an initially isotropic material is represented by n linear segments of constant tangent plastic moduli, as shown in Fig. 50. In stress space, this approximation can be represented by n hypersurfaces f_o, f_1, ..., f_n, where f_o is the initial yield surface, and f_1 to f_n define regions of constant work-hardening moduli. Figure 51 illustrates these hypersurfaces in the σ_1 - σ_2 plane for an initially isotropic material. As seen from this figure, the surfaces f_o, f_1, ... are similar and concentric, and for simplicity are schematically represented by a family of circles. If we consider proportional loading in the σ_2 direction, corresponding to σ in Fig. 50, and if we assume that the surfaces can experience a rigid translation without experiencing a change of size or orientation, then when the stress state reaches point A on Fig. 51a, the surface f_o will translate until it reaches the circle f_1 at the stress corresponding to point B. The circles f_o and f_1 translate together until the point C is reached, where now f_o, f_1, and f_2 are attached at a common point of contact. For unloading and subsequent reversed loading, when the stress reaches a point corresponding to point E (Fig. 51b), reverse plastic flow occurs and the surface f_o translates downward along the σ axis until it reaches the surface f_1 at F. Mróz further proposes that the curve of reverse loading in Fig. 50 joins the

curve $OA'B'G$ that is obtained by symmetry with respect to the origin from $OABC$. Thus, the curve of reverse loading EFG is uniquely defined by the curve of primary loading, represented by an equation of the form $\sigma = f(e)$. If a new coordinate system $(\bar{\sigma},\bar{e})$ with origin at C is used, we have for the curve $CEFG$

$$\tfrac{1}{2}\,\bar{\sigma} = f(\tfrac{1}{2}\,\bar{e}) \ . \qquad \text{(B-13)}$$

In the generalization of this model to nonproportional loading, it is assumed that during translation of the hypersurfaces the individual surfaces do not intersect but consecutively contact and push each other. If we consider two neighboring surfaces f_k and f_{k+1} having centers at O_k and O_{k+1} defined by the position vectors α_{ij}^{k} and α_{ij}^{k+1}, then the equations of these two surfaces are

$$f\left(\sigma_{ij} - \alpha_{ij}^{k}\right) - \left(\sigma_{o}^{k}\right)^{n} = 0 \quad ; \quad f\left(\sigma_{ij} - \alpha_{ij}^{k+1}\right) - \left(\sigma_{o}^{k+1}\right)^{n} = 0 \ , \qquad \text{(B-14)}$$

where σ_o^k and σ_o^{k+1} are constants used to define the size of the surface. From Ref. 80, the instantaneous translation of $f(\sigma_{ij} - \alpha_{ij}^{k})$ is given by

$$d\alpha_{ij}^{k} = \frac{d\mu}{\sigma_{o}^{k}}\left[\left(\sigma_{o}^{k+1} - \sigma_{o}^{k}\right)\sigma_{ij}^{k} - \left(\alpha_{ij}^{k}\sigma_{o}^{k+1} - \alpha_{ij}^{k+1}\sigma_{o}^{k}\right)\right] \ , \qquad \text{(B-15)}$$

where

$$d\mu = \frac{\partial f/\partial\sigma_{ij}\, d\sigma_{ij}}{\partial f/\sigma_{mn}\left(\sigma_{mn}^{k+1} - \sigma_{mn}^{k}\right)} \ .$$

On reaching surface f_{k+1}, the position of f_k can be obtained from the following relation:

$$\sigma_{ij}^{k+1} - \alpha_{ij}^{k+1} = \frac{\sigma_{o}^{k+1}}{\sigma_{o}^{k}}\left(\sigma_{ij}^{k} - \alpha_{ij}^{k}\right) \ , \qquad \text{(B-16)}$$

i.e., the vectors connecting the center of the surface with the stress point are parallel for the surfaces f_k and f_{k+1}. When the centers of the surfaces originally coincide, the mathematical description of the translation of the yield surface is identical to that given by Ziegler (Ref. 28) and presented here in Eq. (B-6).

The work-hardening modulus for each hypersurface is developed in Ref. 80 from a flow rule in the form of Eq. (B-3), and is given as

$$c = \frac{d\sigma_{ij} d\epsilon_{ij}}{d\epsilon_{ij} d\epsilon_{ij}} \tag{B-17}$$

for multiaxial stress. Equation (B-17) represents a generalization of the plastic tangent modulus in the uniaxial stress state. A corresponding modulus of the form $c = h(\bar{\sigma}, \bar{\epsilon})$, where h is a functional representation of the instantaneous slope of an effective stress $(\bar{\sigma})$-effective strain $(\bar{\epsilon})$ curve, is presented in Ref. 25. It should be noted that when f_1 tends to infinity, so that the work-hardening modulus is constant (the work-hardening curve being represented by a straight line), the theory proposed by Mróz is identical to Prager's kinematic hardening model.

The further generalization of the theory of work-hardening moduli is associated with an expansion or contraction of the surfaces f_o, f_1, ..., so that transitory phenomena (work stiffening, work softening or nonisothermal conditions) can be treated. Thus, the hypersurfaces f_k are not constants but functions of a scalar parameter, λ, monotonically increasing during plastic flow. One suggestion for λ is presented in Ref. 80, where it is proposed that

$$\sigma_o^k = \sigma_o^k(\lambda) \ , \tag{B-18}$$

where

$$\lambda = \sqrt{\frac{2}{3}} \int_0^t (d\epsilon_{ij} d\epsilon_{ij})^{\frac{1}{2}} dt \ ,$$

and t represents an interval of time or load, etc.

The effects of cyclic loading, as predicted by kinematic hardening or the theory of Mróz, can be expected to give, at best, a simplified approximation of the actual behavior of structural metals under cyclic loading. These theories idealize the behavior of the location of the yield surface(s) in a general direction of prior plastic deformation. Experiments have shown that the behavior of subsequent yield surfaces are far more complex than a mere translation and/or expansion of the original surface. However, we believe that these theories satisfy our original criteria requiring mathematical simplicity and capability of predicting the essential features of cyclic plastic behavior. Results for several of those problems in which strain hardening is considered in this report were obtained by using the Prager-Ziegler kinematic hardening theory with a constant work-hardening modulus. For others, the concept of fields of work-hardening moduli was used where, for a point undergoing loading in the plastic range, a new modulus is computed for each increment of load. Further, for reversed loading, a new coordinate system, used to define the reversed stress-strain behavior, is chosen at a point corresponding to E in Fig. 51b.

REFERENCES

1. Plastic Design in Steel. A Guide and Commentary, ASCE-Manuals and Reports on Engineering Practice, No. 41, 1971.

2. Interim Specification, developed by the American Association of State Highway Officials, Committee on Bridges and Structures, 1971.

3. Greenstreet, W. et al., High Temperature Structural Design Methods for LMFBR Components, Quarterly Progress Report for Period Ending December 31, 1971, ORNL-TN-3736, March 1972.

4. Padlog, J., Huff, R., and Holloway, G., "The Unelastic Behavior of Structures Subjected to Cyclic, Thermal, and Mechanical Stressing Conditions," WADD-TR-60-271, 1960.

5. Marçal, P., "A Stiffness Method for Elastic-Plastic Problems," Int. J. Mech. Sci., Vol. 7, 1965.

6. Argyris, J., "Continua and Discontinua," Proceedings of Conference on Matrix Methods in Structural Mechanics, Wright-Patterson AFB, Ohio, October 1965, AFFDL-TR-66-80.

7. Lansing, W., Jensen, W., and Falby, W., "Matrix Analysis Methods for Inelastic Structures," Proceedings of Conference on Matrix Methods in Structural Mechanics, Wright-Patterson AFB, Ohio, October 26-28, 1965, AFFDL-TR-66-80.

8. Pope, G., "The Application of the Matrix Displacement Method in Plane Elasto-Plastic Problems," Proceedings of Conference on Matrix Methods in Structural Mechanics, Wright-Patterson AFB, Ohio, October 26-28, 1965, AFFDL-TR-66-80.

9. Marçal, P., "A Comparative Study of Numerical Methods of Elastic-Plastic Analysis," AIAA Journal, Vol. 6, No. 1, January 1968, p. 157.

10. Felippa, C., Refined Finite Element Analysis of Linear and Nonlinear Two Dimensional Structures, Structures and Materials Research Report, Department of Civil Engineering Report No. 66-22, University of California, Berkeley, October 1966.

11. Armen, H. Jr., Isakson, G., and Pifko, A., "Discrete Element Methods for the Plastic Analysis of Structures Subjected to Cyclic Loading," International Journal for Numerical Methods in Engineering,"Vol. 2, No. 2, April-June 1970, pp. 189-208.

12. Popov, E., Khojasteh-Bakht, M., and Yaghmai, S., "Analysis of Elastic-Plastic Circular Plates," ASCE, J. Eng. Mech. Div., Vol. 93, No. EM6, December 1967, pp. 49-65.

13. Armen, H. Jr., Pifko, A., and Levine, H., "A Finite Element Method for the Plastic Bending Analysis of Structures," Proceedings of Air Force Second Conference on Matrix Methods in Structural Mechanics, Wright-Patterson AFB, Ohio, October 15-17, 1968, AFFDL-TR-68-150.

14. Yamada, T., Kawai, T., Yoshimura, N., and Sakurai, T., "Analysis of the Elastic-Plastic Problems by the Matrix Displacement Method," presented at the Second Conference on Matrix Methods in Structural Mechanics, Wright-Patterson AFB, October 15-17, 1968, AFFDL-TR-68-150.

15. Zienkiewicz, O., Valliappan, S., and King, J., "Elasto-Plastic Solutions of Engineering Problems 'Initial Stress,' Finite Element Approach," International Journal for Numerical Methods in Engineering, Vol. 1, No. 1, January-March 1969, pp. 75-100.

16. Armen, H. Jr., Pifko, A., and Levine, H., Finite Element Analysis of Structures in the Plastic Range, NASA CR-1649, February 1971.

17. Mendelson, A. and Manson, S., Practical Solution of Plastic Deformation Problems in the Elastic-Plastic Range, NASA TR-R-28, 1959.

18. Stricklin, J., Haisler, W., and Von Riesemann, W., "Evaluation of Solution Procedures for Material and/or Geometrical Nonlinear Structural Analysis by the Direct Stiffness Method," presented at the AIAA/ASME 13th Structures, Structural Dynamics, and Materials Conference, San Antonio, Texas, April 1972.

19. Murray, D. and Wilson, E., "Finite Element Large Deflection Analysis of Plates," ASCE, J. of Eng. Mech. Div., Vol. 95, No. EM1, February 1969, pp. 143-165.

20. Haisler, W., Stricklin, J., and Stebbins, F., "Development and Evaluation of Solution Procedures for Geometrically Nonlinear Structural Analysis," AIAA Journal, Vol. 10, No. 3, March 1972, pp. 264-272.

21. Mallett, R. and Marçal, P., "Finite Element Analysis of Nonlinear Structures," Proceedings of ASCE, J. Struc. Div., Vol. 94, No. ST9, September 1968.

22. Marçal, P., "Large Deflection Analysis of Elastic-Plastic Shells of Revolution," AIAA Journal, Vol. 8, No. 9, p. 1627, 1970.

23. Levine, H. et al., "Nonlinear Behavior of Shells of Revolution under Cyclic Loading," presented at the National Symposium on Computerized Structural Analysis and Design at George Washington University, Washington, D.C., March 1972; also Grumman Research Report RE-426J, April 1972.

24. Hofmeister, L., Greenbaum, G., and Evensen, D., "Large Strain, Elasto-Plastic Finite Element Analysis," AIAA Journal, Vol. 9, No. 7, 1971, p. 1248.

25. Isakson, G., Armen, H. Jr., and Pifko, A., Discrete-Element Methods for the Plastic Analysis of Structures, NASA CR-803, 1967.

26. Prager, W., "The Theory of Plasticity: A Survey of Recent Achievements," (James Clayton Lecture) Proc. Instn. Mech. Engrs., Vol. 169, 1955, p. 41.

27. Prager, W., "A New Method of Analyzing Stress and Strains in Work-Hardening Plastic Solids," J. Appl. Mech., Vol. 23, 1956, p. 493.

28. Ziegler, H., "A Modification of Prager's Hardening Rule," Quart. Appl. Math., Vol. 17, No. 1, 1959, p. 55.

29. Biot, M., Mechanics of Incremental Deformations, John Wiley & Sons, Inc., New York, 1965.

30. Lin, T., Theory of Inelastic Structures, John Wiley & Sons, Inc., New York, 1968.

31. Gallagher, R., Padlog, J., and Bijlaard, P., "Stress Analysis of Heated Complex Shapes," J. Am. Rocket. Soc., Vol. 32, 1962, pp. 700-707.

32. Hill, R., The Mathematical Theory of Plasticity, Chapter 12, Oxford University Press, 1950.

33. Armen, H. Jr., et al., "Plastic Analysis of Structures," Proceedings of Conference on Finite Element Techniques in Solid Mechanics, University of Southampton, Southampton, England, 1970; also published as Grumman Research Report RE-380J, April 1970.

34. Mallett, R. and Marçal, P., "Finite Element Analysis of Nonlinear Structures, Proc. of the ASCE, J. of the Structures Division, Vol. 94, No. ST9, 1968.

35. Martin, H., "On the Derivation of Stiffness Matrices for the Analysis of Large Deflection and Stability Problems," Proceedings of Conference on Matrix Methods in Structural Mechanics, Wright-Patterson AFB, Ohio, October 26-28, 1965, AFFDL-TR-66-80.

36. Stricklin, J., Haisler, W., and Von Riesemann, W., Formulation, Computation, and Solution Procedures for Material and/or Geometric Nonlinear Structural Analysis by the Finite Element Method, Sandia Corporation Report SC-CR-72-3102, Albuquerque, New Mexico, January 1972.

37. Garvey, S., "The Quadrilateral 'Shear' Panel," Aircraft Engineer, May 1951, p. 134.

38. Inglis, C., "Stresses in a Plate Due the Presence of Cracks and Sharp Corners," Trans. Inst. of Naval Architects, Vol. LV, 1913, pp. 219-230; also Timoshenko and Goodier, Theory of Elasticity, McGraw-Hill, 1951, p. 197.

39. Bell, K., "Analysis of Thin Plates in Bending Using Triangular Finite Elements," Institutt for Statikk, Norges Tekniske Hogskole, Trondheim, Norway, February 1968.

40. Armen, H. Jr., Levine, H., and Pifko, A., "Elastic-Plastic Behavior of Plates under Combined Bending and Stretching," presented at AIAA/ASME Eleventh Structures, Structural Dynamics and Materials Conference, Denver, Colorado, April 22-24, 1970; also Grumman Research Department Report RE-379J, April 1970.

41. Wilson, E., "Structural Analysis of Axisymmetric Solids," AIAA Journal, Vol. 3, No. 12, December 1965.

42. Levine, H. and Armen, H. Jr., A Refined Doubly-Curved Axisymmetric Orthotropic Shell Element, Grumman Research Department Memorandum RM-496, February 1971.

43. Cohen, G., "Computer Analysis of Asymmetric Buckling of Ring-Stiffened Orthotropic Shells of Revolution," AIAA Journal, Vol. 6, No. 1, January 1968.

44. Levine, H. and Klosner, J., "Axisymmetric Elasticity Solutions of Spherical Shell Segments," PIBAL Report No. 68-12, May 1968, Polytechnic Institute of Brooklyn, Brooklyn, N.Y.

45. Prager, W. and Hodge, P. Jr., Theory of Perfectly Plastic Solids, J. Wiley and Sons, Inc., 1951.

46. Khojasteh-Bakht, M., "Analysis of Elastic-Plastic Shells of Revolution under Axisymmetric Loading by the Finite Element Method," Ph.D. Dissertation, University of California at Berkeley, SESM67-8, 1967.

47. Drucker, D. and Shield, R., "Limit Analysis of Symmetrically Loaded Thin Shells of Revolution," J. Appl. Mech., Vol. 26, No. 1, 1959, pp. 61-68.

48. Havner, K., "On Convergence of Iterative Methods in Plastic Strain Analysis," Int. J. Solids and Structures, Vol. 4, 1968, pp. 491-508.

49. Popov, E., Khojasteh-Bakht, M., and Yaghmai, S., "Bending of Circular Plates of Hardening Material," Int. J. Solids and Structures, Vol. 3, 1967, pp. 975-988.

50. Zienkiewicz, O. et al., "Iso-Parametric and Associated Element Families for Two and Three Dimensional Analysis," Finite Element Methods in Stress Analysis, TAPIR, Technical University of Norway, Trondheim, 1969.

51. Iyengar, R., Raja, Sundara, and Prabhakara, M., "A Three Dimensional Elasticity Solution for Rectangular Prism under End Loads," ZAMM, Vol. 49, No. 6, June 1969, p. 21.

52. Sternberg, E. and Sadowsky, M., "Three Dimensional Solution for the Stress Concentration around a Circular Hole in a Plate of Arbitrary Thickness," J. Appl. Mech., Vol. 16, No. 1, March 1949.

53. Isakson, G. and Levy, A., "Finite-Element Analysis of Interlaminar Shear in Fibrous Composites," J. Comp. Materials, Vol. 5, 1971, p. 273.

54. Levy, A., Armen, H. Jr., and Whiteside, J.,"Elastic and Plastic Interlaminar Shear Deformation in Laminated Composites under Generalized Plane Stress," presented at Air Force Third Conference on Matrix Methods in Structural Mechanics, Wright-Patterson AFB, Ohio, October 19-21, 1971; also Grumman Research Department Memorandum RM-535J, February 1972.

55. Way, S., "Bending of Circular Plates with Large Deflection," Trans. ASME, Vol. 56, 1934, pp. 627-636.

56. Mescall, J., "Large Deflections of Spherical Shells under Concentrated Loads," J. of Appl. Mech., Vol. 32, No. 4, 1965, pp. 936-938.

57. Wilkinson, M. and Fulton, R., "Axisymmetric Buckling of Uniformly Loaded Spherical Caps Undergoing Plastic Deformation," to be published in AIAA Journ., 1972.

58. Haythornthwaite, R. and Onat, E., "The Load Carrying Capacity of Initially Flat Circular Steel Plates under Reversed Loading," J. Aero. Sci., Vol. 22, No. 12, 1955, p. 867.

59. Hibbitt, H., Levy, N., and Marçal, P., "On General Purpose Programs for Nonlinear Finite Element Analysis," presented at the Winter Annual Meeting of ASME, New York, N.Y., November 1970, and published in On General Purpose Finite Element Computer Programs, edited by P. V. Marçal, ASME.

60. Cowper, G. et al., "A High Precision Triangular Plate-Bending Element," Aeronautical Report LR-514, National Research Council of Canada, Ottowa, December 1968.

61. Visser, W., "The Finite Element Method in Deformation and Heat Conduction Problems," Dr. Ir. Dissertation, T. H. Delft, March 1968.

62. Harris, H. and Pifko, A., "A Finite Element Technique for the Elastic-Plastic and Anisotropic Buckling Analysis of Stiffened Rectangular Plates," Grumman Advanced Development Report No. FSR-AD2-01-68.6, November 1968; also presented at the Symposium on Application of Finite Elements in Civil Engineering, November 1969, Vanderbilt University, Nashville, Tenn.

63. Gifford, L. Jr., "Finite Element Analysis for Arbitrary Axisymmetric Structures," Naval Ship Research and Development Center, NSRDC-2641, March 1968.

64. Marçal, P. and King, I., "Elastic-Plastic Analysis of Two Dimensional Stress Systems by the Finite Element Method," Int. J. of Mech. Sci., Vol. 9, 1967, pp. 143-155.

65. Armen, H. Jr., Levine, H., and Pifko, A., "Plasticity-Theory and Applications," presented at the 2nd U.S.-Japan Seminar on Matrix Methods of Structural Analysis and Design, Berkeley, California, August 1972, and appears in Advances in Computational Methods in Structural Mechanics and Design, University of Alabama at Huntsville Press, Huntsville, Alabama, 1972.

66. Sanders, J. Jr., "Nonlinear Theories for Thin Shells," Quarterly of Applied Mathematics, Vol. 21, No. 1, April 1963, pp. 21-36.

67. Broom, T. and Ham, R., "The Hardening and Softening of Metals by Cyclic Stresses," Proceedings of the Royal Society, Vol. 242A, 1957, pp. 166-179.

68. Morrow, J., Cyclic Plastic Strain Energy and Fatigue of Metals, ASTM STP No. 378, American Society for Testing and Materials, 1965.

69. Drucker, D., "Plasticity," Structural Mechanics (Proceedings, First Symposium on Naval Structural Mechanics, Goodier, J. and Hoff, N., eds.), Pergamon Press, 1960, p. 407.

70. Kadashevitch, Y. and Novozhilov, B., "The Theory of Plasticity Taking Residual Micro-Stresses into Consideration," Prikl. Mat. Meckh., Vol. 22, No. 1, 1955, p. 78.

71. Budiansky, B., Discussion of Reference 27, J. Appl. Mech., Vol. 24, 1957, p. 481.

72. Shield, R. and Ziegler, H., "On Prager's Hardening Rule," ZAMP, Vol. 9a, 1958, p. 260.

73. Perrone, N. and Hodge, P. Jr., Applications of a Consistent Theory for Strain-Hardening Plastic Solids, PIBAL Report 403, September 1957.

74. Phillips, A. and Kaechele, L., "Combined Stress Tests in Plasticity," J. Appl. Mech., Vol. 23, 1956, p. 43.

75. Marin, J. and Hu, L., "Biaxial Plastic Stress-Strain Relations of a Mild Steel for Variable Stress Ratios," Trans. ASME, April 1956, p. 499.

76. Hu, L. and Bratt, J., "Effect of Tensile Plastic Deformation on the Yield Condition," J. Appl. Mech., Vol. 25, September 1958, p. 111.

77. Marin, J. and Hu, L., "On the Validity of Assumptions Made in Theories of Plastic Flow for Metals," Trans. ASME, Vol. 75, No. 6, 1953, p. 1181.

78. Coffin, L. Jr., "The Stability of Metals under Cyclic Plastic Strain," J. Basic Eng., Vol. 82D, 1960, pp. 671-682.

79. Mróz, Z., "On the Description of Anisotropic Workhardening," J. Mech. Phys. Solids, Vol. 15, 1967, pp. 163-175.

80. Mróz, Z., "An Attempt to Describe the Behavior of Metals under Cyclic Loads Using a More General Workhardening Model," Acta Mechanica, Vol. 7, 1969, pp. 199-212.

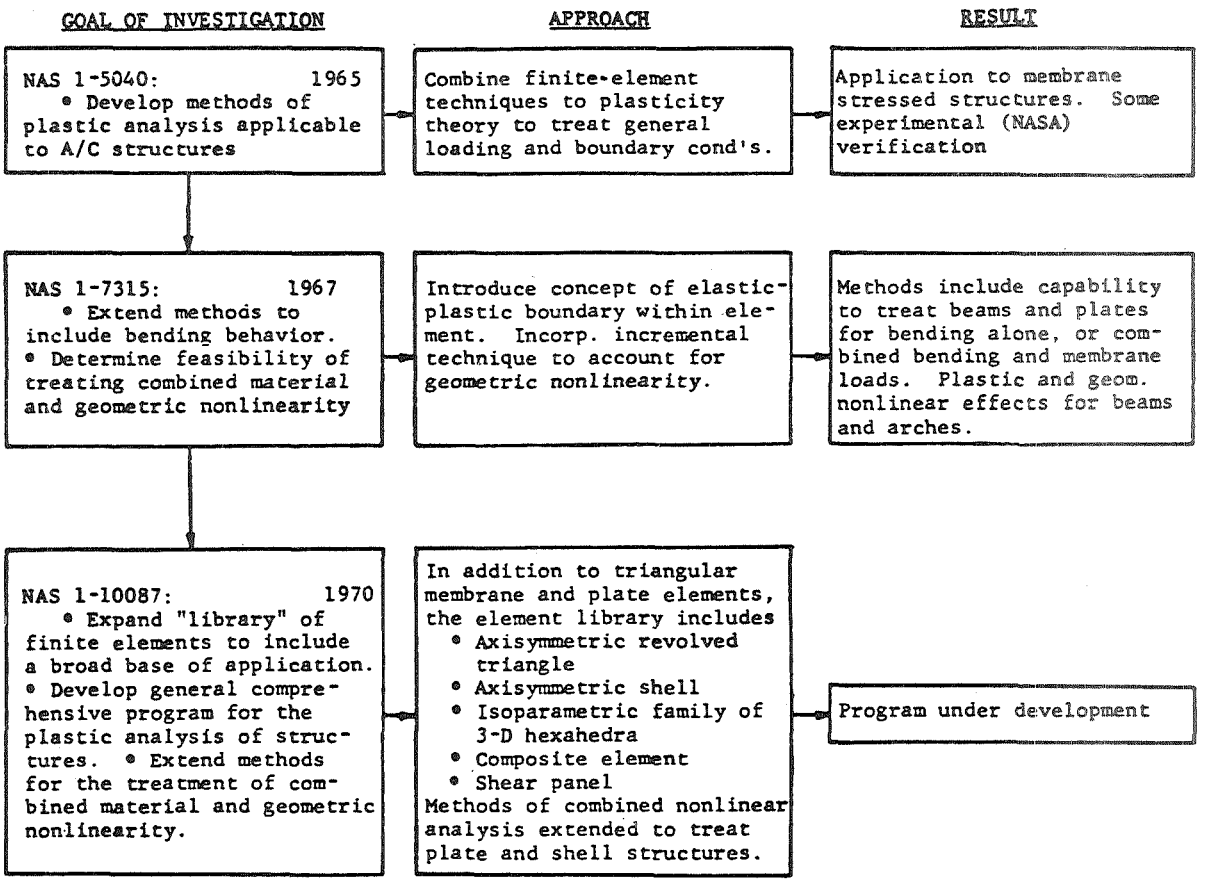

Fig. 1 Chronological Summary of Nonlinear Finite Element Analysis Studies at Grumman

Type of Analysis	Loading	Application
I. Membrane Stress	• Arbitrary concentrated and/or distributed in-plane (membrane) loads. • Unloading from any plastic state and reversed loading.	Thin walled membrane stressed structures, such as sheets with arbitrarily shaped holes and cutouts; general out-of-plane thin walled membrane structures.
II. 1. Bending 2. Combined bending and membrane	• Arbitrary concentrated and/or distributed normal and in-plane loads. • Unloading from any plastic state and reversed loading.	Plates of arbitrary shape with holes and cutouts; stiffened panel; general out-of-plane thin walled structures
III. Axisymmetric bodies of revolution	• Axisymmetric line or distributed loads. • Unloading from any plastic state and reversed loading.	Thin walled axisymmetric stiffened and unstiffened shells of revolution; thick walled axisymmetric structures; junctions between branched structures; transitional shells (thin - thick).
IV. Three dimensional	• Arbitrary concentrated and/or undistributed loads. • Unloading from any plastic state.	Behavior of arbitrarily shaped three dimensional bodies.
V. Composite plates under plane stress	• Arbitrary concentrated and/or distributed in-plane loads. • Unloading from any plastic state and reversed loading.	Laminated composite plates under generalized plane stress conditions.

Fig. 2a Nonlinear Analysis Capabilities of the PLANS System

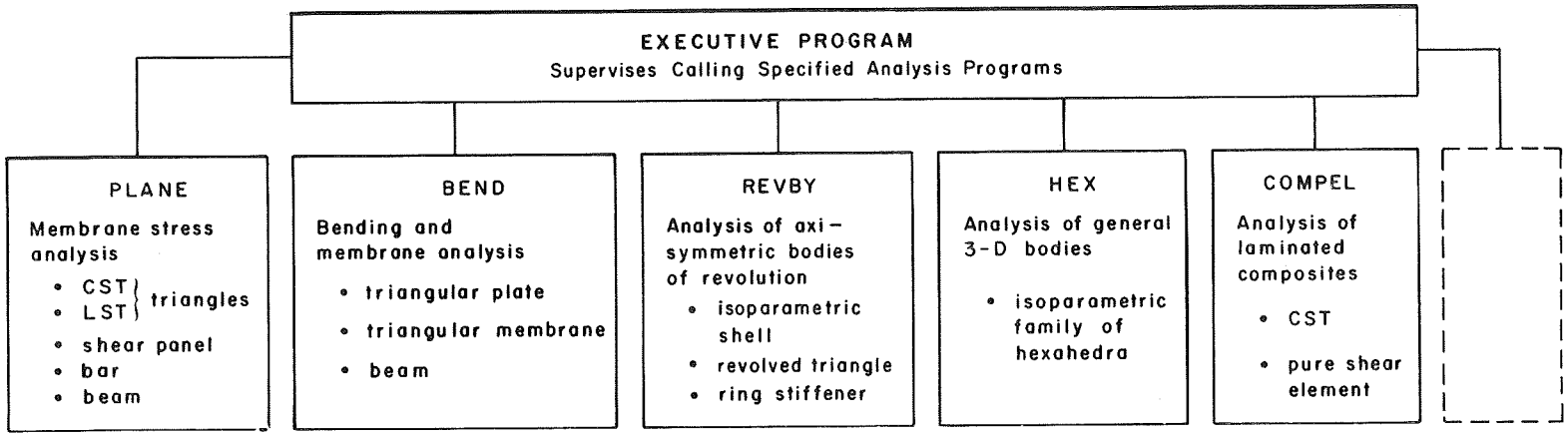

Fig. 2b ORGANIZATION OF PLANS

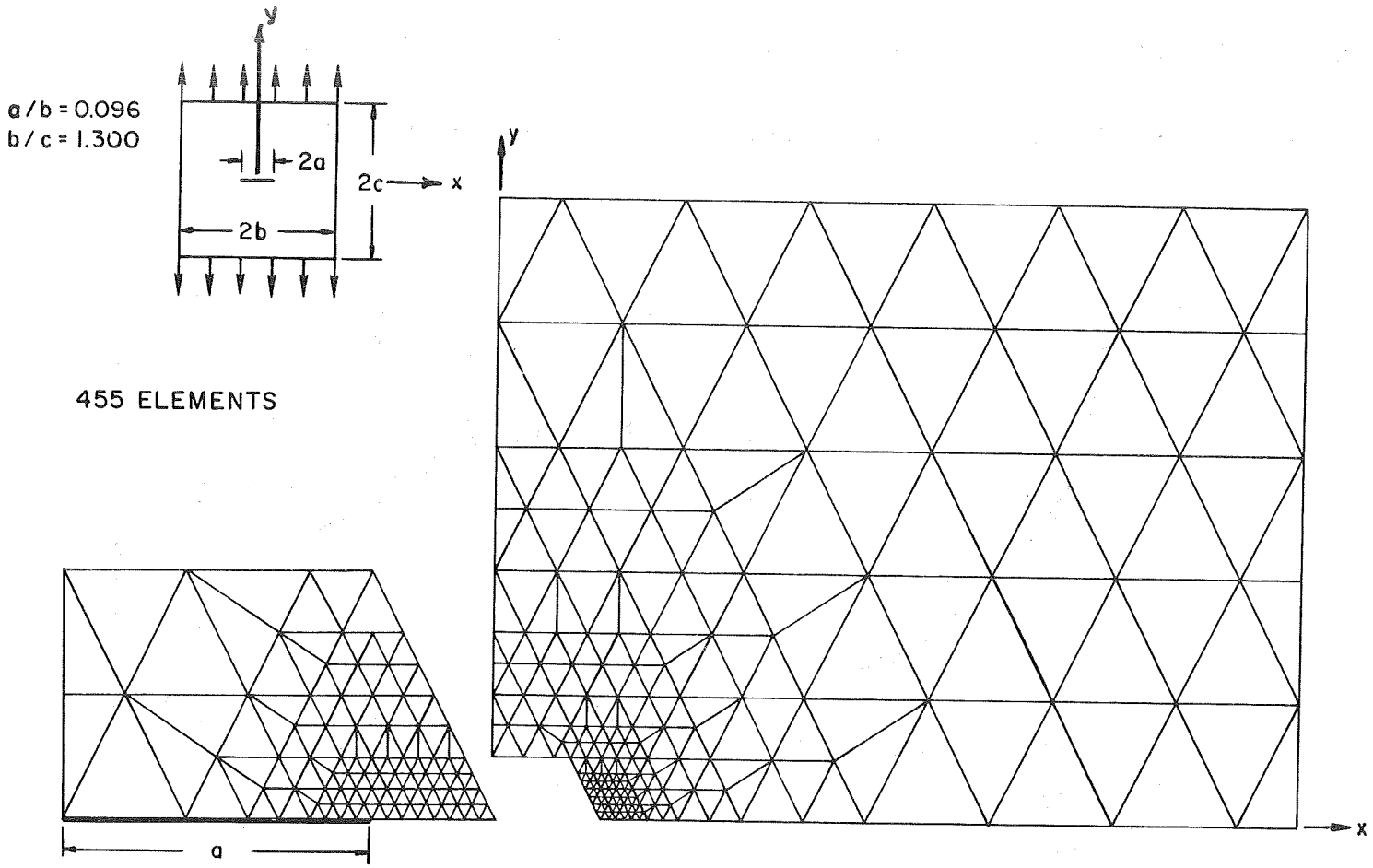

Fig. 3 IDEALIZATION OF A QUADRANT OF A SHEET WITH A CENTRAL CRACK

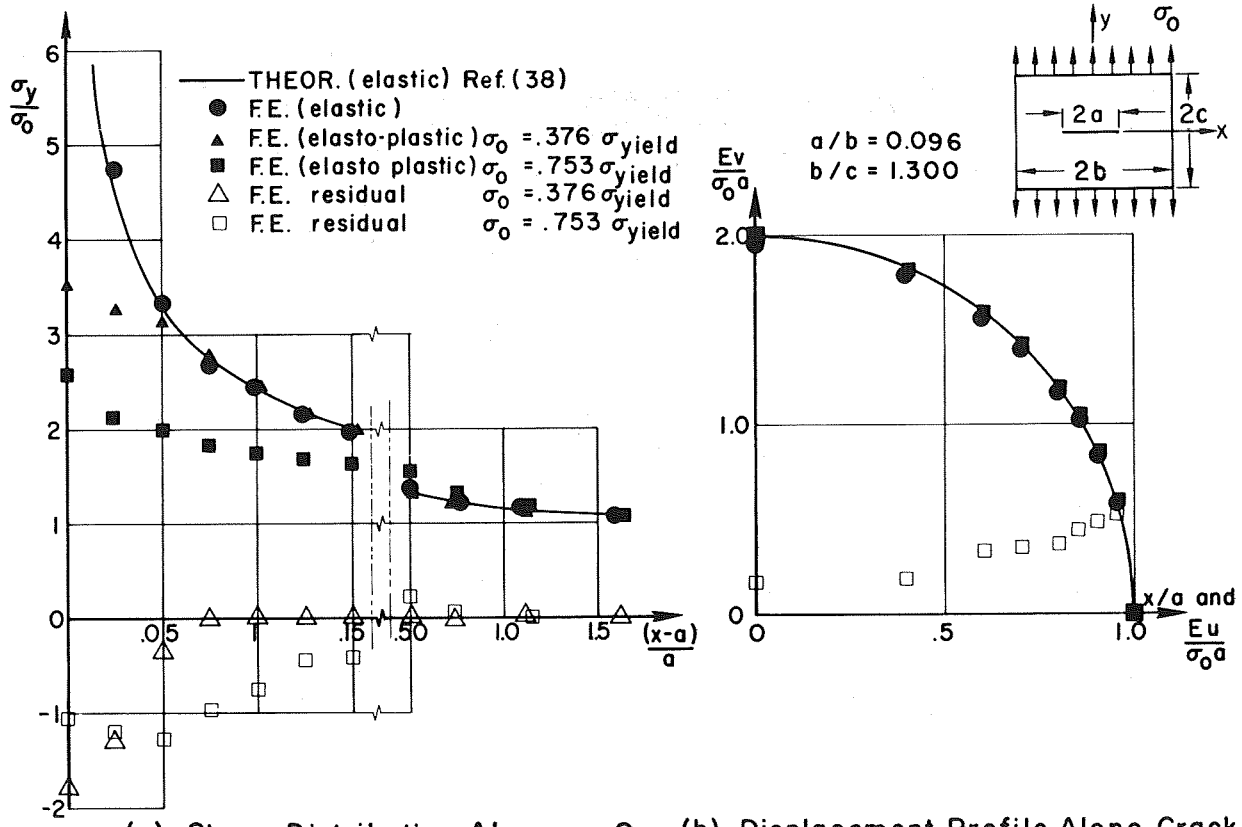

(a) Stress Distribution Along y = 0 (b) Displacement Profile Along Crack Length

Fig 4. ELASTIC-PLASTIC ANALYSIS OF A UNIFORMLY LOADED SHEET WITH A CENTRAL CRACK

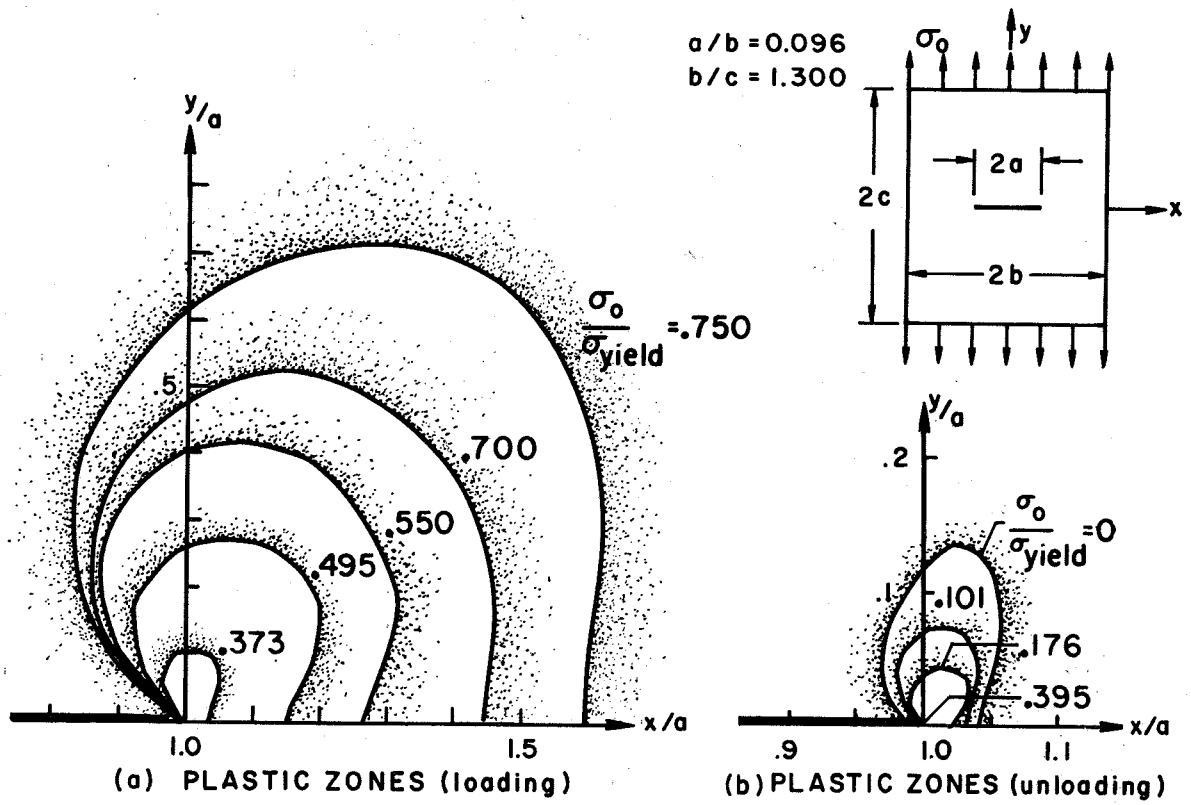

Fig. 5 PROPAGATION OF PLASTIC ZONE IN A UNIFORMLY LOADED SHEET WITH A CENTRAL CRACK.

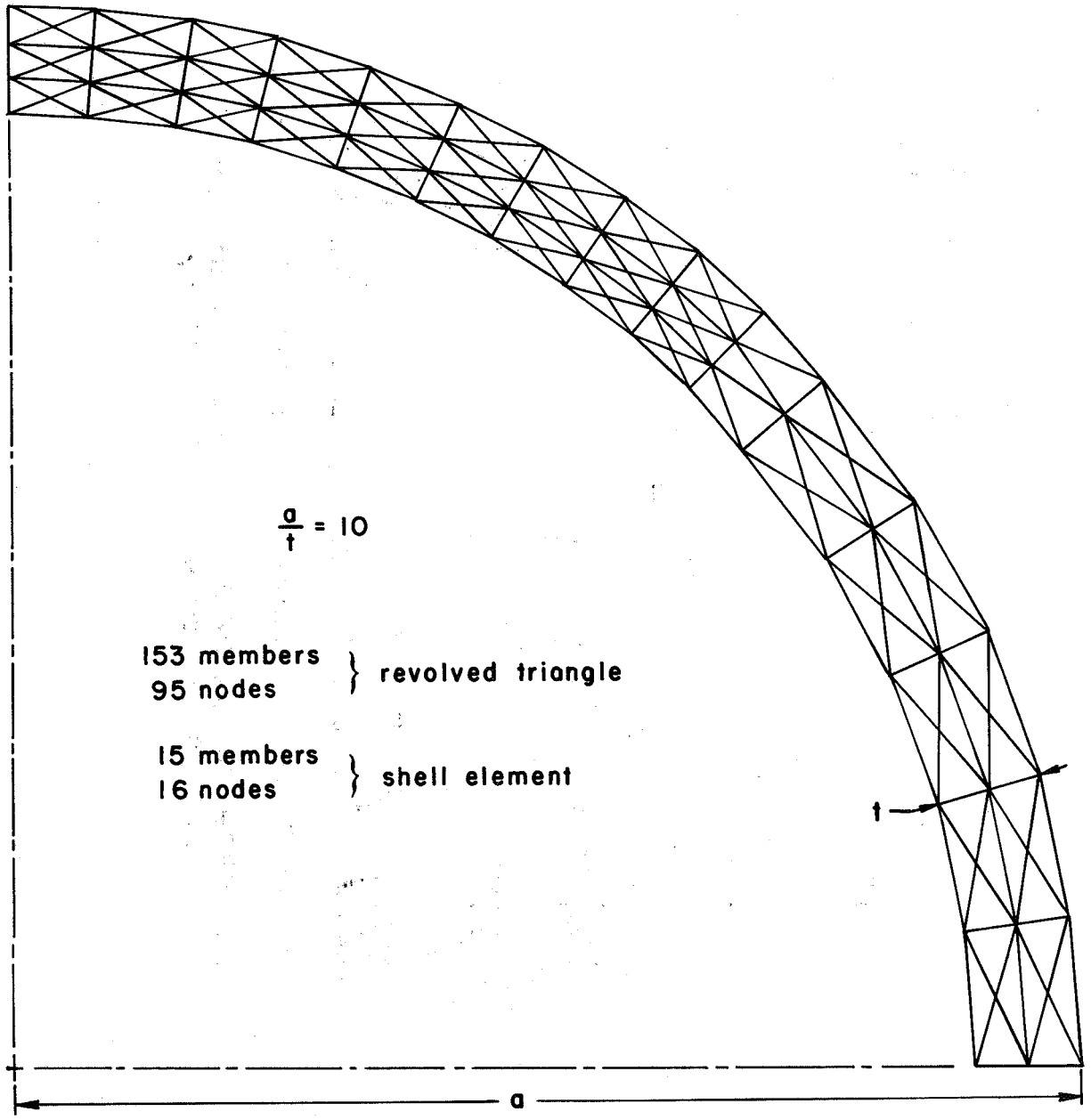

Fig. 6 IDEALIZATION OF QUADRANT OF FULL SPHERE

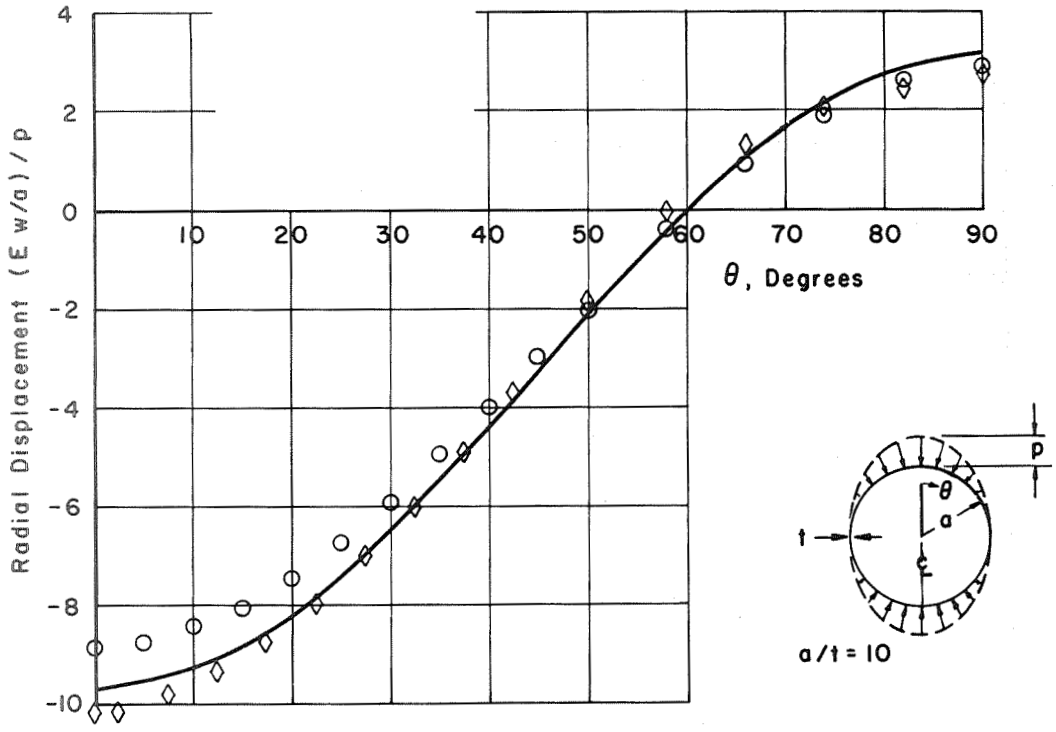

Fig.7 RADIAL DISPLACEMENT DISTRIBUTION vs MERIDIONAL DIRECTION

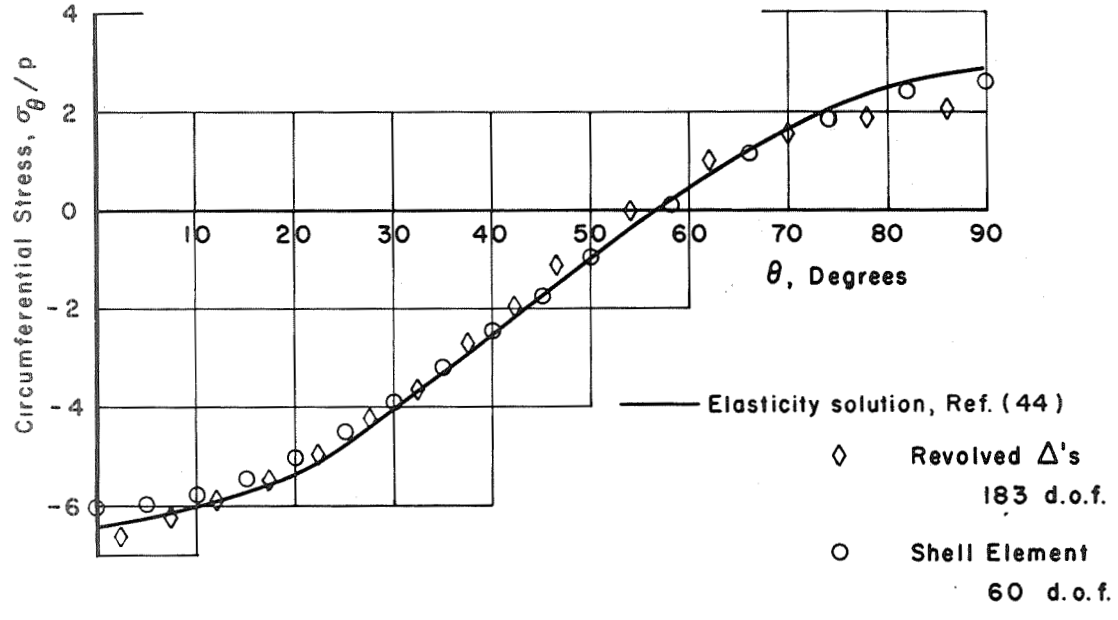

Fig. 8 CIRCUMFERENTIAL STRESS, σ_ϕ, vs MERIDIONAL DIRECTION

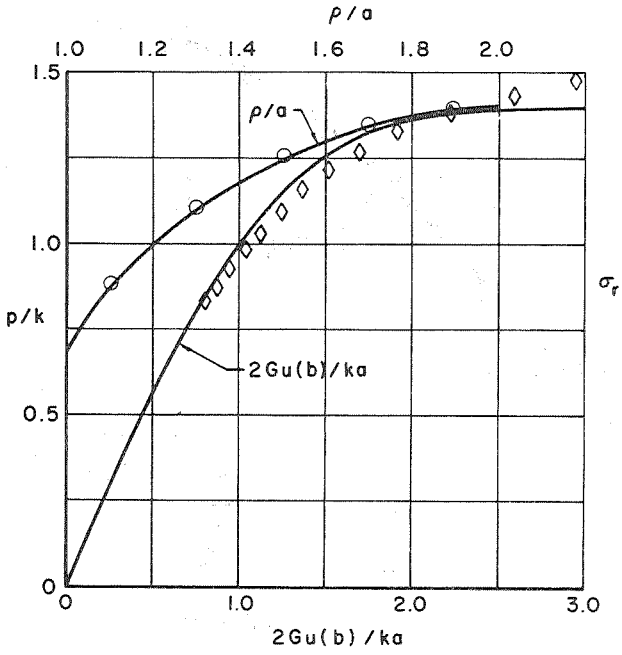

Fig.9 PRESSURE p VERSUS RADIAL DISPLACEMENT u(b) AND RADIUS OF ELASTIC-PLASTIC BOUNDARY, ρ.

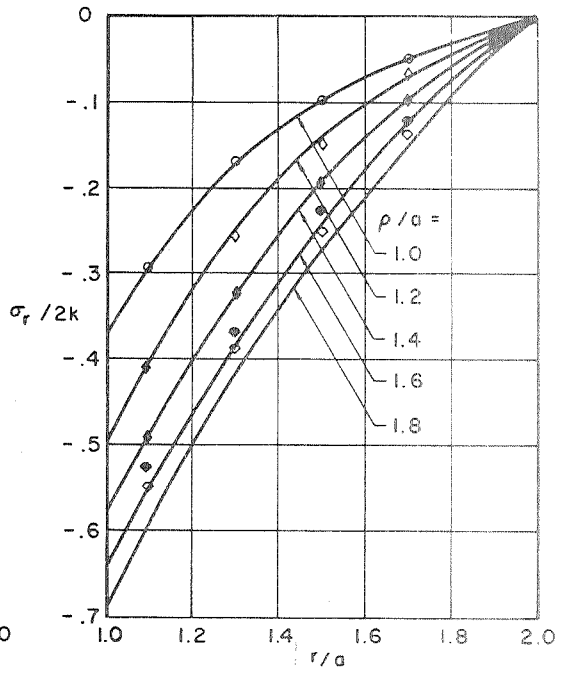

Fig. 10 DISTRIBUTION OF RADIAL STRESS

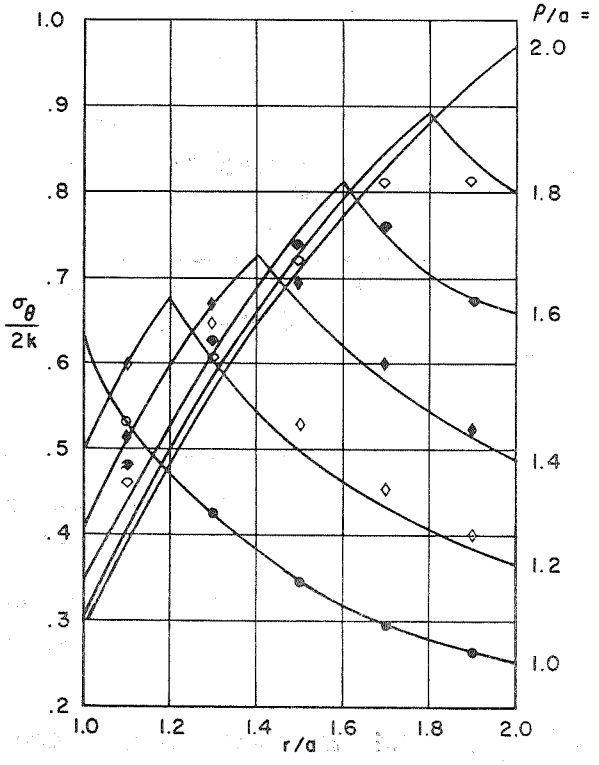

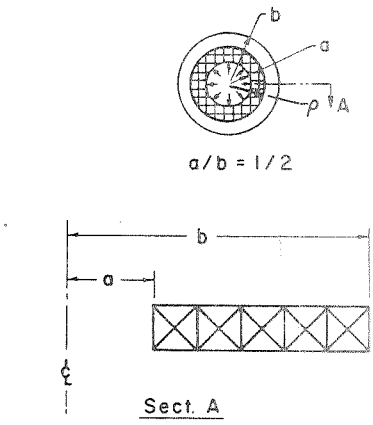

Fig. 11 DISTRIBUTION OF CIRCUMFERENTIAL STRESS

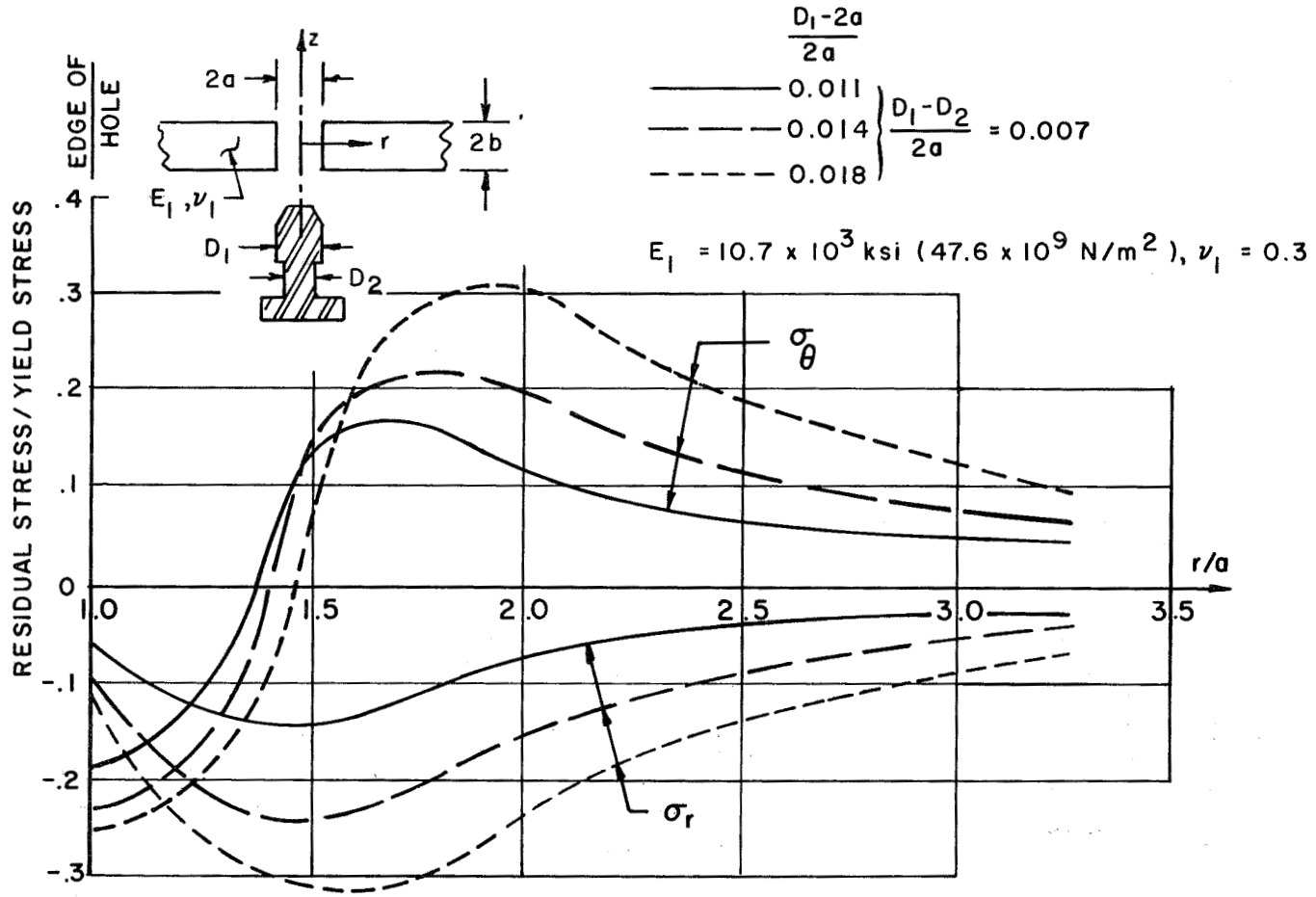

Fig. 12 RADIAL AND CIRCUMFERENTIAL RESIDUAL STRESSES IN SHEET WITH RIGID OVERSIZE FASTENERS ($z = \pm b$)

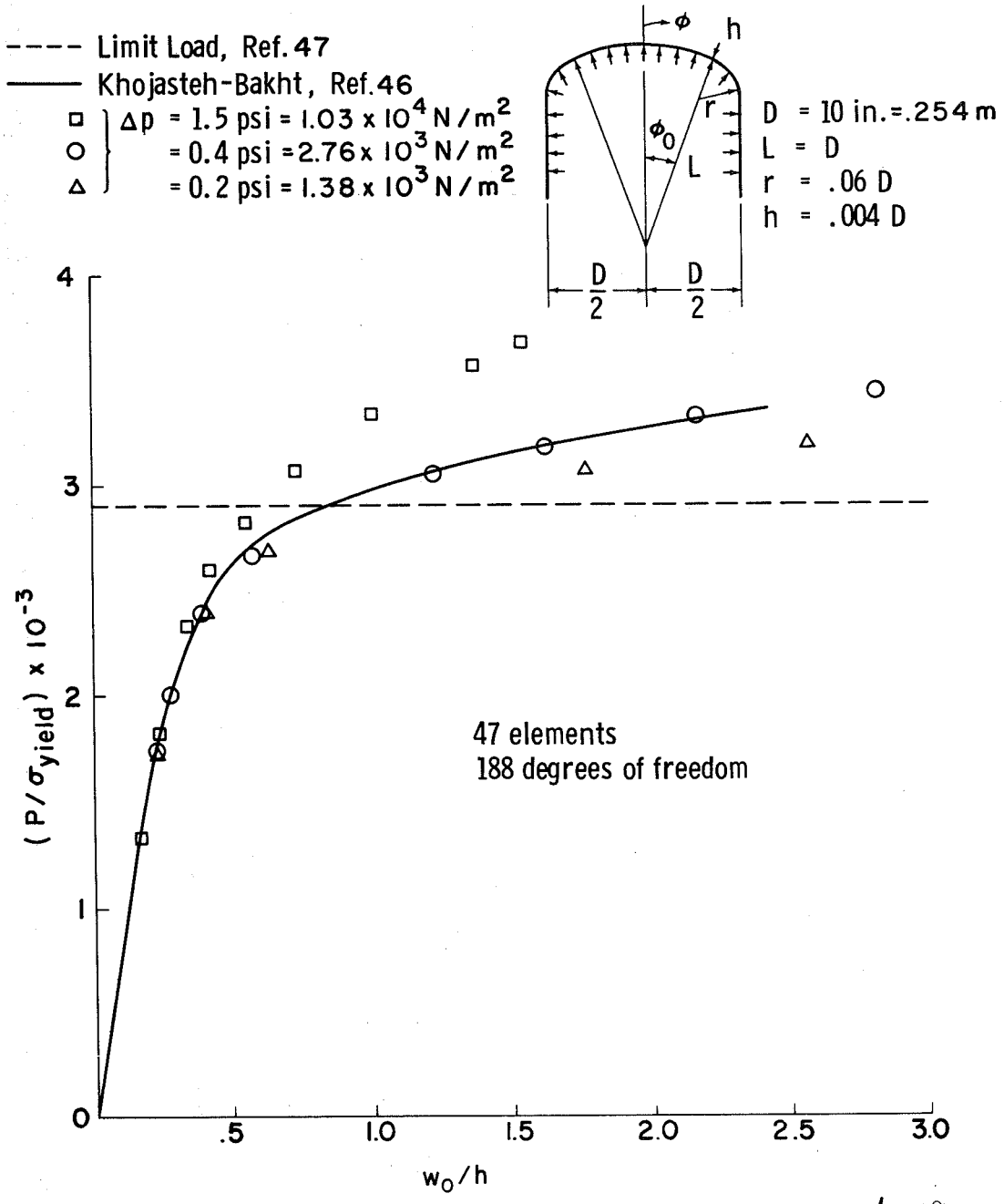

Fig. 13 PRESSURE VERSUS NORMAL DISPLACEMENT, w_0, AT APEX ($\phi = 0°$) FOR DIFFERENT LOAD INCREMENTS - TORISPHERICAL SHELL

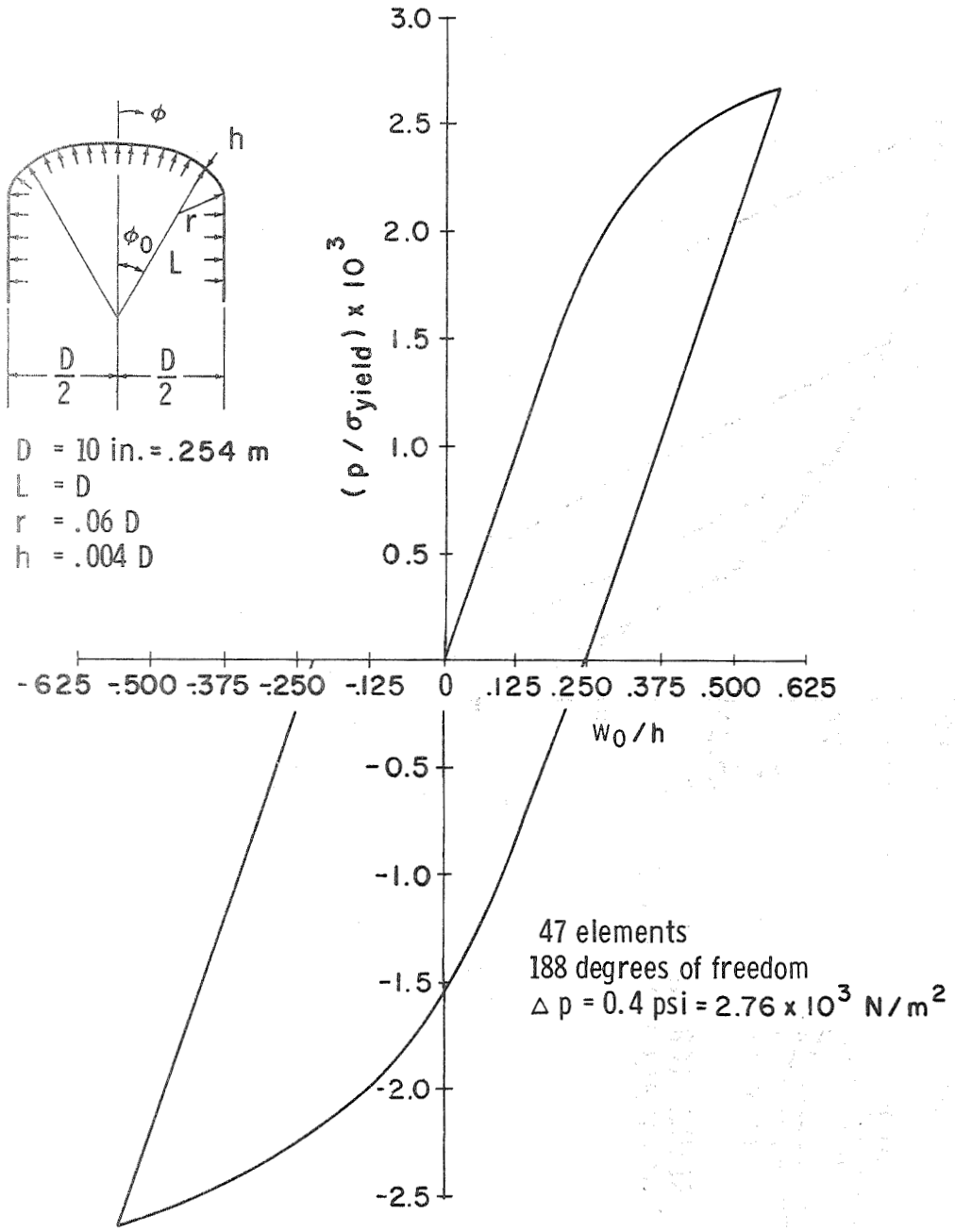

Fig. 14 CYCLIC PRESSURE VERSUS NORMAL DISPLACEMENT, w_0, AT APEX ($\phi = 0°$) TORISPHERICAL SHELL

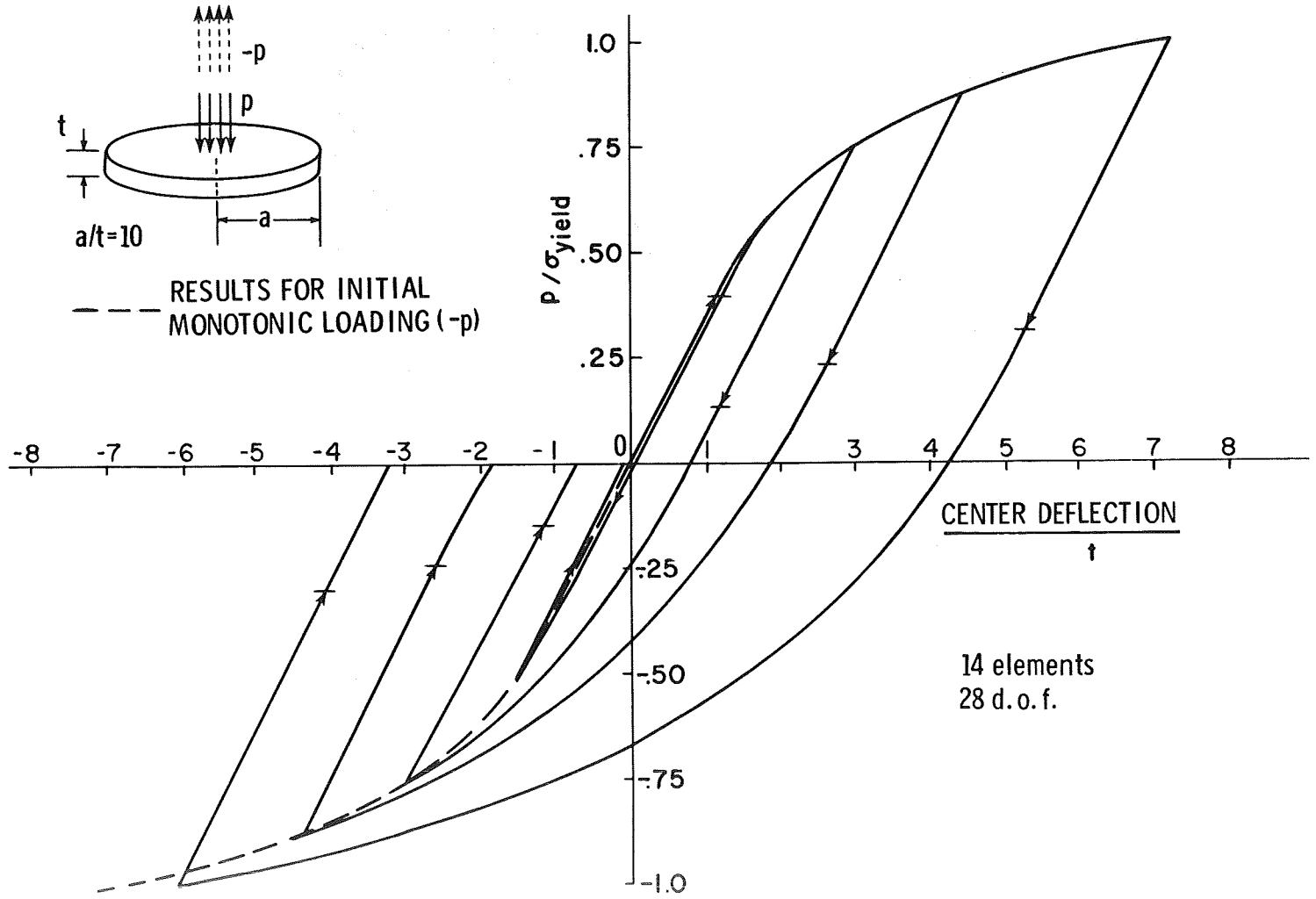

Fig.15 LOAD VERSUS CENTER DEFLECTION OF A SIMPLY-SUPPORTED, CENTRALLY LOADED CIRCULAR PLATE

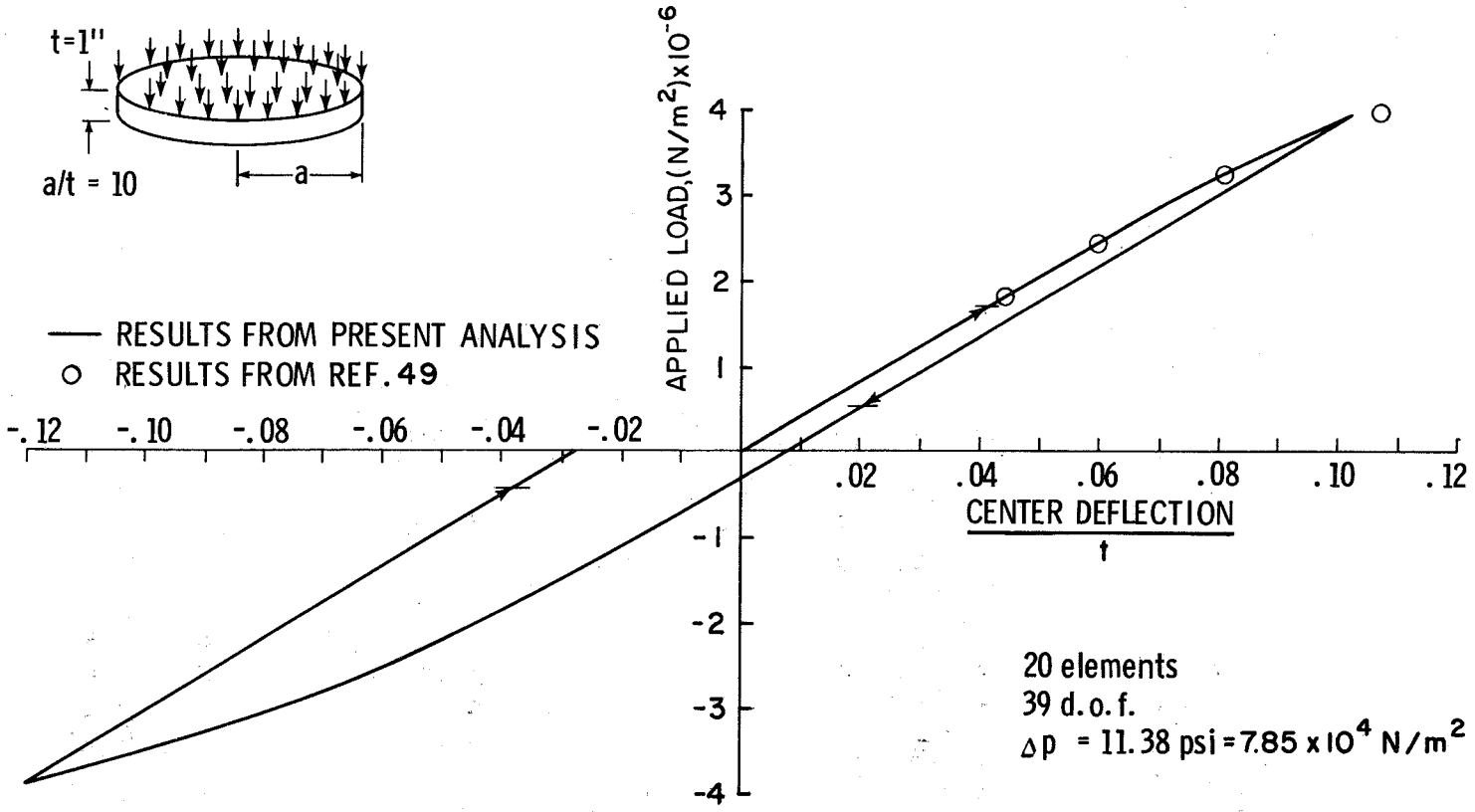

Fig. 16 LOAD VERSUS CENTER DEFLECTION OF A UNIFORMLY LOADED CLAMPED CIRCULAR PLATE

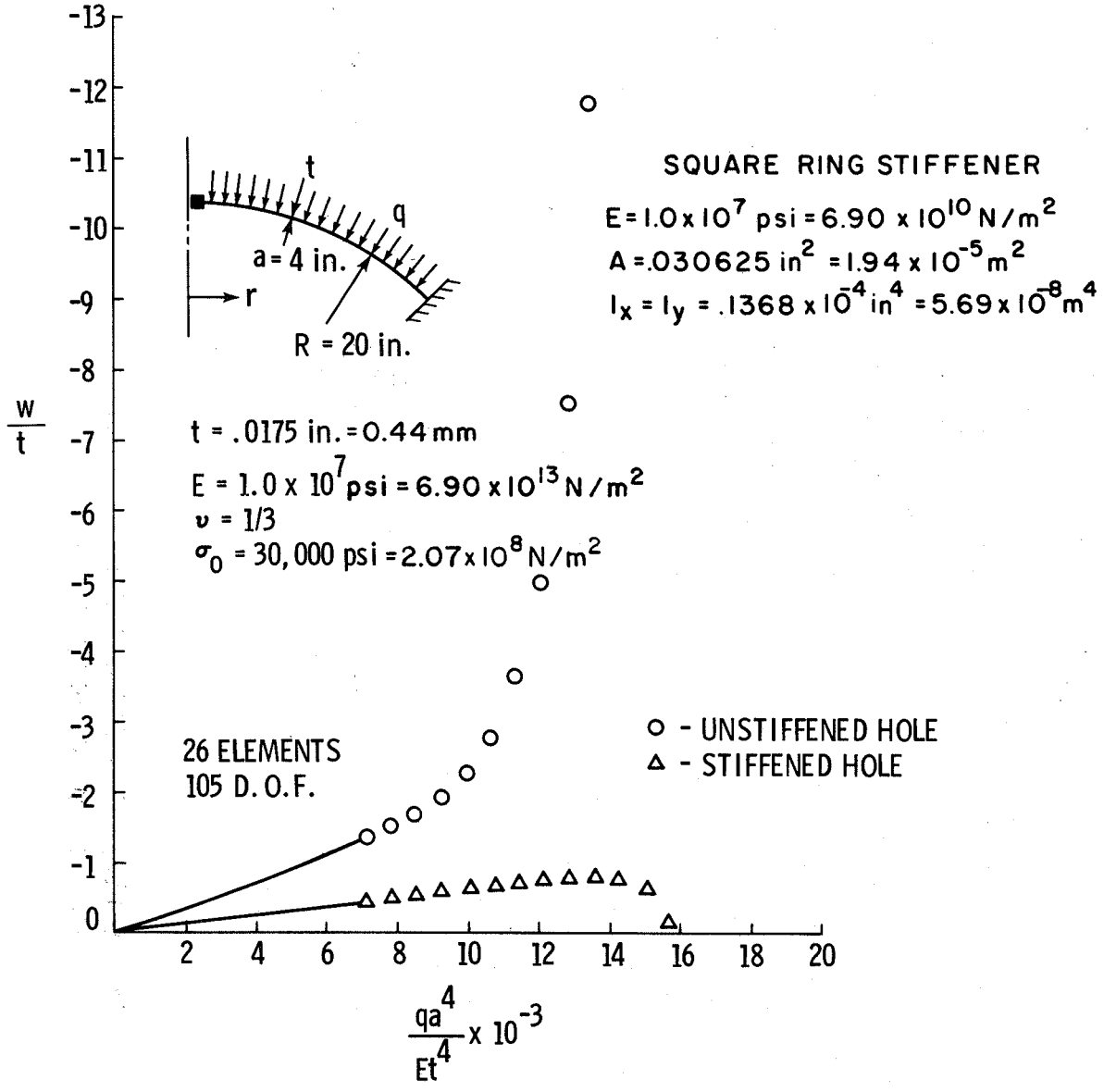

(a) Normal displacement at the hole boundary.

Fig. 17 LOAD-DEFLECTION CURVES FOR RING-STIFFENED SPHERICAL SHELL UNDER EXTERNAL PRESSURE

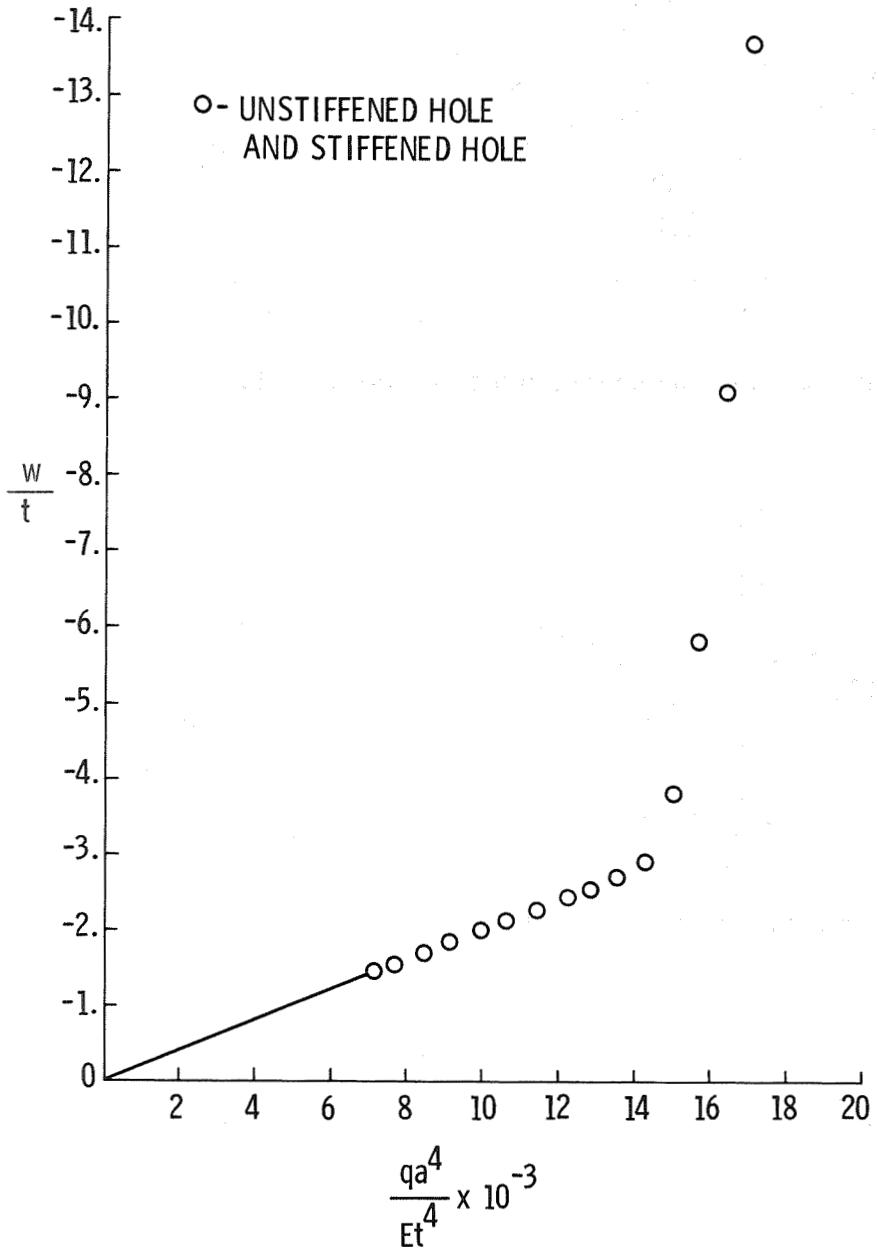

(b) Normal displacement at r = 2.5 in = 6.35 cm

Fig. 17. LOAD-DEFLECTION CURVES FOR RING-STIFFENED SPHERICAL SHELL UNDER EXTERNAL PRESSURE

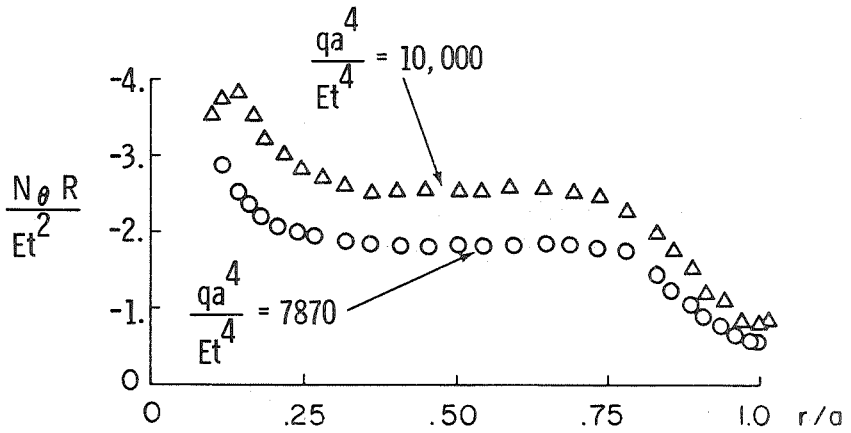

(a) Distribution of circumferential stress resultant for unstiffened hole.

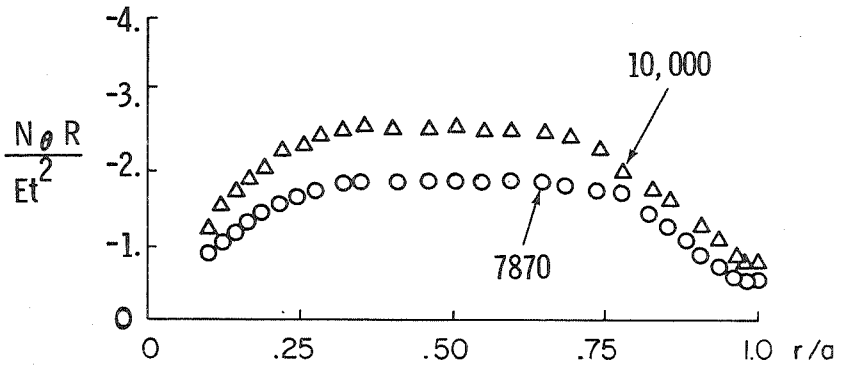

(b) Distribution of circumferential stress resultant for stiffened hole.

Fig.18 RING-STIFFENED SPHERICAL SHELL UNDER EXTERNAL PRESSURE

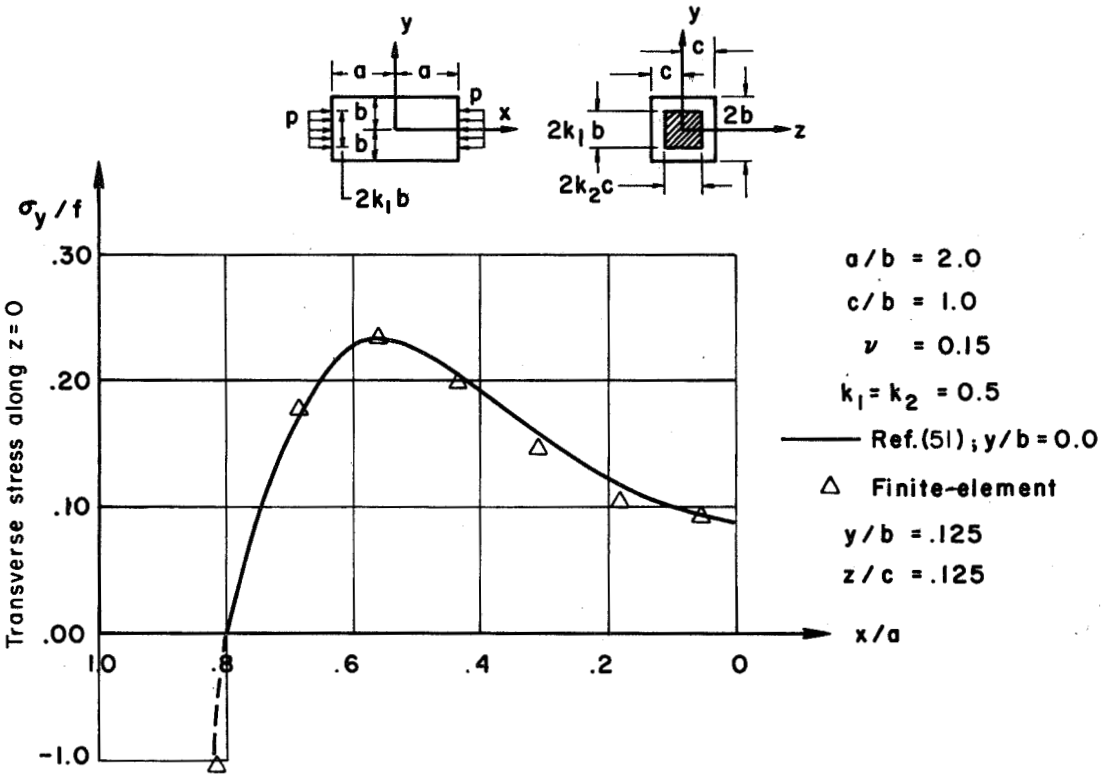

(a) Distribution of transverse stress σ_y along x axis, z = 0 (f = p/4bc)

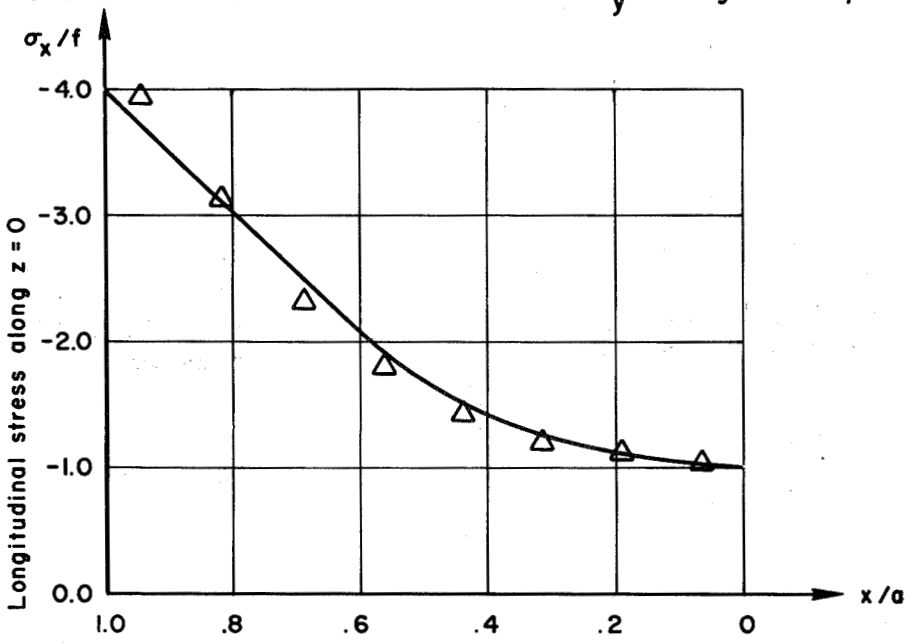

(b) Distribution of longitudinal stress σ_x along x axis, z = 0 (f = p/4bc)

Fig. 19 RECTANGULAR PRISM

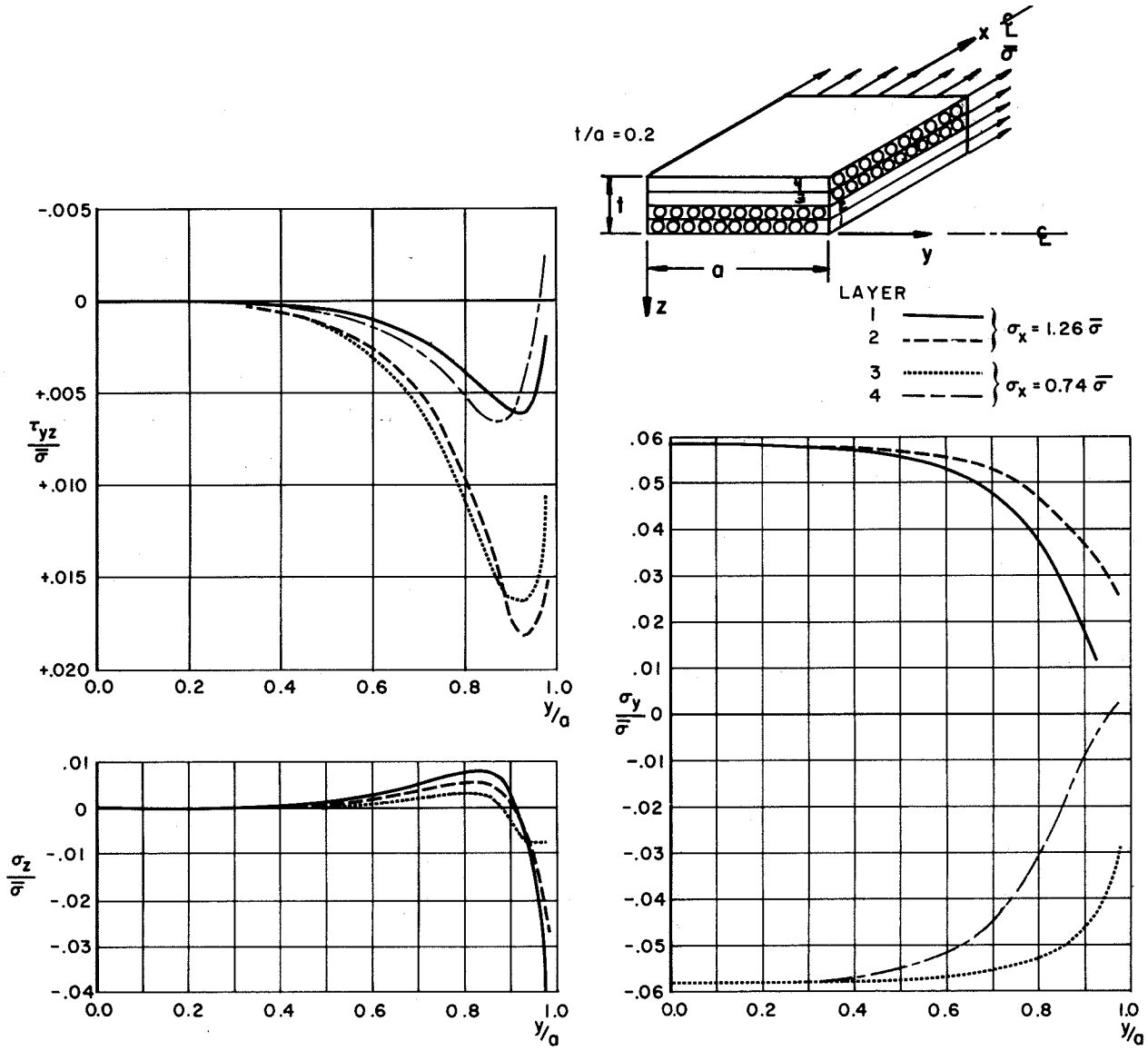

Fig.20. ELASTIC STRESS DISTRIBUTION IN A BORON-ALUMINUM LAMINATE $[90/90/0/0]_s$

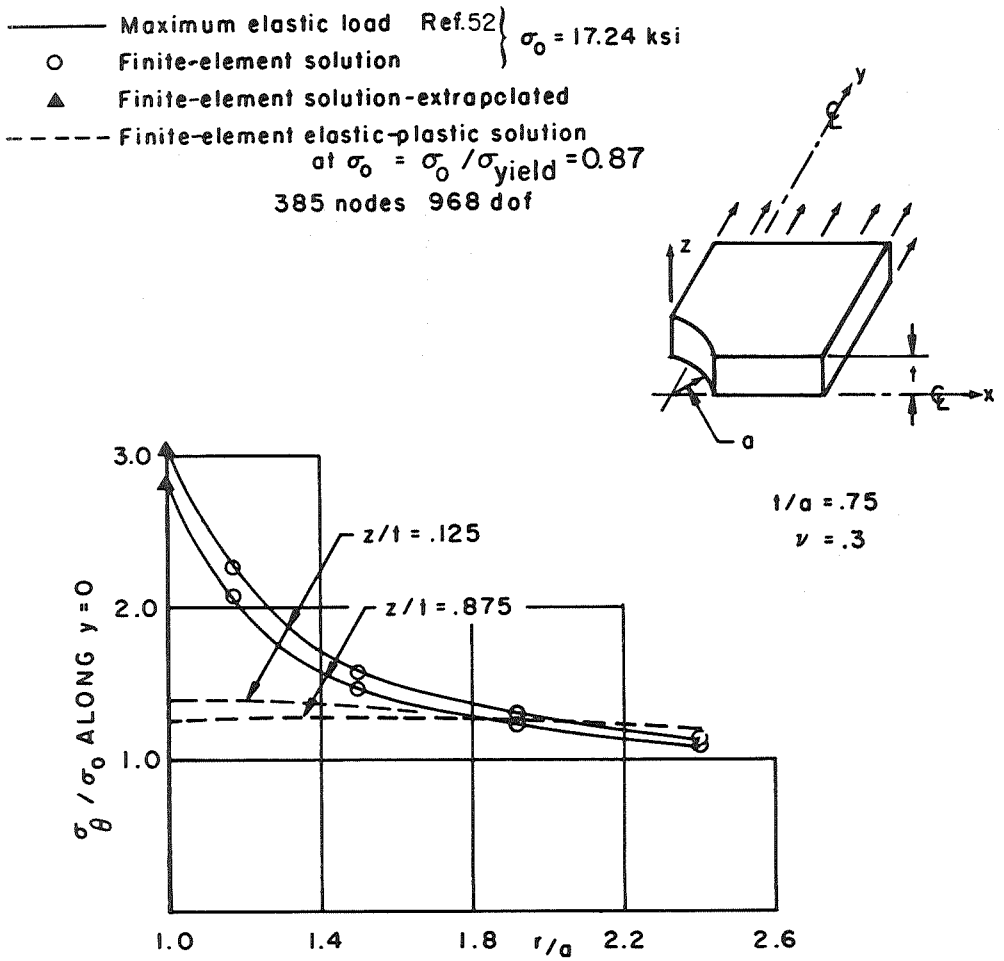

Fig. 21 DISTRIBUTION OF CIRCUMFERENTIAL STRESS IN A THICK PLATE WITH A CENTRAL HOLE.

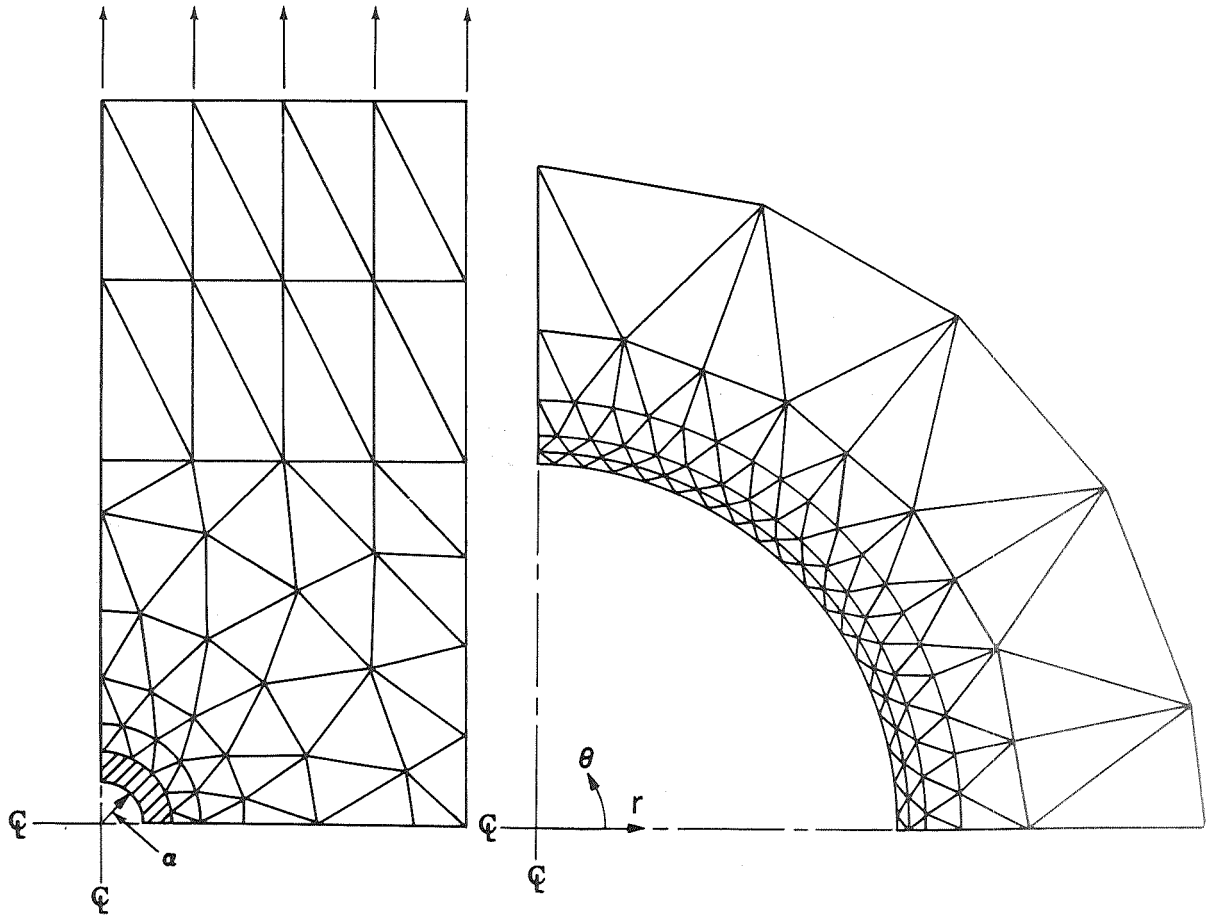

Fig. 22 IDEALIZATION FOR PANEL WITH A CUTOUT

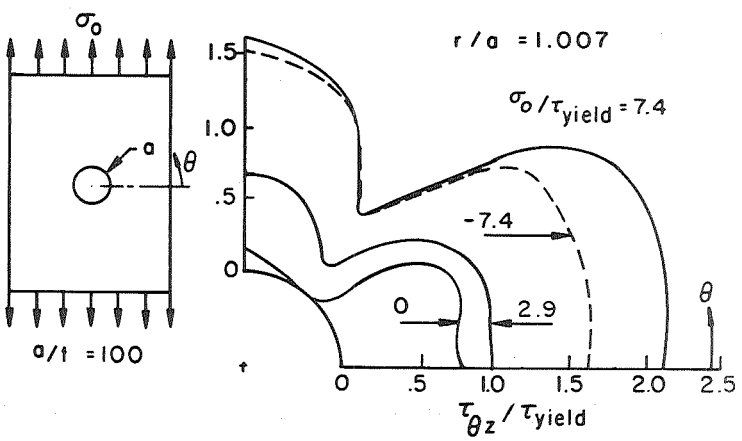

Fig. 23 INTERLAMINAR SHEAR STRESSES AROUND CUTOUT IN BORON-EPOXY $[\pm 45]_s$ LAMINATES

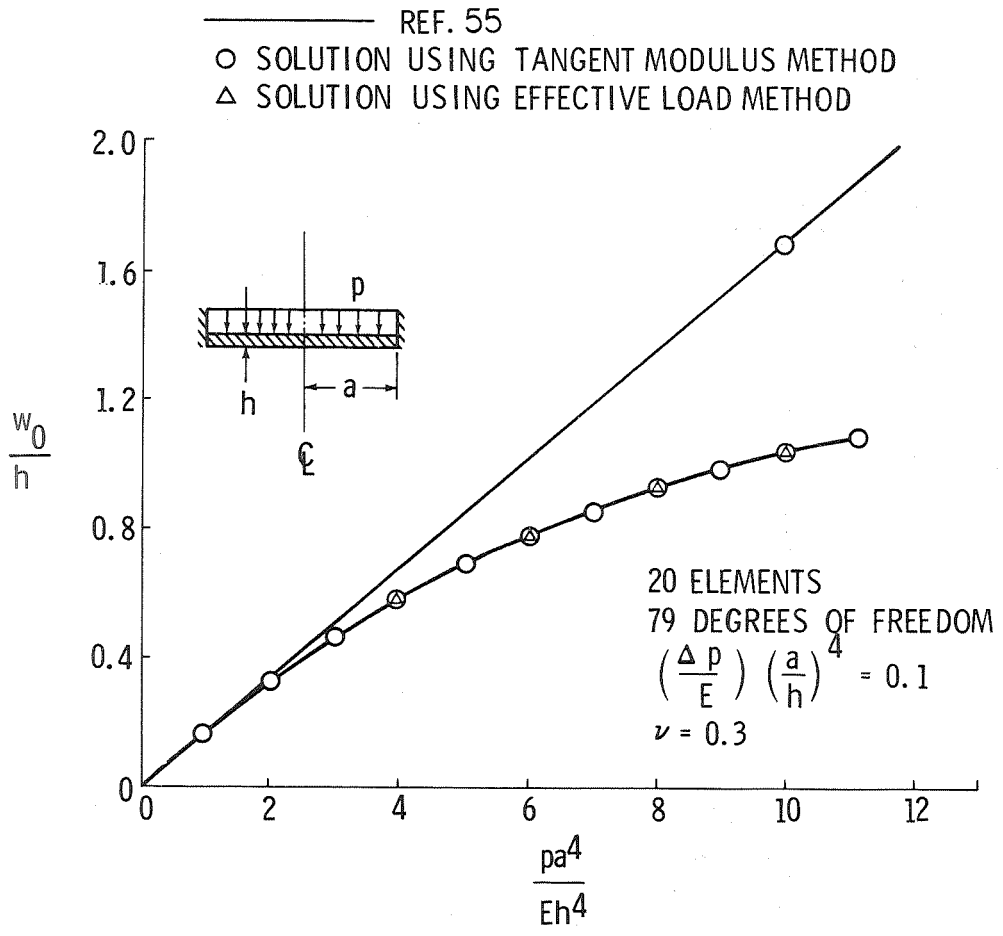

FIG. 24 CENTRAL DEFLECTION VERSUS LOAD FOR A UNIFORMLY LOADED CLAMPED CIRCULAR PLATE

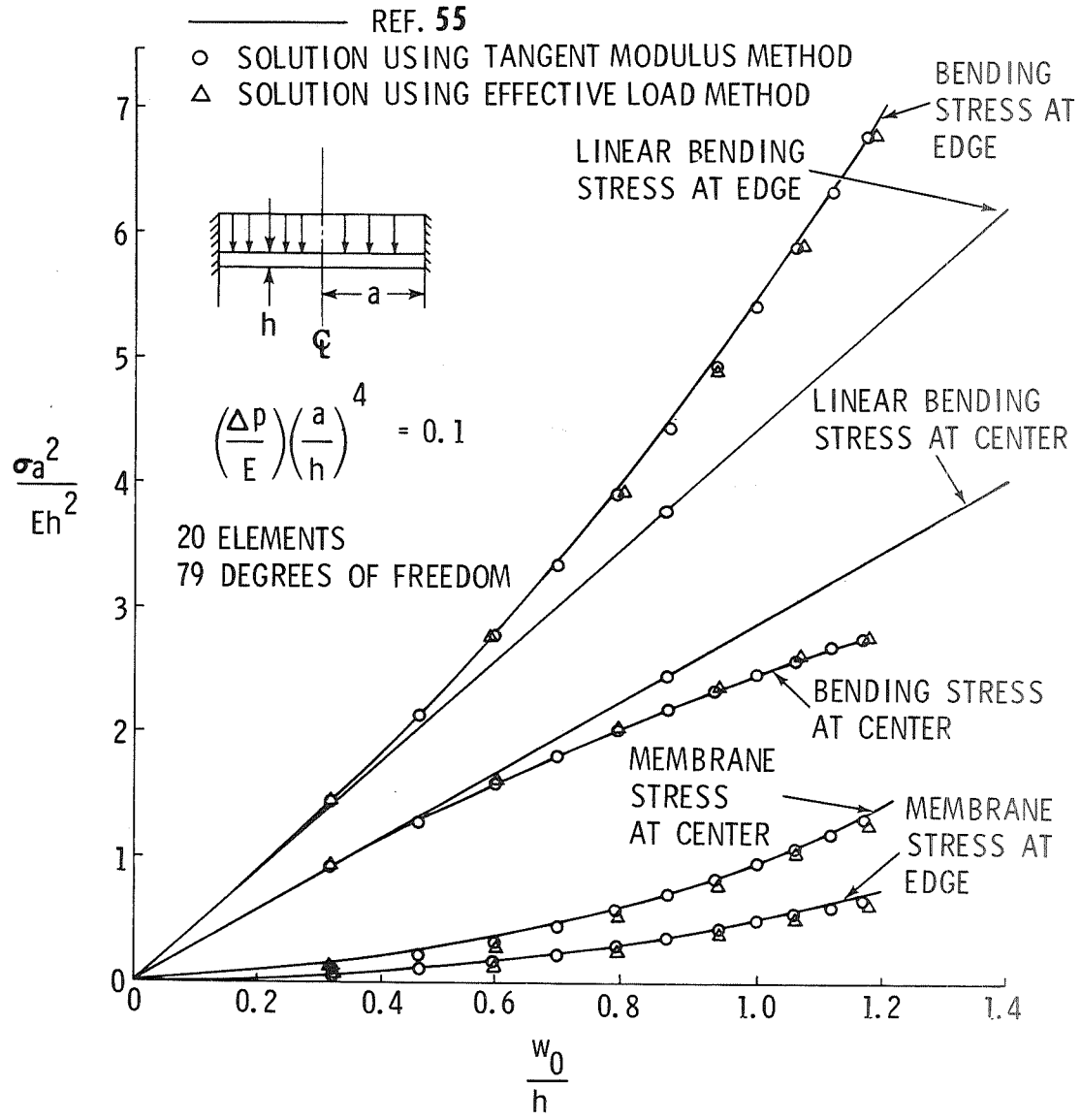

Fig. 25. STRESS VERSUS CENTRAL DEFLECTION FOR A UNIFORMLY LOADED CLAMPED CIRCULAR PLATE

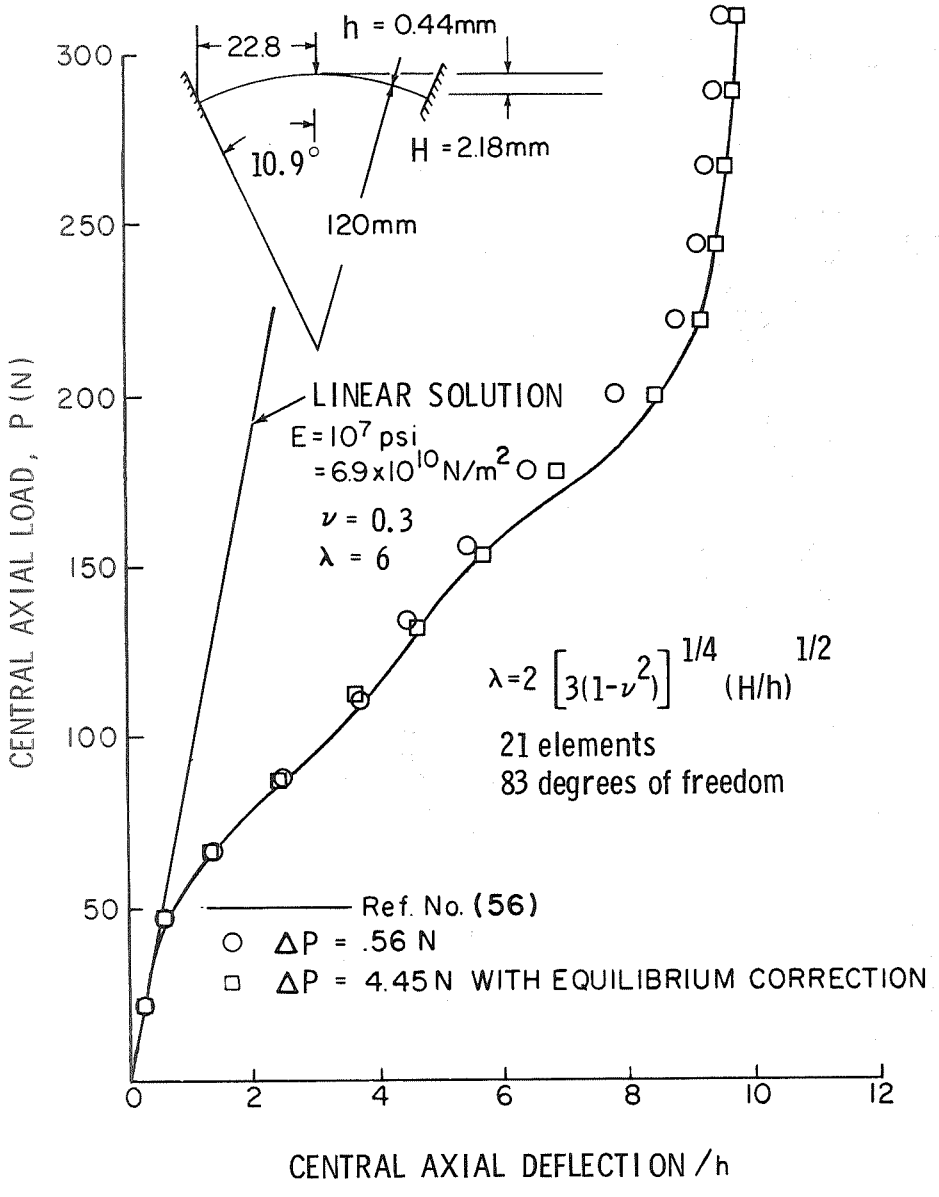

Fig.26 LOAD VERSUS CENTRAL DEFLECTION FOR A CENTRALLY LOADED CLAMPED SPHERICAL CAP ($\lambda = 6$)

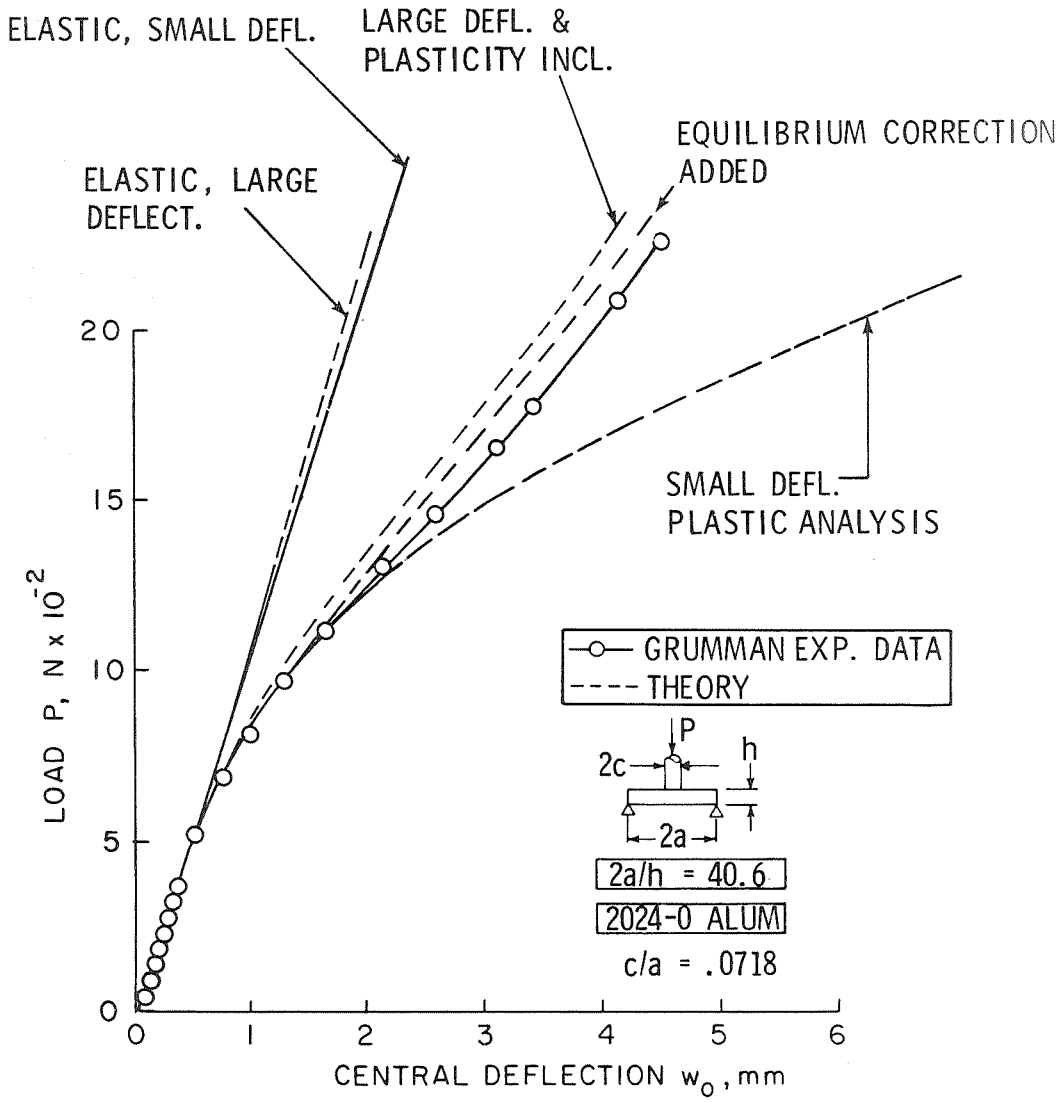

Fig.27a LOAD VERSUS CENTER DEFLECTION FOR A SIMPLY-SUPPORTED CIRCULAR PLATE (2a/h = 40.6)

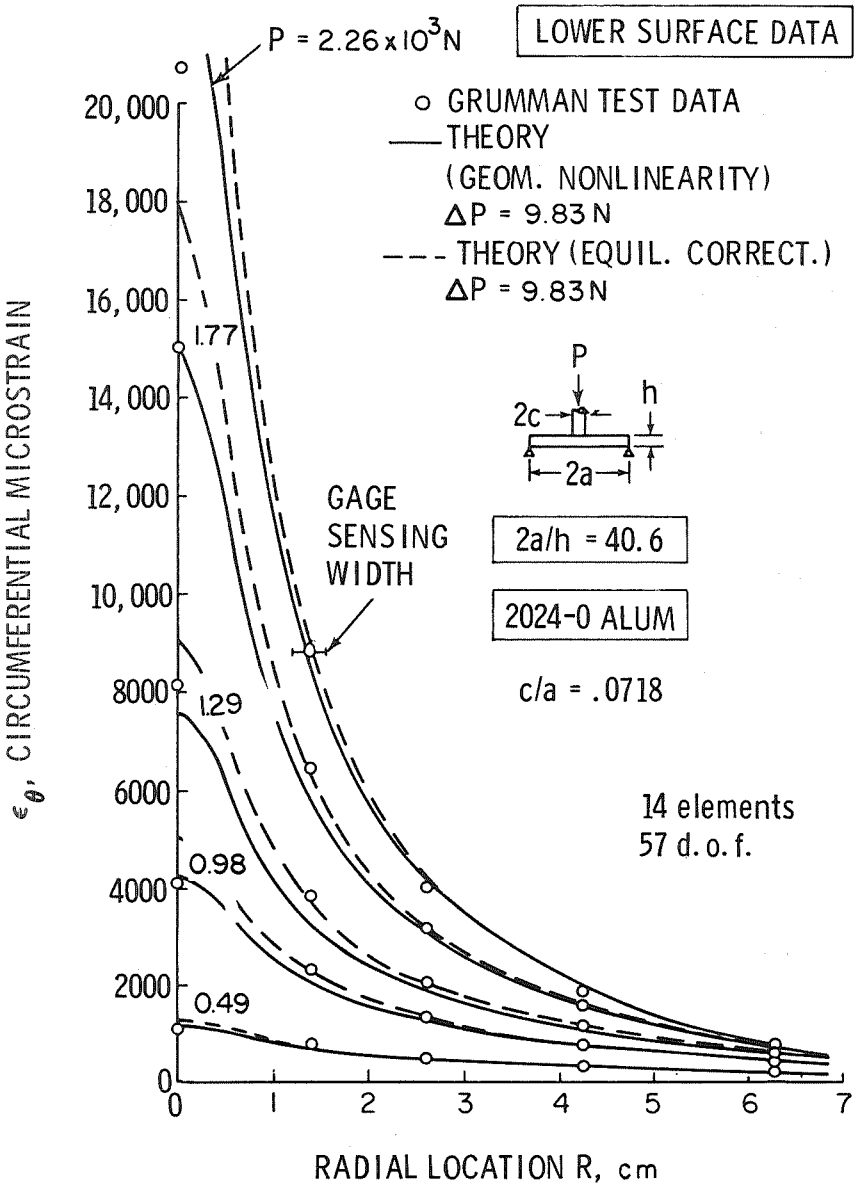

Fig. 27b CIRCUMFERENTIAL STRAIN DISTRIBUTION AT LOWER SURFACE FOR A SIMPLY-SUPPORTED CIRCULAR PLATE (2a/h = 40.6)

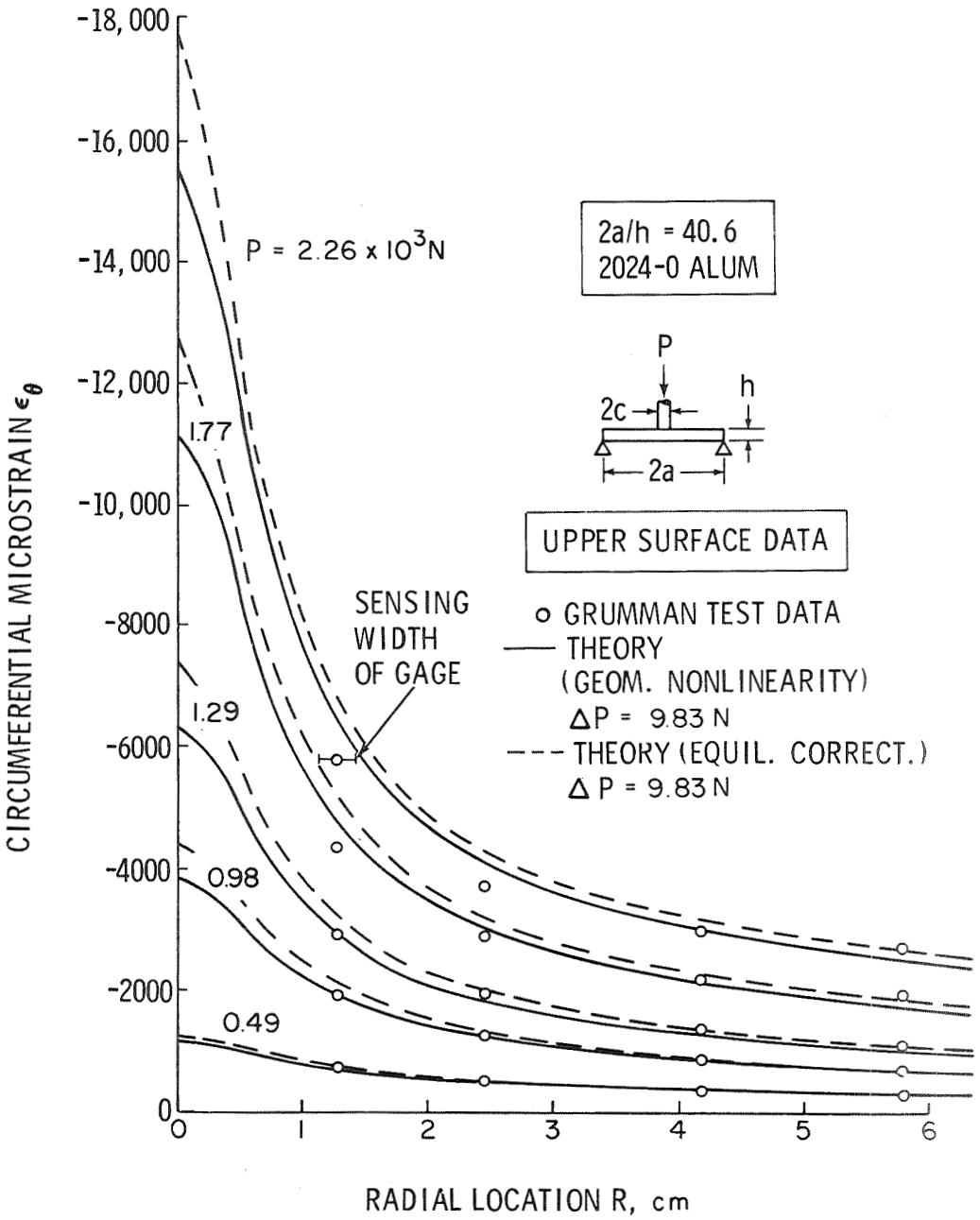

Fig.27c CIRCUMFERENTIAL STRAIN DISTRIBUTION AT UPPER SURFACE FOR A SIMPLY-SUPPORTED CIRCULAR PLATE (2a/h = 40.6)

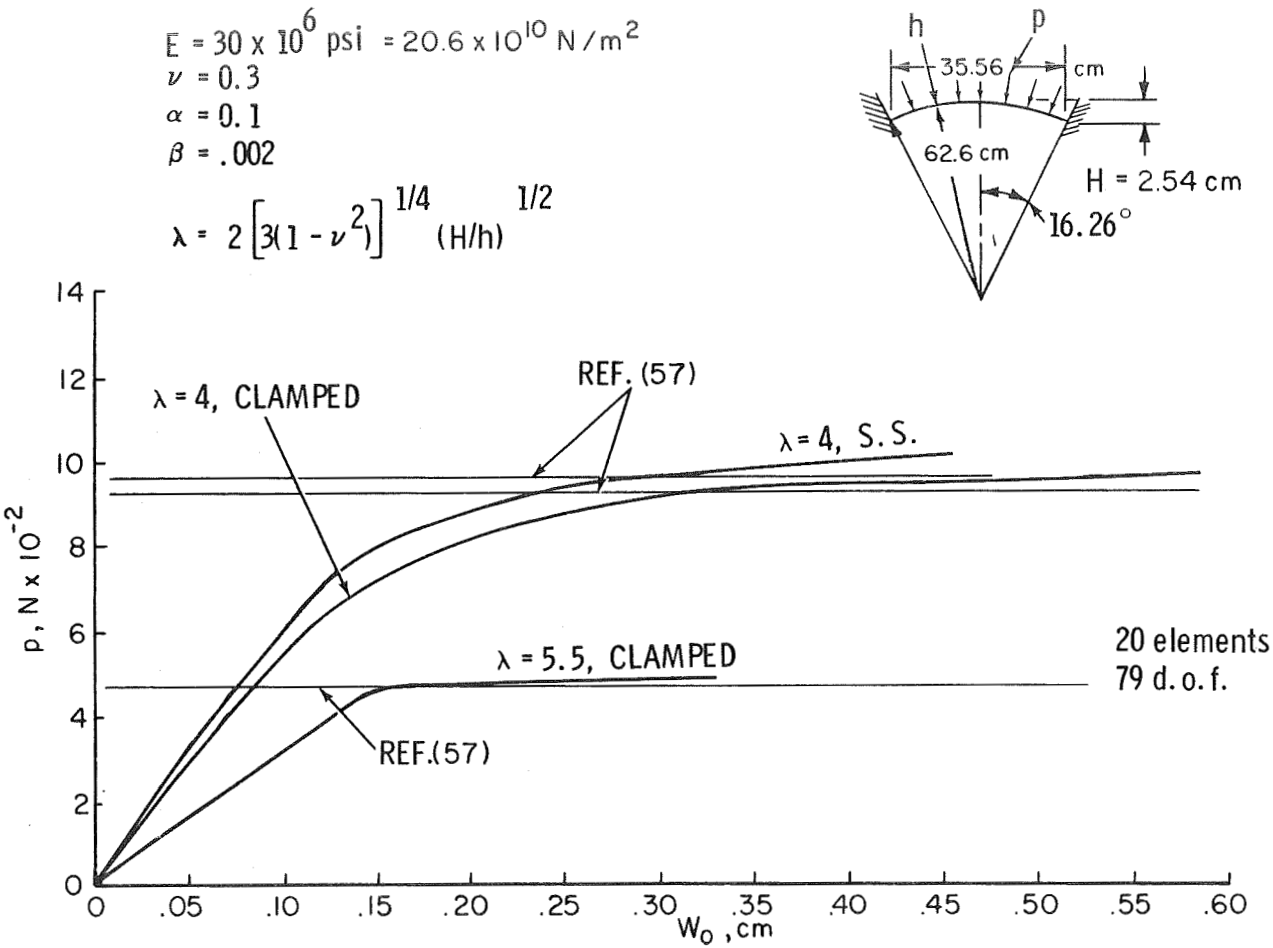

FIG. 28. ELASTO-PLASTIC BUCKLING OF SIMPLY-SUPPORTED AND CLAMPED SPHERICAL CAPS UNDER UNIFORM EXTERNAL PRESSURE (LOAD VS. CENTRAL DEFLECTION CURVES)

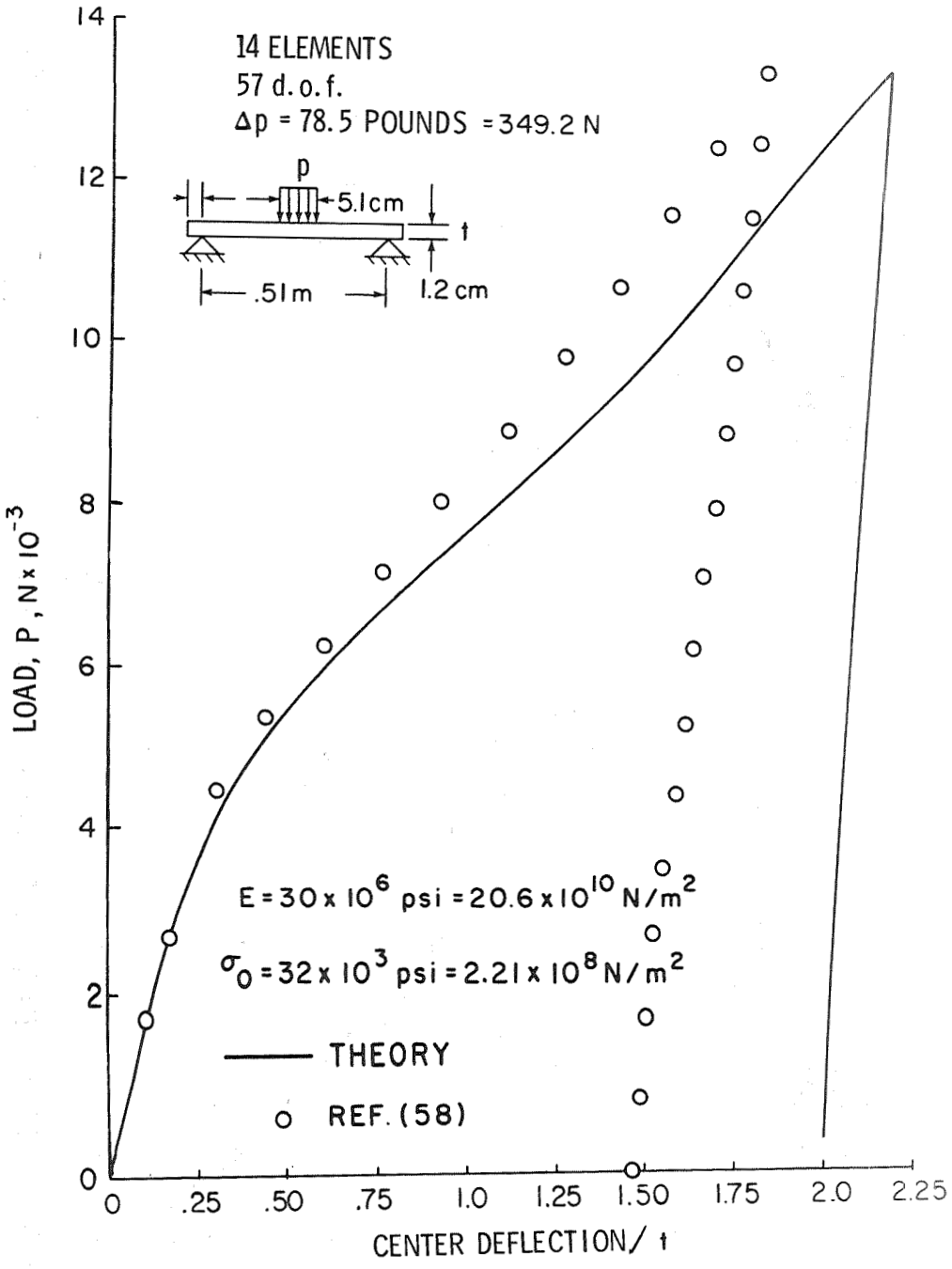

Fig. 29 LOAD VS. CENTER DEFLECTION OF A SIMPLY-SUPPORTED CIRCULAR PLATE

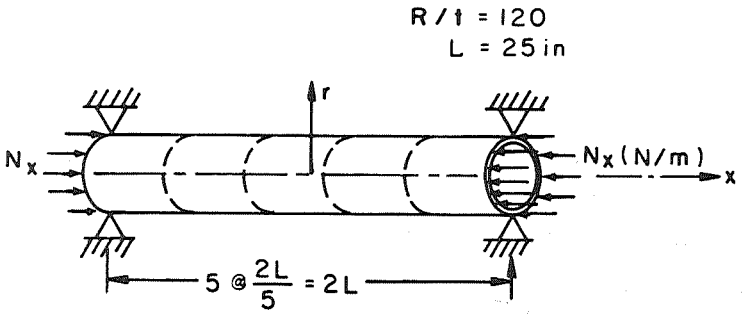

——— Elastic, Ideally plastic

– – – – Elastic

R/t = 120

E = 10×10^3 ksi = 6.9×10^{10} N/m^2

ν = 0.3

σ_{yield} = 30 ksi = 2.1×10^7 N/m^2

L = 25 in = 0.64 m

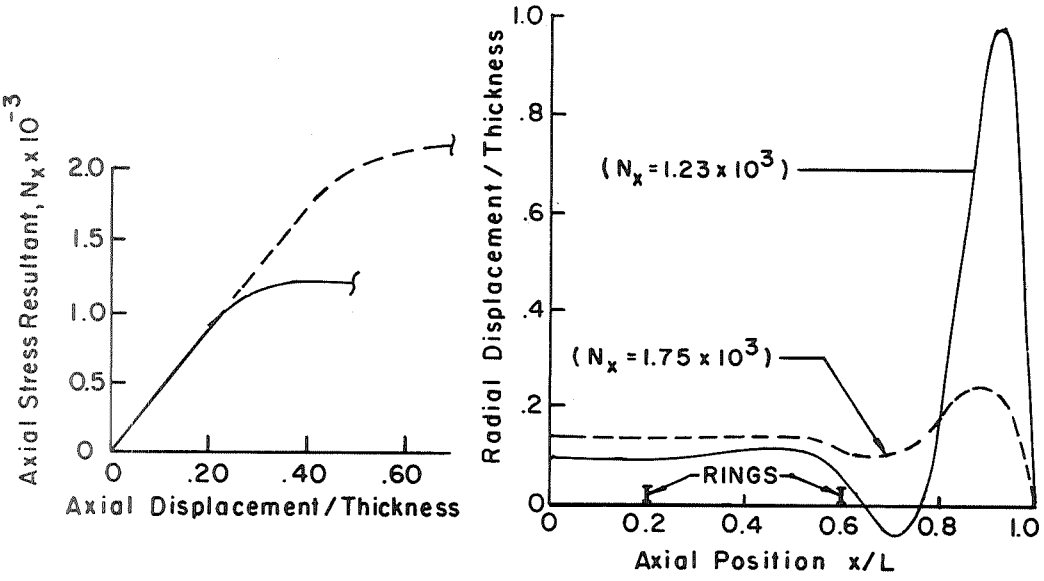

(a) Load vs axial end displacement. (b) Elastic and plastic radial displacement profile.

Fig. 30 SIMPLY-SUPPORTED, STIFFENED CIRCULAR CYLINDER SUBJECTED TO COMPRESSIVE AXIAL LOADS.

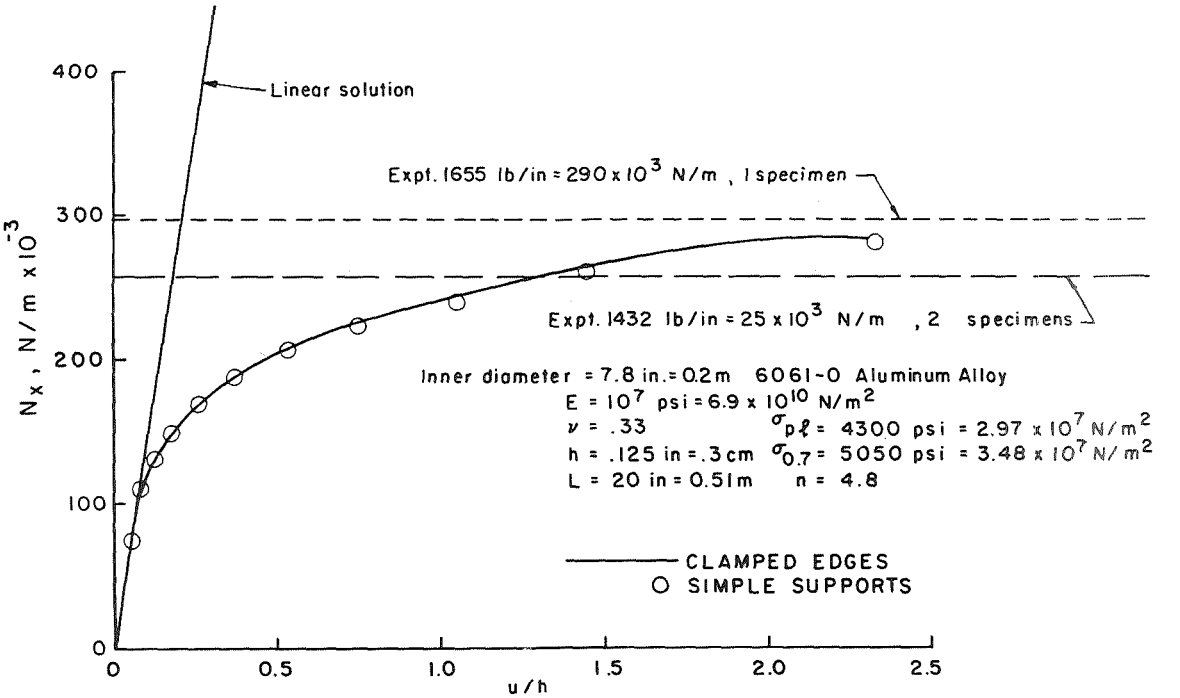

(a) Applied end load vs end deflection for clamped and simply-supported circular cylinders

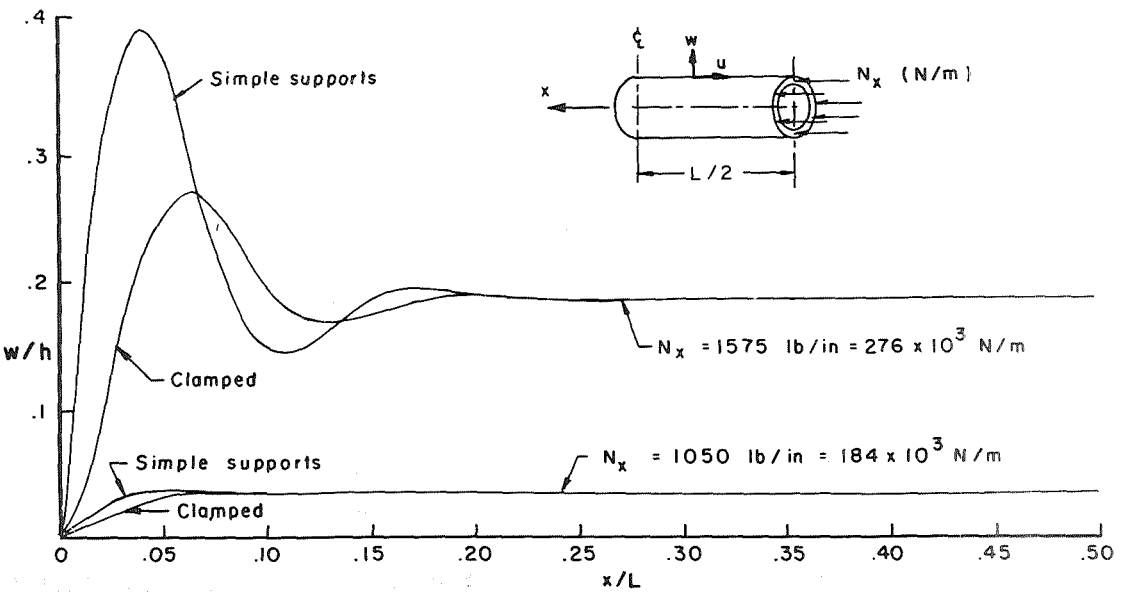

(b) Radial shell displacement along axis for clamped and simply-supported end loaded cylinders.

Fig.31 UNSTIFFENED CIRCULAR CYLINDERS

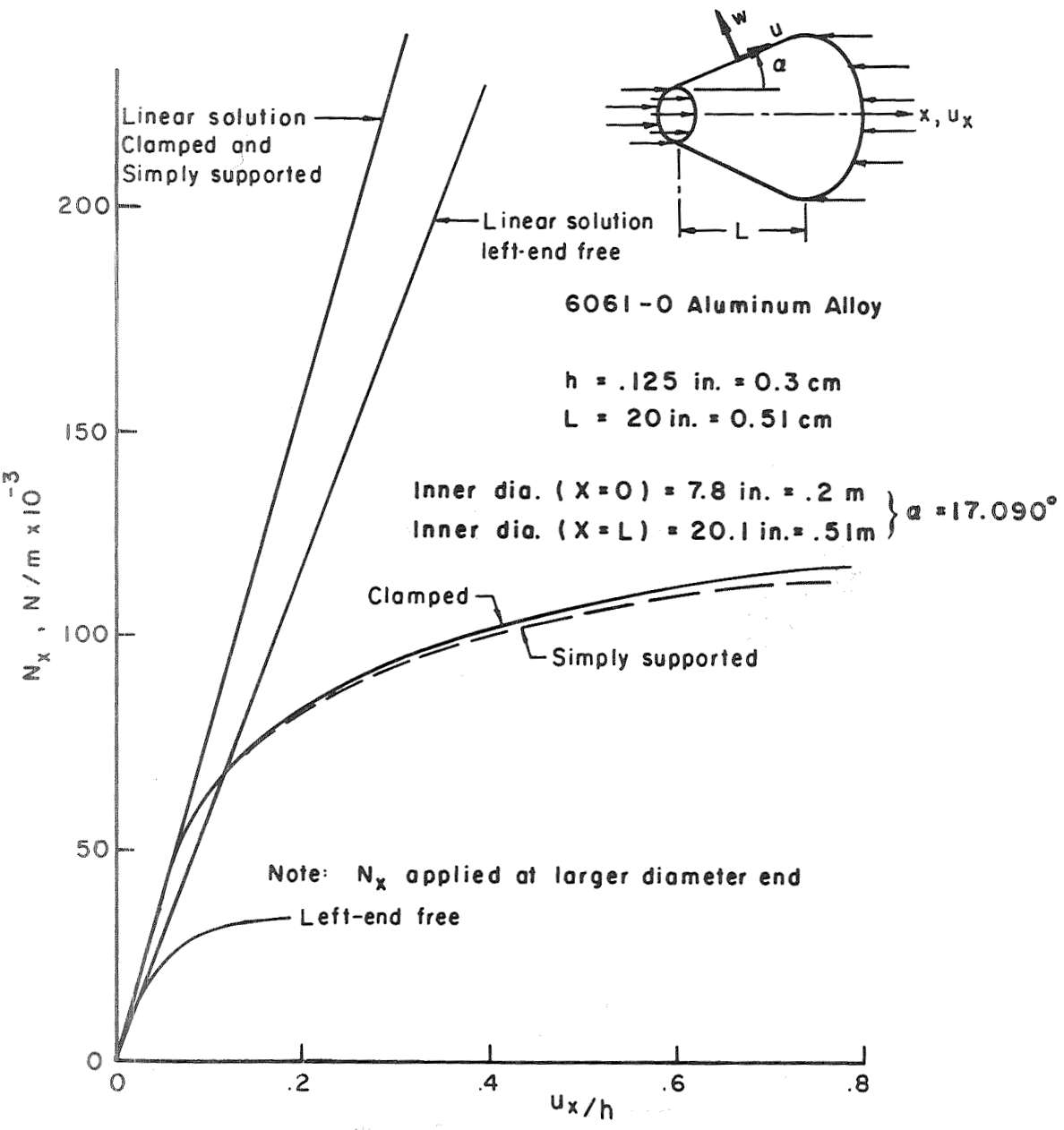

(a) Axial load versus axial end deflection.

Fig. 32 TRUNCATED CONICAL SHELL

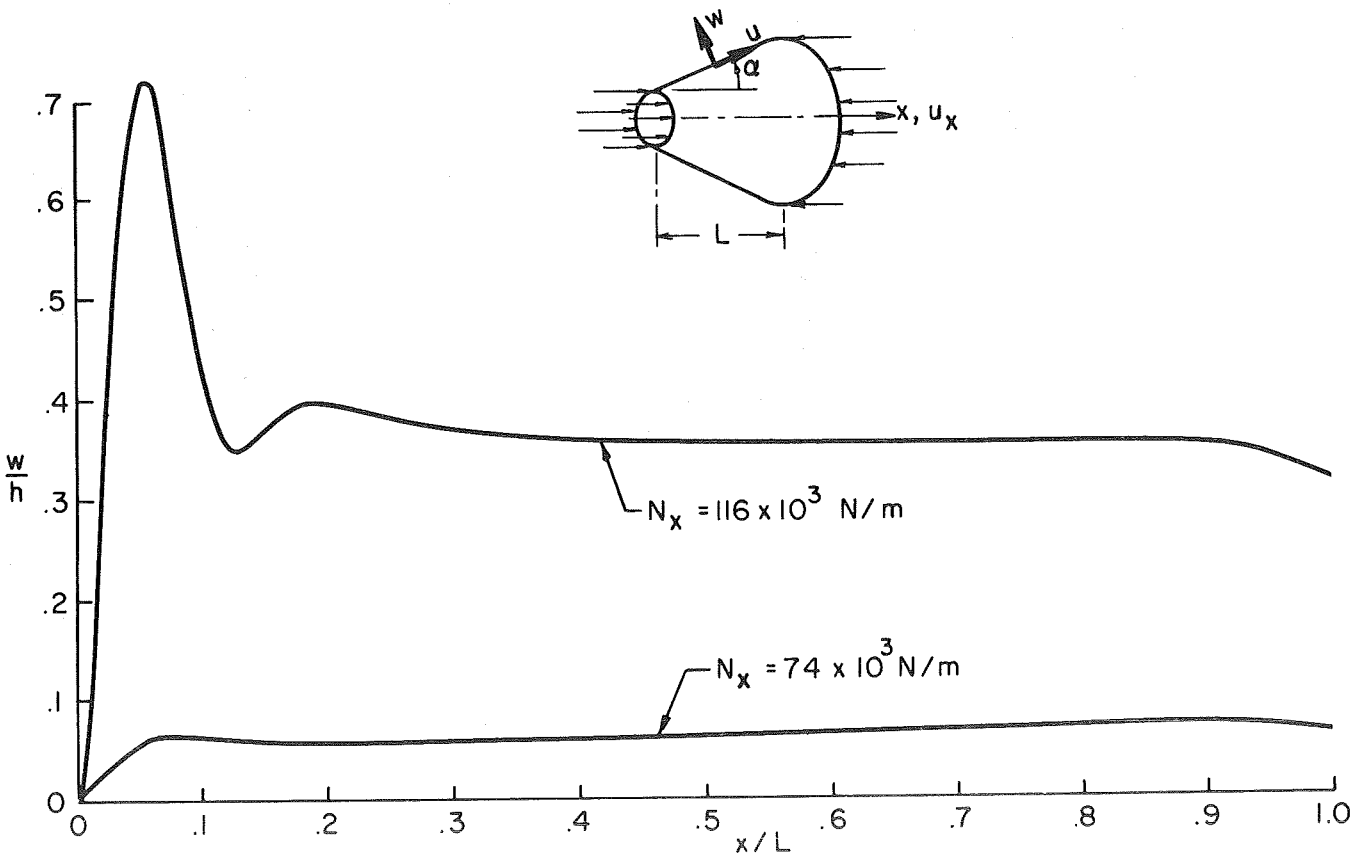

(b) Normal shell displacement along shell axis.

Fig. 32 (cont.) CLAMPED TRUNCATED CONICAL SHELL

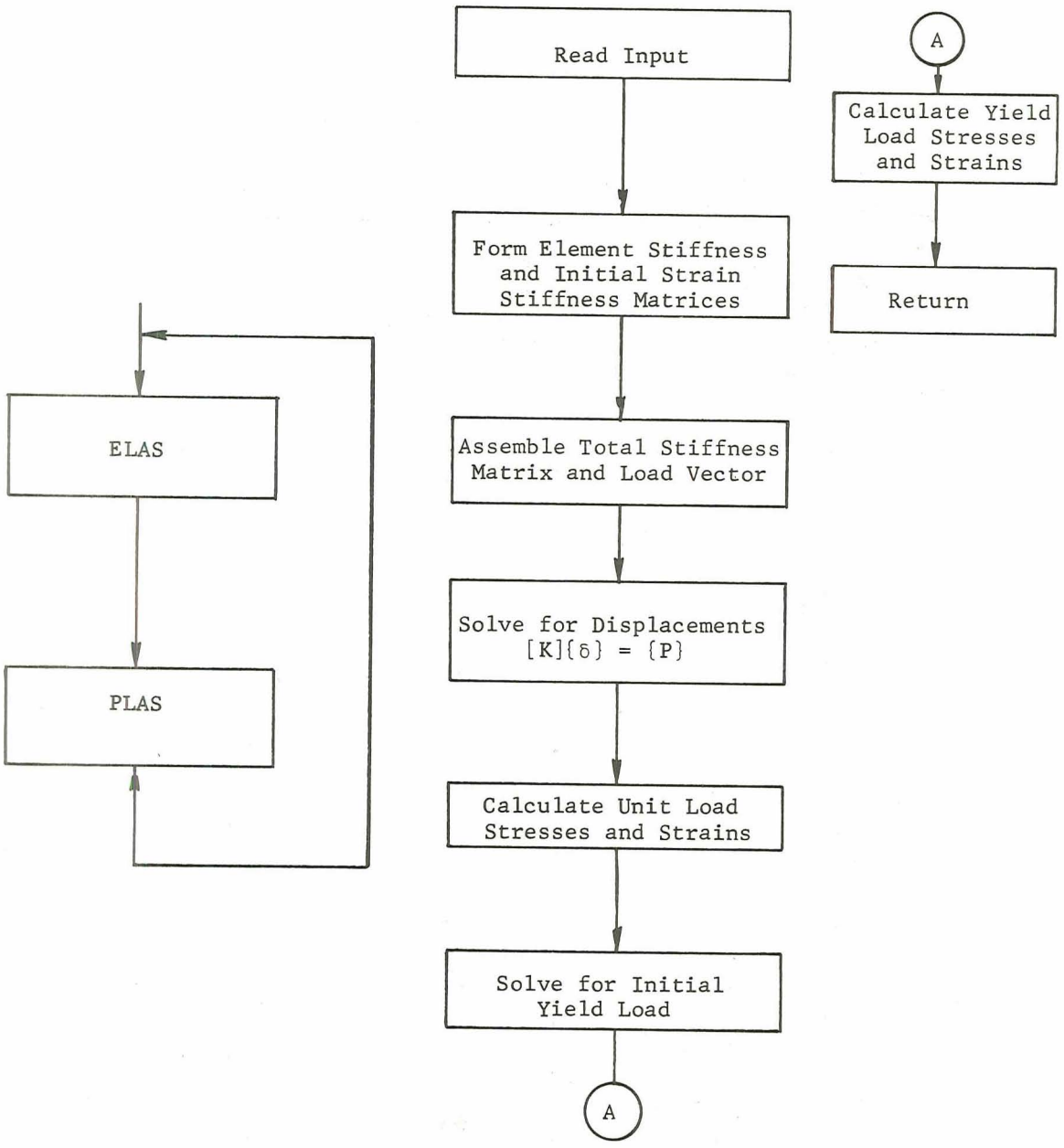

a) Main Program

b) ELAS

Fig. 33 Basic Flow of Each Analysis Program in "PLANS"

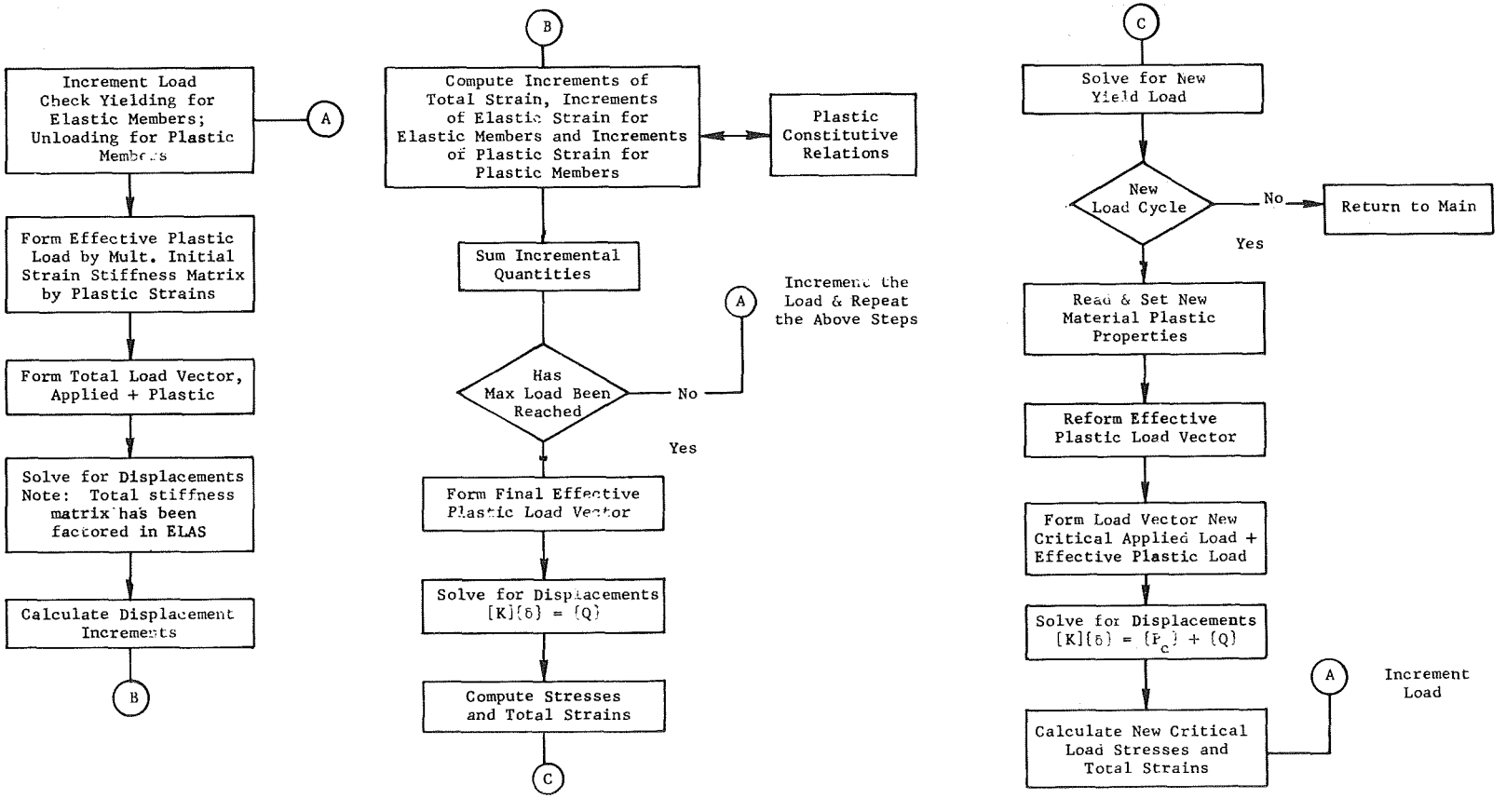

c) PLAS

Fig. 33 (Cont.) Basic Flow of Each Analysis Program in "PLANS"

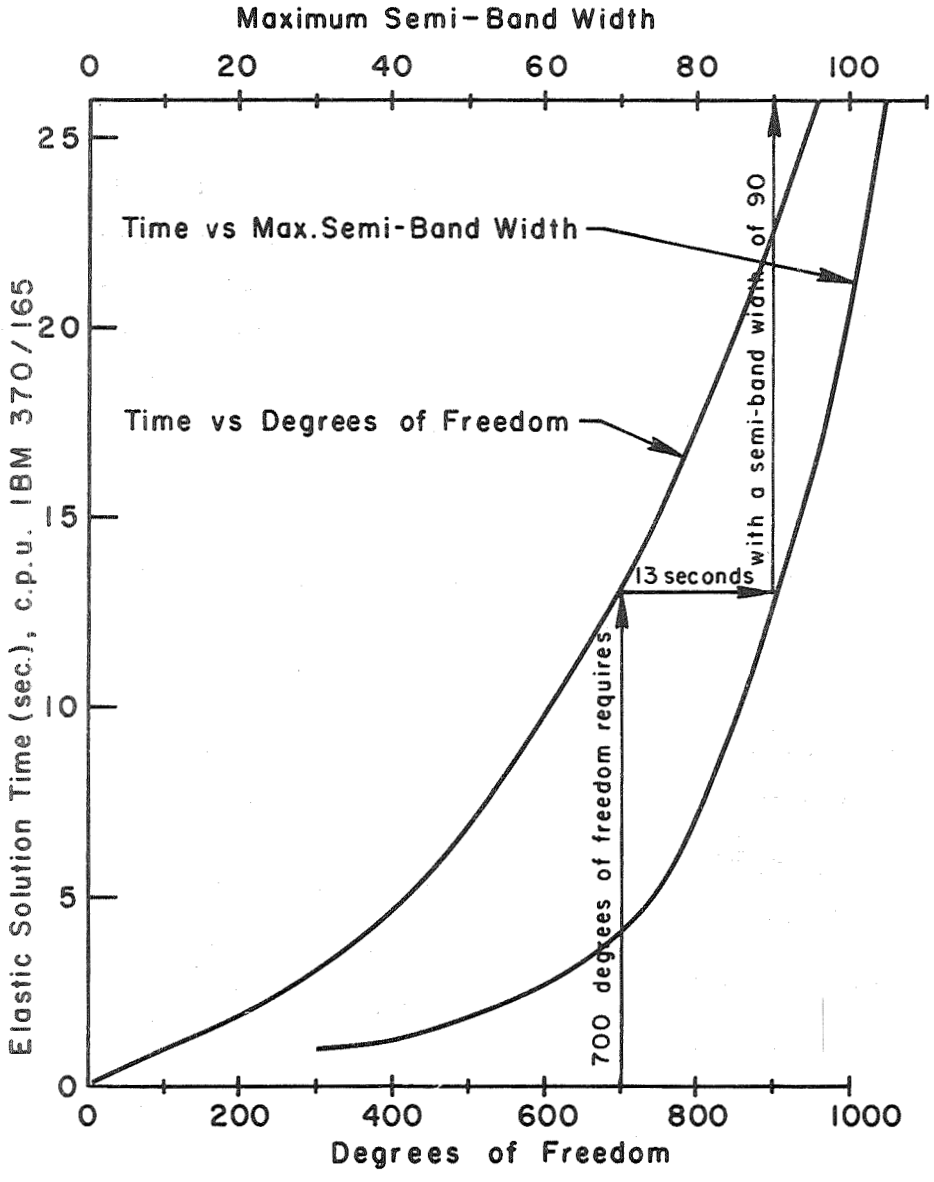

Fig. 34 ELASTIC SOLUTION TIME REQUIREMENTS "PLANE"

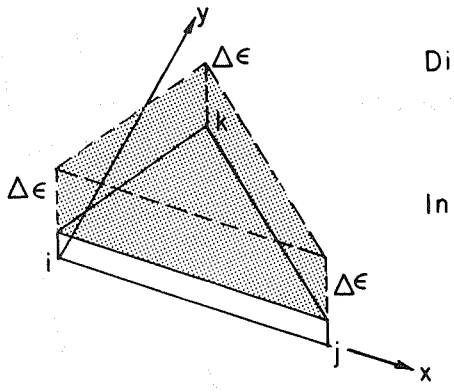

Displacement Assumption :

$u(x,y) = a_1 + a_2 x + a_3 y$

$v(x,y) = a_4 + a_5 x + a_6 y$

Initial Strain Distribution :

ϵ_{ij} (x,y) = constant

Fig.35 CONSTANT STRESS TRIANGLE (CST)

Displacement Assumption:

$u = a_1 + a_2 x + a_3 y + a_4 x^2 + a_5 xy + a_6 y^2$

$v = a_7 + a_8 x + a_9 y + a_{10} x^2 + a_{11} xy + a_{12} y^2$

Initial Strain Distribution :

ϵ = constant

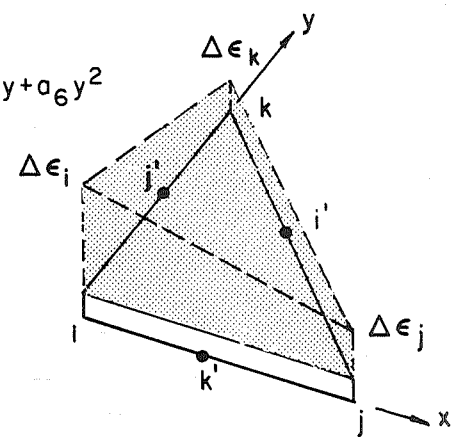

Fig.36 LINEAR STRAIN TRIANGLE (LST)

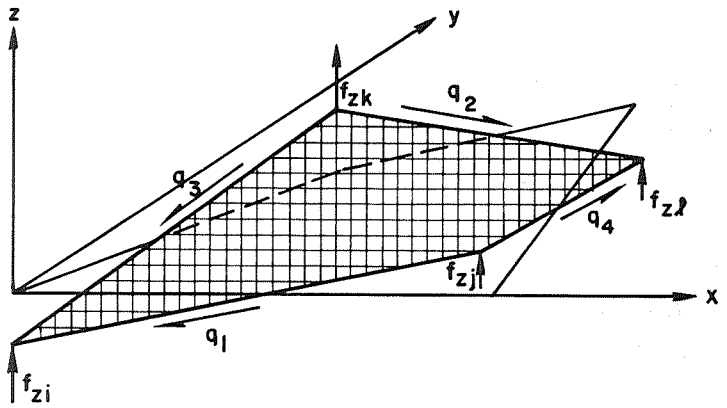

Fig.37 WARPED SHEAR PANEL (GARVEY)

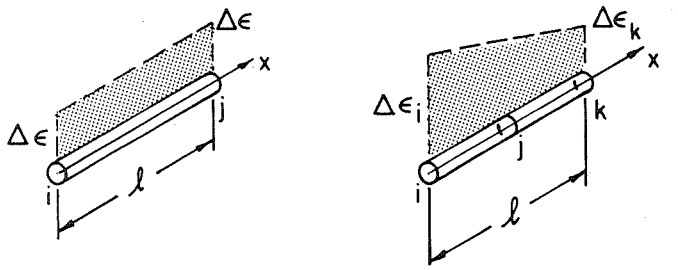

(a) Constant strain element (b) Linear strain element

Displacement Assumption:

$u = a_1 + a_2 x$ $u = a_1 + a_2 x + a_3 x^2$

Initial Strain Distribution

ϵ = constant

Fig.38 STRINGER ELEMENTS

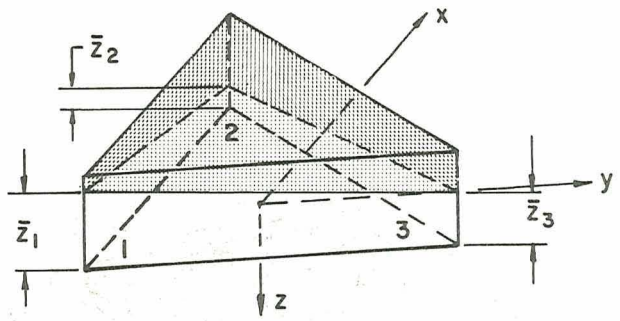

Displacement Assumption :

$$w = a_1 + a_2 x + a_3 y + a_4 x^2 + a_5 xy + \cdots + a_{21} y^5$$

$$u = b_1 + b_2 x + b_3 y + b_4 x^2 + b_5 xy + \cdots + b_{10} y^3$$

$$v = c_1 + c_2 x + c_3 y + c_4 x^2 + c_5 xy + \cdots + c_{10} y^3$$

Initial Strain Distribution :

$$\epsilon(x,y,z) = f(z) \sum_{i=1}^{3} \omega_i \epsilon_i(z)$$

Fig.39 TYPICAL TRIANGULAR ELASTIC-PLASTIC PLATE ELEMENT (PURE B)

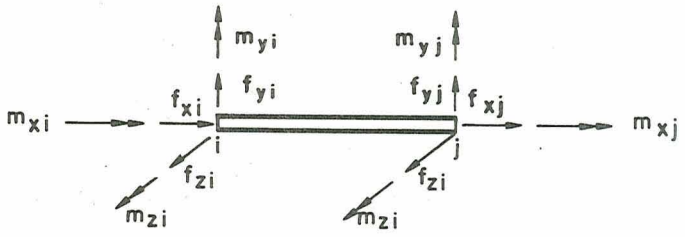

Displacement Assumption:

$$\begin{Bmatrix} u \\ v \\ w \end{Bmatrix} = \sum_{i=1}^{2} H_{oi}^{(1)}(\xi) \begin{Bmatrix} u_i \\ v_i \\ w_i \end{Bmatrix} + H_{ii}^{(1)}(\xi)\, \ell \begin{Bmatrix} u,_{xi} \\ v,_{xi} \\ w,_{xj} \end{Bmatrix}$$

$$\{\beta_x\} = \sum_{i=1}^{2} H_{oi}^{(0)}(\xi) \{\beta_i\}$$

$H^{(k)}$ = Hermitian polynomial of order k

Fig.40 BEAM ELEMENT

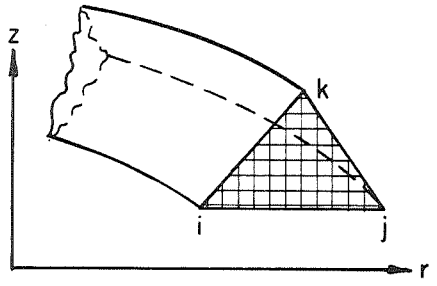

Displacement Assumption:

$$u_r = a_1 + a_2 r + a_3 z$$

$$u_z = a_4 + a_5 r + a_6 z$$

$$u_\theta = a_7 + a_8 r + a_9 z$$

Initial Strain Distribution:

$$\epsilon_{ij}\ (r,z) = \text{constant}$$

Fig. 41 AXISYMMETRIC REVOLVED TRIANGLE

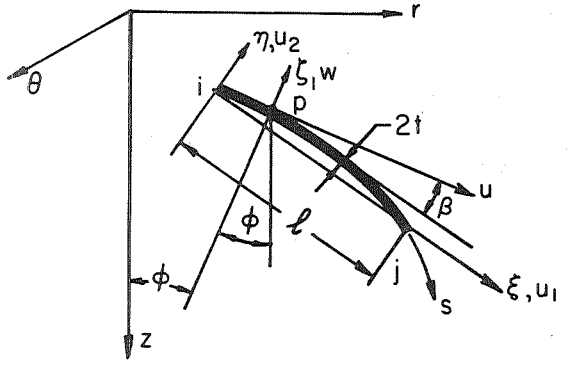

Displacement Assumptions:

$$w = a_1 + a_2 \xi + a_3 \xi^2 + a_4 \xi^3$$

$$u = a_1 + a_2 \xi + a_3 \xi^2 + a_4 \xi^3$$

Initial Strain Distribution:

$$\left\{ \epsilon_s \right\}_\theta = (1-\xi)\, \epsilon^i_{s\,\theta}\ (\zeta) + (\xi)\, \epsilon^j_{s\,\theta}\ (\zeta)$$

Fig. 42 AXISYMMETRIC THIN SHELL ELEMENT

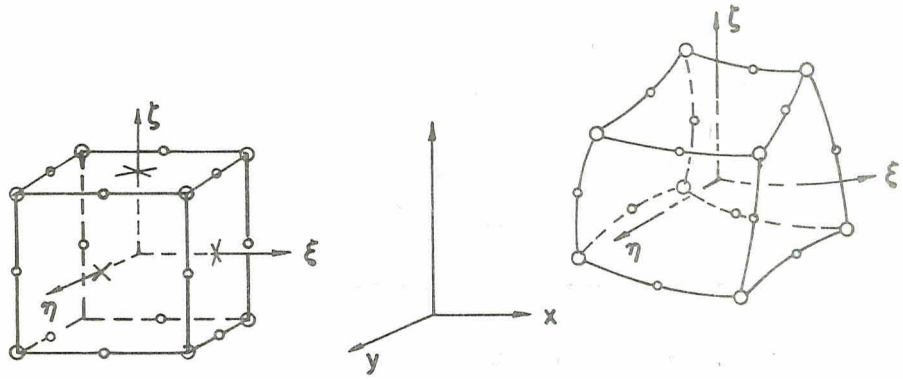

Local Coordinates

Cartesian Coordinates

Displacement Assumption

$$\begin{Bmatrix} U \\ V \\ W \end{Bmatrix} = \begin{bmatrix} P & 0 & 0 \\ 0 & P & 0 \\ 0 & 0 & P \end{bmatrix} \begin{Bmatrix} \bar{U} \\ \bar{V} \\ \bar{W} \end{Bmatrix}$$

$$P = P_1 \; P_2 \; P_3 \cdots P_8 \cdots P_{20}$$

$$P_i = -(1+\zeta_i \xi)(1+\eta_i \eta)(1+\xi_i \xi+\eta_i \eta+\zeta_i \zeta-2) \quad i = 1,8$$

for a typical mid-edge node (e.g. $\xi_i = 0, \eta_i = \pm 1, \zeta_i = \pm 1$)

$$P = \frac{1}{4}(1-\xi^2)(1+\eta_i \eta)(1+\zeta_i \zeta)$$

Plastic Strain Distribution

$$\epsilon_{ij} = \text{uniform}$$

Fig.43 ISOPARAMETRIC HEXAHEDRA

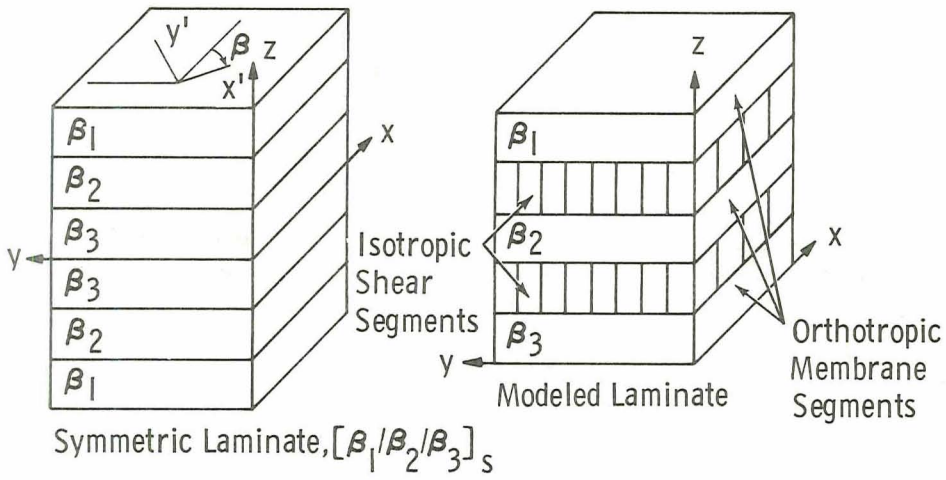

(a) Laminate Model

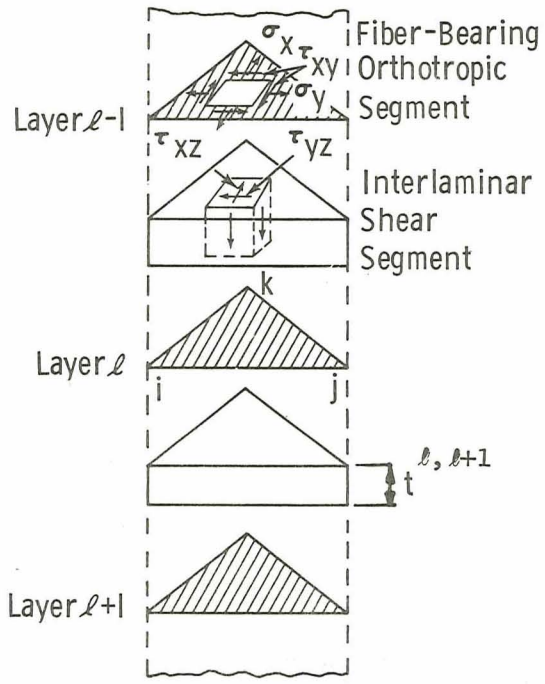

(b) Finite-Element Model

Fig. 44 COMPOSITE ELEMENT

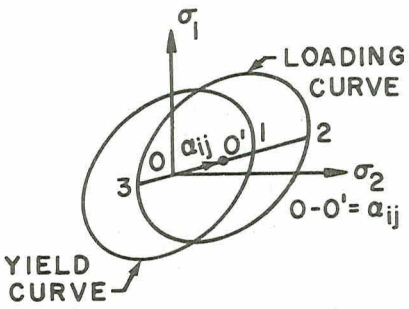

Fig. 45 KINEMATIC HARDENING

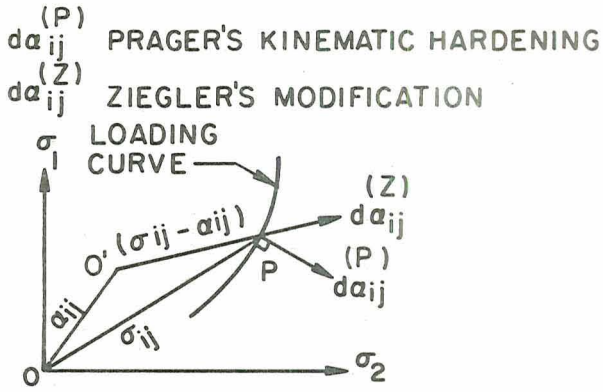

Fig. 46 COMPARISON OF PRAGER'S RULE WITH ZIEGLER'S MODIFICATION

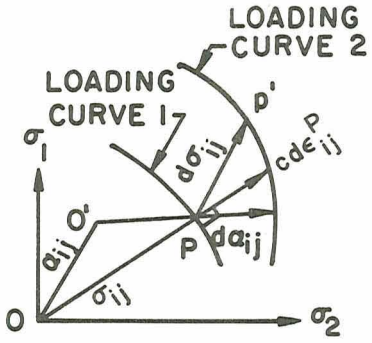

Fig. 47 HARDENING RULE AND FLOW LAW FOR WORK-HARDENING MATERIAL USING ZIEGLER'S MODIFICATION

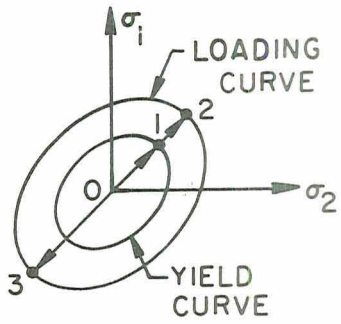

Fig. 48 ISOTROPIC HARDENING

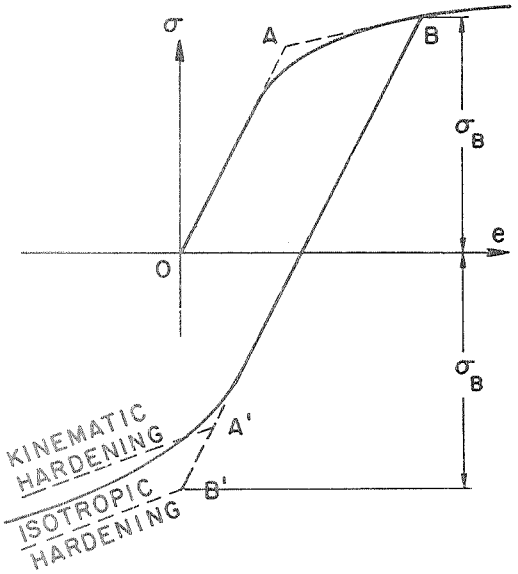

Fig. 49 TYPICAL CYCLIC STRESS-STRAIN CURVE

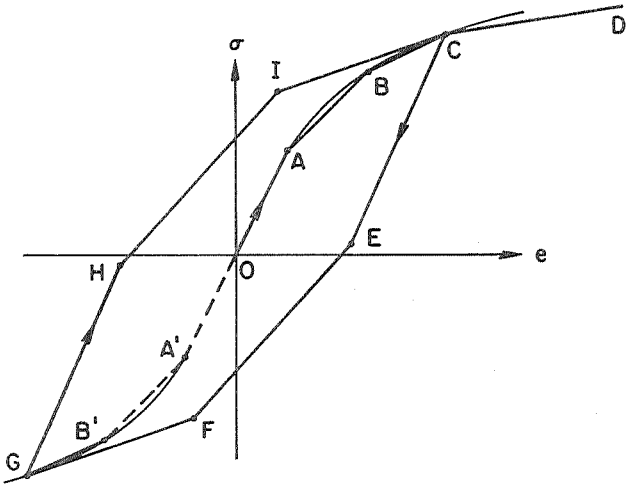

Fig. 50 REPRESENTATION OF TYPICAL CYCLIC STRESS-STRAIN CURVE BY CONSTANT TANGENT MODULI.

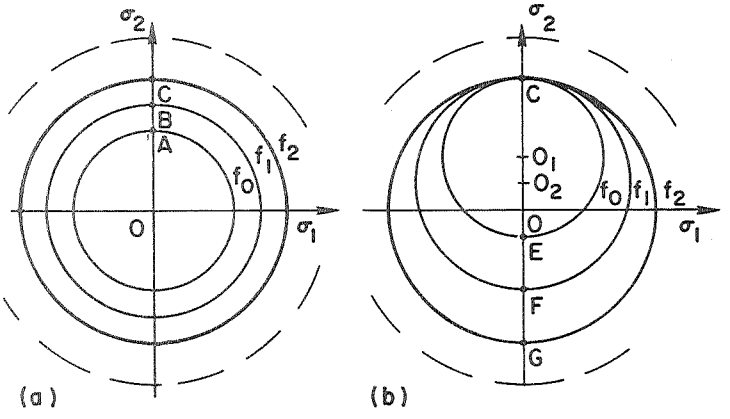

Fig. 51 REPRESENTATION OF HYPERSURFACES OF CONSTANT WORK-HARDENING MODULII.

☆U.S. GOVERNMENT PRINTING OFFICE: 1974-739-158/100

NATIONAL AERONAUTICS AND SPACE ADMINISTRATION
WASHINGTON, D.C. 20546

OFFICIAL BUSINESS
PENALTY FOR PRIVATE USE $300

SPECIAL FOURTH-CLASS RATE BOOK

POSTAGE AND FEES PAID
NATIONAL AERONAUTICS AND SPACE ADMINISTRATION
451

U.S.MAIL

POSTMASTER : If Undeliverable (Section 158 Postal Manual) Do Not Return

"The aeronautical and space activities of the United States shall be conducted so as to contribute . . . to the expansion of human knowledge of phenomena in the atmosphere and space. The Administration shall provide for the widest practicable and appropriate dissemination of information concerning its activities and the results thereof."

—NATIONAL AERONAUTICS AND SPACE ACT OF 1958

NASA SCIENTIFIC AND TECHNICAL PUBLICATIONS

TECHNICAL REPORTS: Scientific and technical information considered important, complete, and a lasting contribution to existing knowledge.

TECHNICAL NOTES: Information less broad in scope but nevertheless of importance as a contribution to existing knowledge.

TECHNICAL MEMORANDUMS: Information receiving limited distribution because of preliminary data, security classification, or other reasons. Also includes conference proceedings with either limited or unlimited distribution.

CONTRACTOR REPORTS: Scientific and technical information generated under a NASA contract or grant and considered an important contribution to existing knowledge.

TECHNICAL TRANSLATIONS: Information published in a foreign language considered to merit NASA distribution in English.

SPECIAL PUBLICATIONS: Information derived from or of value to NASA activities. Publications include final reports of major projects, monographs, data compilations, handbooks, sourcebooks, and special bibliographies.

TECHNOLOGY UTILIZATION PUBLICATIONS: Information on technology used by NASA that may be of particular interest in commercial and other non-aerospace applications. Publications include Tech Briefs, Technology Utilization Reports and Technology Surveys.

Details on the availability of these publications may be obtained from:

SCIENTIFIC AND TECHNICAL INFORMATION OFFICE

NATIONAL AERONAUTICS AND SPACE ADMINISTRATION

Washington, D.C. 20546